공학박사 학위 논문

연료전지-배터리-슈퍼커패시터 하이브리드 전력시스템 에너지 관리
전략 개발

DEVELOPMENT OF ENERGY MANAGEMENT STRATEGIES FOR FUEL CELL-BATTERY-SUPERCAPACITOR HYBRID POWER SYSTEM

울산대학교 대학원

기계자동차 공학과

TRINH HOAI AN

UNIVERSITY OF ULSAN

DEVELOPMENT OF ENERGY MANAGEMENT STRATEGIES FOR FUEL CELL-BATTERY-SUPERCAPACITOR HYBRID POWER SYSTEM

by

TRINH HOAI AN

Supervisor: Professor KYOUNG KWAN AHN

A dissertation submitted in partial fulfillment of the requirements for the degree of

Doctor of Philosophy

to the

School of Mechanical and Automotive Engineering,

University of Ulsan, Korea

June 2023

연료전지-배터리-슈퍼커패시터 하이브리드 전력시스템 에너지 관리 전략 개발

DEVELOPMENT OF ENERGY MANAGEMENT STRATEGIES FOR FUEL CELL-BATTERY-SUPERCAPACITOR HYBRID POWER SYSTEM

지도교수   **안경관**

이논문을 공학박사 학위 논문으로 제출함

2023 년 06 월

울산대학교 대학원
기계자동차공학과

DEVELOPMENT OF ENERGY MANAGEMENT STRATEGIES FOR FUEL CELL – BATTERY – SUPERCAPACITOR HYBRID POWER SYSTEM

This certifies that the dissertation of

TRINH HOAI AN is approved by

Committee Chairman:	Prof. BYUNG-RYONG LEE	
Committee Member:	Prof. KYOUNG KWAN AHN	
Committee Member:	Prof. CHEOL KEUN HA	
Committee Member:	Assistant Prof. GI-SEO PARK	
Committee Member:	Prof. JI-SUNG JANG	
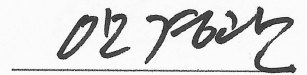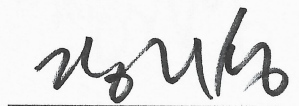
School of Mechanical and Automotive Engineering

University of Ulsan, Korea

June 2023

TRINH HOAI AN 의

공학박사 학위 논문을 인준함

심사위원	이병룡	
심사위원	안경관	
심사위원	하철근	
심사위원	박기서	
심사위원	장지성	

울 산 대 학 교 대 학 원

기계자동차공학과

2023 년 06월

I would like to dedicate this dissertation to my beloved parents, my wife, and my son:

Trần Ngọc Phước Hạnh
Trịnh Hoài Khang

Acknowledgments

Contents

List of Figures

List of Tables

Abbreviations

BAT	Battery
DC	Direct current
DSP	Digital signal processor
ECMS	Equivalent consumption minimization strategy
EMS	Energy management strategy
ES	Extremum seeking
ESS	Energy storage system
ESD	Energy storage device
FCEV	Fuel cell electric vehicle
FD	Frequency decoupling
FLC	Fuzzy logic control
FLR	Fuzzy logic rule
H2	Hydrogen
HPS	Hybrid power system
IEA	International Energy Agency
LPF	Low-pass filter
PEMFC	Proton exchange membrane fuel cell
PID	Proportional-integral-derivative
PWM	Pulse width modulation
SC	Supercapacitor
SOC	State of charge

Abstract

Using renewable energy is becoming a new tendency for vehicular applications to reduce fossil fuel consumption and minimize greenhouse gas emissions. Well-known as an eco-friendly energy source, the proton exchange membrane fuel cell (PEMFC) is extensively used in hybrid power systems to achieve the objective of zero-emission and air protection. However, this type of fuel cell offers slow dynamics and cannot adapt to abrupt load variations when used as a primary energy source. To overcome this shortcoming, battery (BAT) and/or supercapacitor (SC) are supplemented as auxiliary sources. Thus, the hybrid configuration of PEMFC-BAT-SC is developed to improve the performance of the PEMFC system, achieve high operating effectiveness for a hybrid power system (HPS), address the issue of fuel economy, decrease system size, and increase device longevity.

In the hybrid power system, it is important to manage the power distribution from energy sources for adapting load power demand under different working conditions. To effectively make use of this hybridization, various energy management strategies (EMSs) have been intensively studied. Essentially, they are classified into rule-based and optimization-based EMSs as two main strategies. Conventionally, rule-based control strategies have been widely used to handle the power distribution of energy sources in real-time. However, these conventional control methods can not be generalized to any optimal objective because the implementation of the rule-based approach significantly depends on the expert knowledge of designers; thus, being not able to fulfill the optimal solution. On the contrary, the optimization-based approach refers to several fundamental algorithms that can specify the optimal objective to enhance the system qualification. Therefore, this thesis presents a comprehensive control strategy to address these inaccurate power distributions, maintain the stability of DC bus voltage, and optimize the economic issues for HPS.

Firstly, a comprehensive EMS for an HPS powered by PEMFC, BAT, and SC is proposed with high- and low-level control to improve the accuracy of power distribution from energy sources to the load power demand. In detail, a deterministic-frequency decoupling method is developed in the high-level control to handle the load power adaptation under different working conditions. Then, the low-level control is designed to define correct gains for compensators of current and voltage control loops that maintain the stability of DC bus voltage. The obtained results reveal that the proposed EMS can guarantee power distribution and maintain the robustness of the DC bus under various load scenarios.

Next, a high-level control based on fuzzy logic rules and a frequency decoupling method is proposed to improve model uncertainty and complex decisions of deterministic rules. The

proposed method ensures a flexible power distribution not only for PEMFC but also for each energy source based on their dynamic characteristics and operating frequency ranges. Next, current and voltage control loops are designed to provide the appropriate gains for compensators that can maintain a stable voltage on the DC bus. As a result, the proposed EMS reduces voltage ripple on the DC bus, while increasing the working efficiency of the PEMFC system.

Finally, a novel real-time optimization-based EMS is proposed with a comprehensive structure of high- and low-level controls for a hybrid power system. The proposed methodology is constructed based on an extremum seeking (ES) method combined with a new equivalent SOC and a new adaptive co-state to maintain constraints in the cost function. It is found that the proposed strategy achieves optimal power distribution, minimizes fuel consumption, and improves the PEMFC stack efficiency.

All control strategies are validated using the Matlab/Simulink simulations and experiments based on the scaled-down HPS testbench. The obtained results show that the proposed control strategies are both feasible and effective. The final section of this thesis presents conclusions and proposes future studies.

Chapter 1

INTRODUCTION

1.1 Background and Motivation

Nowadays, environmental pollution becomes an urgent issue that undoubtedly influences the health of humans and other creatures living in the world. The development of renewable energy sources is quickly becoming an indispensable solution for inhibiting environmental pollution caused by types of machines or power generation systems that consume fossil fuels [1, 2]. In addition, research by the International Energy Agency (IEA) shows that the majority of CO2 emissions are caused by coal, oil, and natural gas which accounted for 89% of energy-related greenhouse gas emissions in 2022 [3]. Total energy-related greenhouse gas emissions reached 41.3 Gt CO2-eq in 2022 and the increasing trend continues steadily over the years as shown in Figure 1.1. As a result, green power sources like solar, wind, or fuel cell are regarded as economically feasible renewable sources for multiple applications and promising solutions for future development in times of energy crisis. According to IEA, from 1990 to 2018, renewable electricity generation rose rapidly with wind, solar photovoltaic (PV), and hydrogen resources. In which, the growth of hydrogen energy increases by 97.3% and is forecast to remain the world's largest source of renewable generation as shown in Figure 1.2.
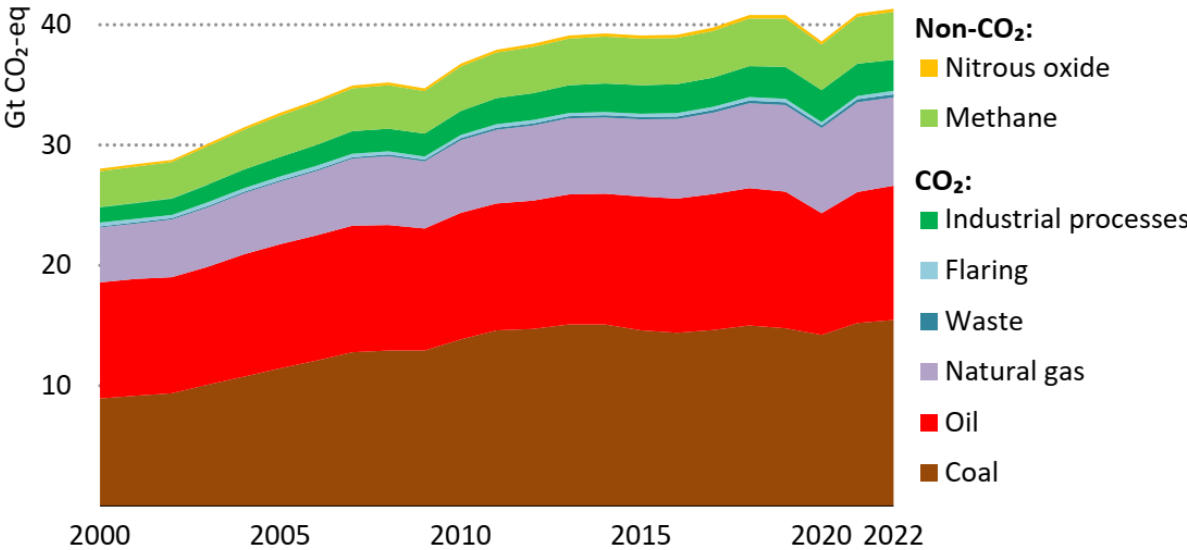
Figure 1.1 Global energy-related greenhouse CO_2 emission [3].
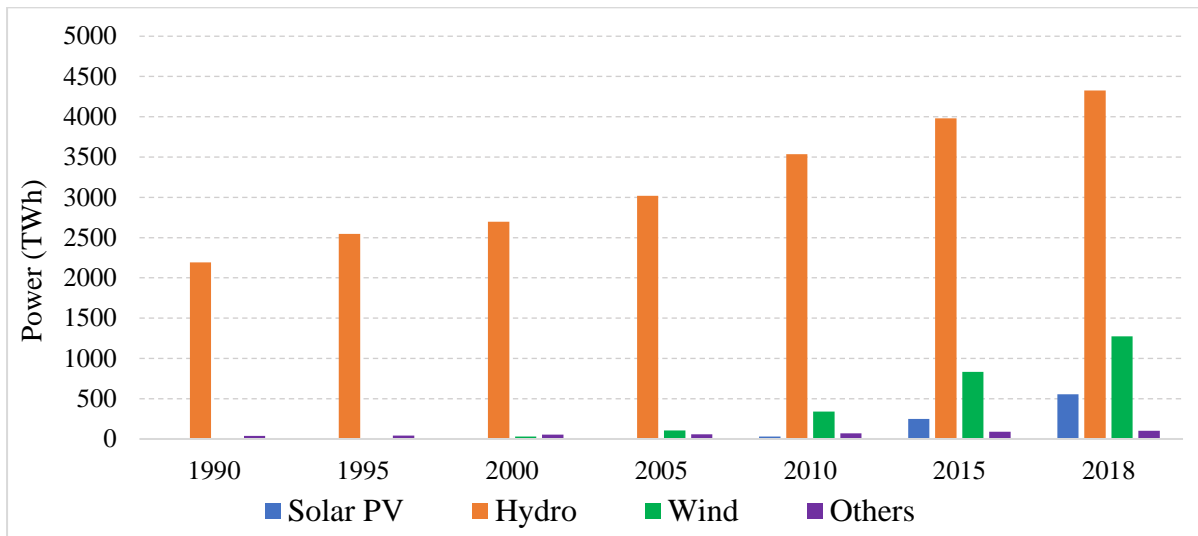
Figure 1.2 Renewable electricity generation by source, World 1990 - 2018 [4].

Recently, the PEMFC has been attracted as a prominent and potential candidate to alternatively replace the traditional energy storage systems (ESSs) such as BAT or SC [5]. Moreover, the PEMFC earns worthy properties of lower operating temperatures, higher power density, and higher energy conversion in comparison with other types of fuel cells [6]. However, variable nature characteristics such as slow response and inability to satisfy abrupt load demands and absorb regenerative energy are existing obstacles when employing standalone PEMFC. Hence, the PEMFC system is highly dependent on an ESS to provide power delivery to load continuity with a fluctuating power source. As a result, these drawbacks come up with high maintenance costs, short lifetime, and restrict widespread applications for standalone usage [7]. Therefore, it is necessary to develop an integration of the PEMFC with other interconnected electrical storage devices. In this configuration, the PEMFC serves as the primary power supply while the electrical storages function as secondary units to support the main source. Conventionally, either BATs or SCs, or both are employed as supplements due to their compatible characteristics for hybridization. The hybrid systems of PEMFC-BAT-SC have been used in a variety of research fields including DC microgrids [8-10], hybrid electric vehicles [11-13], construction machinery [14, 15], hybrid tramway powertrains [16-18], and so on. The aforementioned literature showed that this hybrid configuration could yield improved performance, decrease system size, address the issue of fuel economy, and increase device longevity. Furthermore, in order to achieve high operating effectiveness for a complicated hybrid power system (HPS), the EMS should be designed to properly manage power distribution from energy sources for the load power demand. The EMS design is considered not only to guarantee overall system efficiency, and optimize the power allocation in accordance with available sources but also to reduce

the stress of power supplies, extend the lifetime of the energy storage devices, and narrow the size of the BAT/SC or other storage devices. Therefore, this dissertation aims to address the fundamentals of energy management and power controls in the HPS and to develop advanced EMS that enables optimal system energy efficiency and guarantees the reliability of the system operations under various working conditions.

1.2 Literature Review of Energy Management for Fuel Cell Hybrid Power System

The energy management strategy has recently become an interesting topic for researchers and many studies have been conducted to control HPS. In [19], a distributed energy management system was constructed for the HPS based on a rule-based power distribution strategy. By using the charge and discharge limitations of power capability and residual capacity, the presented EMS might increase the lifespan and enhance the economics of the hybrid energy storage system. Similar to [20-22], rule-based EMSs were also developed for the fuel cell electric vehicle (FCEV) to determine the required power of electrical sources and obtain fuel economy by regulating the power distribution of BAT and SC through charge and discharge mechanisms. To save hydrogen consumption and extend the life of system components, Kaya et al. [23] proposed two control strategies based on the simplicity of their structure and characteristics, which may be readily applied to the many types of FCEVs. These strategies have only been verified in two separate road models, the "stop-go road model" and the "uphill-downhill road model", and more complicated road models should be done for further research. For the fuel cell hybrid excavator, Do et al. presented an EMS in [7], to properly manage the power distribution of energy sources based on load power demand and increase the power performance under various operating scenarios. To improve the efficiency of a hybrid tramway system, Qi Li et al. [24, 25] developed a state machine technique based on droop management to coordinate numerous power sources when load states change. In [26], a simple control system was designed for a switcher locomotive-powered PEMFC-BAT-SC hybrid system to manage the power flows and load power demand levels while maintaining the proper state of charge (SOC) on the ESSs. In [27, 28], Garcia et al. proposed an operational mode control and cascade control loop that could allocate the load power demand for each energy source, ensuring power performance and satisfying the hybrid tramway system's drive cycle under varying operating circumstances. In addition, depending on the different characteristics of power sources, the frequency decomposition techniques were applied to regulate the dynamic response, improve the power-sharing accuracy, and extend the lifetime of devices. Based on the Ragone diagram, LPFs were used in [29, 30] to decompose the frequency ranges allowed by each power source and improve the power performance of HPS while reducing stress and power fluctuation on the PEMFC and ESS.

To achieve the optimum distribution of energy between the sources, Snoussi et al. [31] proposed an adaptive filtering-based EMS for minimizing hydrogen consumption and maintaining the constraints of each device, such as the permissible limits of storage system capacities and battery current variation. According to the results of the aforementioned studies, these EMSs could ensure the HPS's overall efficiency and fulfill the load power demand. However, the rule-based method remains a drawback of not flexible operation because of switching modes that are usually based on the on/off mechanism to adapt to the particular working conditions. This may cause instability and delay to the system if the order of charge and discharge for ESSs is not appropriate such as power shortage for the hybrid system in the case of a sudden load change. Nevertheless, these EMSs focus solely on power distribution for energy sources as the high-level control, but the voltage control scheme of the DC bus is not taken into account comprehensively to design, so the output voltage could not be maintained at the desired value. This thing can cause instability and decrease the working performance of the hybrid system. Furthermore, the controllers of DC-DC converters in low-level control are designed by the trial and error method without investigating the dynamic characteristics of these converters. As a result, it is difficult to identify suitable compensator gains. This can result in a shortage of supplied power for the load, especially if the required power varies abruptly. Therefore, the development of an EMS considering a comprehensive design of the high- and low-level control is required to achieve the overall system qualification and improve the stable DC bus voltage delivered to the load under different working conditions.

Considered as a powerful toolbox, fuzzy logic has been applied to solve the complex issues of the logical process, especially in the power allocation for the hybrid system. Unlike the classical logic algorithm that requires clear knowledge, accurate equations, and exact numeric data of a system, fuzzy logic combines a different way of thinking, which allows complicated systems to be modeled using a higher degree of flexibility based on human knowledge and experience. In the fuel cell hybrid vehicular system, the fuzzy logic-based approach has been applied to develop the power management strategy in many works. For an electric vehicle application, Qi Li et al. [32] used fuzzy logic control (FLC) to build EMSs for hybrid FC-BAT and FC-BAT-SC configurations to improve the fuel economy of the car and extend the mileage of the journey. In [33], Ameur et al. exploited the master-slave model-based FLC strategy for an EMS design to improve the system efficiency and prolong the component lifespan for a renewable hybrid system. Ahmadi et al. constructed a fuzzy-based EMS with a genetic algorithm for a PEMFC integrated with BATs-SCs to improve hybrid vehicle behaviors [34]. The feasibility of the FLC methods for the PEMFC hybrid system-based transportation applications was investigated in [6]. In this work, the multi-level Haar-Wavelet transform was incorporated into the structure of the 2-FLC approach to separate the high- and low-

frequency features of the power demand. The results indicated that the proposed strategy achieved high efficiency without compromising the stack efficiency of the PEMFC and coordinated the power demand to each power source appropriately. To guarantee an ideal BAT power in an FC-BAT-SC tramway system, Piraino et al. [17] applied the FLC to find out the suitable factor of the BAT. In this strategy, the BAT power, BAT SOC, and SC SOC were input variables while the BAT corrective factor was the output variable. The simulation was implemented with a real driving cycle and the results proved that the suggested strategy not only made sufficient BAT power to meet sudden and unexpected demand variations but also avoided critical SOC levels of the BAT and SC. Based on the advantages of FLC, Fragiacomo et al. [35] combined this technique and an equivalent consumption minimization strategy (ECMS) to design an EMS for the hybrid locomotive. Based on detailed evaluations of stochastic uncertainties in tramway operation, a suboptimal real-time power-sharing technique was proposed to deal with operation uncertainties, enhance fuel efficiency, and guarantee system durability. In this work, the FLC was conducted to coordinate the power flows of energy sources that could adapt to the requirement of load power. In the aforementioned studies, the requirements of power distribution between the PEMFC and ESSs are effectively implemented by using fuzzy logic techniques. Although there are more challenges in the design procedure to achieve high efficiency, the fuzzy logic approach is still a good solution to construct an EMS for a hybrid PEMFC-BAT-SC system. This technique can handle most situations of operating behavior and mutual impacts of the charging and discharging process of ESSs to keep the high performance of all energy sources.

It is a fact that the rule-based approach is a real-time control strategy based on heuristic knowledge and engineering experience, which can be simply applied to practical hybrid systems, such as state machines [19, 22], frequency-decoupling [30], and so forth. Nonetheless, it cannot be generalized to any objective because the implementation of the rule-based approach significantly depends on the expert knowledge of designers; thus, being not able to fulfill the optimal solution. On the contrary, the optimization-based approach refers to several fundamental algorithms that can specify the optimal objective to enhance the system qualification. This approach can be categorized into global and local (real-time) optimizations. Specific global optimizations such as dynamics programming, genetic algorithm, particle swarm algorithm, ECMS, and so forth have been successfully deployed for several objectives such as electric vehicles [36, 37], construction machines [38, 39], and tramway systems [40, 41]. In the HPS, optimal control strategies have been developed to solve several requirements of system performance, economic indicators, optimal sizing, safety protection, and so forth. In detail, the system performance primarily consists of dynamic responses of power sources and stability on the

steady-state operating condition [42]. The economic issues are evaluated by optimizing the sizing of the hybrid system, minimizing fuel consumption, maintaining the SOC balance for energy storage devices, and prolonging the lifetime of power sources [43]. Because the capacity of energy sources installed on HPS is limited, the EMSs are developed to optimize the power allocation in accordance with available sources, reduce the stress of power supplies, improve the system efficiency, and extend the lifetime of the energy storage devices (ESDs) [44]. For safety demands, the conditions of over-charging or -discharging, current fluctuation, voltage ripple, and operating temperature of energy sources are mainly considered to prevent risks affecting system performance [45]. For objectives of electric vehicles, as the limitation of the rule-based approaches when they are not able to exhibit an optimal solution and require a lot of heuristic efforts, Yi et al. employed dynamic programming to achieve the optimal solution in the EMS design [46]. Recently, Li et al. proposed a novel online ECMS for the hybridization of three devices, but for electric vehicles [47]. Concerning the optimization-based approaches for hybrid tramway system, Zhang et al. [48] investigated the PEMFC-BAT-SC for an ECMS-based EMS execution. However, the author neglected the SC consumption in the cost function where the SC operated freely without any constraint and was just used for absorbing peak and transient load power. Despite being well-known as a powerful optimization method, the ECMS requires internal parameters such as charged and discharged resistors and coefficients corresponding to each circumstance to execute the equivalent consumption and objective function, which may meet difficulty in achieving good system identification. Besides, the ECMS is a typical method of global optimization, which offers offline implementation and requires pre-determined or well-known driving cycles. Compared to global optimizations, real-time optimizations take advantage of flexibly satisfying load variations owing to the online updating process. In [49], Wang et al. proposed a hierarchical power distribution based on the ES technique for the HET with a novel configuration of dual PEMFC battery. The ES is useful to seek out the optimal working point due to its advantages as the model-free method where it also does not require internal parameters of energy storage devices [50]. It can be seen that the EMS design is also considered not only to guarantee overall system efficiency, narrow the size of the BAT/SC or other storage devices but also to achieve high efficiency of energy recovery, and lower pollutant emissions. Therefore, to meet the demanding requirements of real-world applications, the optimal EMS challenges must be continuously improved to serve the ever-increasing expectations of customers as well as to enrich the variety of research directions and encourage the development of greater HPSs.

1.3 Research Objectives

Motivated by the aforementioned analysis, this dissertation aims to address the existing issues in the EMS for an HPS such as guaranteeing the power distribution and load power adaptation, DC bus voltage regulation, improving the PEMFC stack efficiency, and reducing hydrogen consumption. The research will focus on two interrelated areas of the energy management strategy consisting of power distribution strategies (high-level control) and the electrical system design (low-level control). In order to emphasize the interaction between both areas concurrently, it was decided to investigate them rather than just concentrate on one. The power distribution will have a significant impact on the optimal system design; however, the system design will also influence the power split decisions. As a result, they must be considered concurrently in order to arrive at a better final design.

The specific objectives of this dissertation are defined as follows:

➤ Investigate the system characteristics including overall HPS configuration, PEMFC model, ESD models, DC/DC converter models, and load profile model.

➤ Design a comprehensive control strategy and verification for the HPS that focuses on the hierarchical high- and low-level control to improve the overall system performance and stability of load power adaptation.

➤ Develop EMSs to enhance the proper power distribution of each energy source based on their dynamic characteristics and operating frequency ranges.

➤ Optimize the operating points of the PEMFC system based on the cost function that allows maintaining high-efficiency operating region, saving hydrogen consumption, and maintaining the SOC of BAT and SC vary in the suitable intervals.

➤ Regulate the DC bus voltage meets the desired value and minimize the voltage ripple under different working scenarios.

➤ Validate the effectiveness of the proposed strategies through comparative simulations and experiments.

1.4 Limitations

In this study, rule-based and optimization-based energy control strategies are developed for the HPS with several requirements for power distribution, DC bus voltage regulation, efficiency improvement, and hydrogen consumption saving. The verifications are implemented in both simulations and experiments based on the hybrid configuration of PEMFC, BAT, and SC. However, some limitations of the dissertation are still existing as follows:

➢ The proposed hybrid configuration is constructed based on the assumption that the PEMFC stack works following the polarization curves of U-I and P-I from the company's user manual. Indeed, the balance-of-plant (BOP) control issues for the PEMFC system such as hydrogen/oxygen supply control, humidity/thermal control, and so forth, are not available for investigation.

➢ Quantification of fuel cell and battery degradation models is not yet considered due to a lack of real-time logged data.

➢ The experimental implementation is only carried out with rule-based strategies (deterministic and fuzzy) due to the limitation of physical test-rig and controller configuration for optimization tasks.

1.5 Outline

The thesis is organized into 6 chapters as follows:

Chapter 1 introduces the motivations, research objectives, limitations, and outline of this dissertation.

Chapter 2 presents the overall configuration of the hybrid power system, characteristics of power sources, DC/DC converters, load profile model, and theoretical classifications and requirements of energy management strategy.

Chapter 3 describes a comprehensive EMS for an HPS powered by PEMFC/BAT/SC based on high- and low-level control. A deterministic-frequency decoupling strategy is developed in high-level control to distribute the load power demand optimally to the power sources under different working conditions. In addition, a low-level control is designed to determine correct gains for compensators of current and voltage control loops that maintain the stability of DC bus voltage based on the BAT.

Chapter 4 presents an improved EMS to solve model uncertainty and complex decisions of deterministic rules. A combination of fuzzy logic rules and frequency decoupling method is proposed to improve the proper power distribution of each energy source based on their dynamic characteristics and operating frequency ranges. Next, current and voltage control loops are designed to provide the appropriate gains for compensators that can maintain a stable voltage on the DC bus.

Chapter 5 describes a real-time optimization EMS based on an extremum-seeking method to achieve the reference optimal power of the PEMFC. This strategy can be more effectively regulated to operate in the high-efficiency region with smooth response whereas the SOCs of the battery and SCs are maintained to vary in the suitable intervals.

Chapter 6 summarizes the works in this dissertation and provides feasible recommendations for future research.

Chapter 2

HYBRID POWER SYSTEM MODEL

In this chapter, a hybrid power system model is described that will be used in the following chapters to design energy management strategies.

2.1 Hybrid Power System Description

Due to the slow dynamic response, using a standalone PEMFC cannot adapt to abrupt load power variations or store the energy regeneration from the load system. For this reason, a hybrid configuration is developed to guarantee the power supply for load demand and system performance. In this hybrid system, the SC and BAT, with high energy density and high power density, are utilized to supplement the lacking power in the initial stage, the transient period or peak power demands, or store the regenerative energy. Both BAT and SC are devices that can charge, discharge, and store energy in which the BAT, with high capacity and low energy leakage, is supposed as an ideal electrochemical storage system, whereas the SC is appropriate for high power in a short time. Therefore, a combination of PEMFC, BAT, and SC is expected to construct a fast dynamics system, enhance working performance, optimize fuel savings, and reduce the PEMFC size and power consumption. Based on the power response of energy sources, the PEMFC operates with the lowest frequency power source, while the SC performs with the highest frequency and BAT works at the frequency between PEMFC and SC [51]. The dynamic responses of the PEMFC, BAT, and SC are described in Figure 2.1.
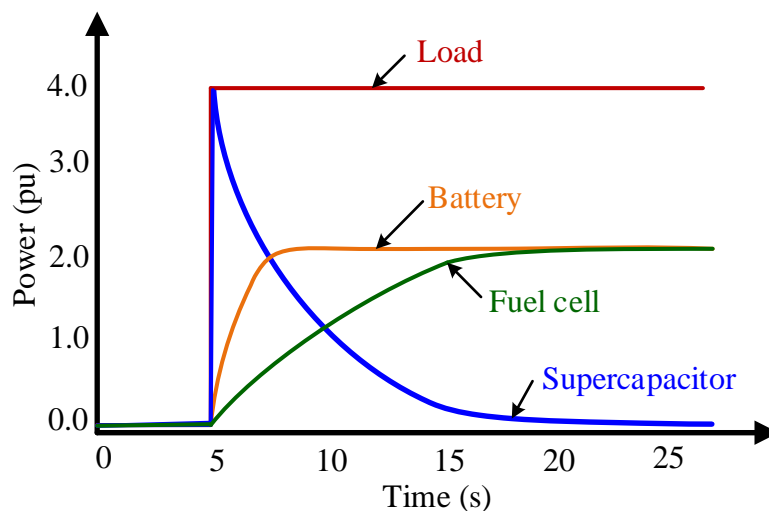
Figure 2.1 The response of PEMFC and energy sources [51].

The suggested configuration of the hybrid power system is described in Figure 2.2. This hybrid system consists of a PEMFC system as a primary energy source, lithium-ion BAT and SC bank as ESDs, DC/DC converters that compose of two bidirectional converters and one unidirectional boost converter, and electric propulsion system as the load power demand. In this system, the PEMFC system is connected to a unidirectional DC/DC converter to boost its output low voltage to the required voltage of the DC bus. Meanwhile, both BAT and SC are connected to bidirectional DC/DC converters to provide power during the acceleration, absorb the regenerative energy in the braking process, and compensate or consume the peak power of the traction load that the PEMFC cannot accommodate in a short time. These DC/DC converters are used to connect three power sources with the DC bus based on a parallel configuration to transfer the power flow to the electric propulsion system with the charge and discharge modes. In detail, a boost converter controls the fuel cell output voltage to adapt to the reference value. A bidirectional converter transfers the power flow in both directions to the ESDs for delivery and recovery cycles. It can be seen that this configuration provides a flexible mechanism for controlling the DC bus voltage, enhancing working performance, and achieving fuel economy for the PEMFC system.
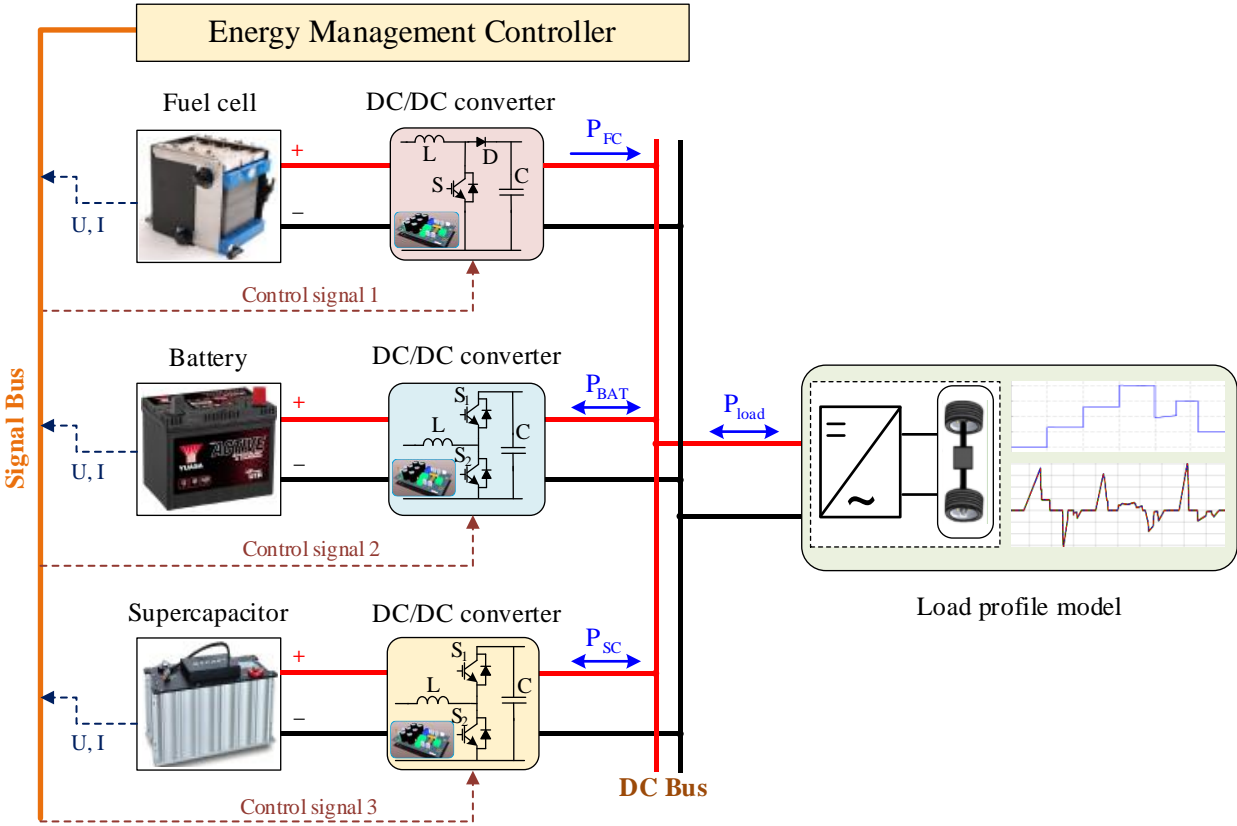
Figure 2.2 Configuration of the hybrid power system.

For simulation purposes, the dynamics of each subsystem component will be modeled first to understand the system behavior and for an effective EMS design. The detailed characteristics of power sources and DC/DC converters are described in the next sub-sections.

2.2 Power Sources and Converters Models

2.2.1 Fuel Cell System Model

In the hybrid power system, the PEMFC is used as the primary source that converts chemical energy from hydrogen to electric energy for load operation. To reproduce its characteristics, a detailed model in [52] is applied to construct the simulation model for the PEMFC that composes of a stack module as a core of the fuel cell system, auxiliary components of hydrogen and air delivery, water-cooling circulation, humidification, while neglecting the reactant flow inside the electrode. In this model, system parameters can be easily set up from the datasheet or by using the simple polarization curve of the testing process. The equivalent circuit of the PEMFC stack is described in Figure 2.3.
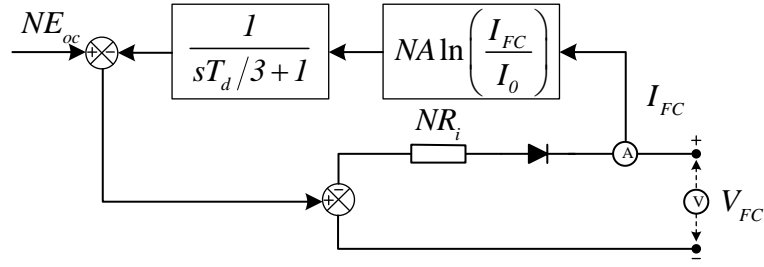
Figure 2.3 The detailed model of the PEMFC stack [52].

From the dynamic model of PEMFC in [52] and the simulation and experiment test results in [53], the cell output voltage can be expressed as follows:

$$V_{ce} = E_{oc} - V_{act} - V_r \tag{2.1}$$

where V_{ce} is the cell output voltage (V), E_{oc} is the open-circuit voltage (V), V_{act} is the activation voltage loss (V), and V_r denotes the resistive and diffusion voltage loss (V).

The open-circuit voltage can be presented by:

$$E_{oc} = K_c E_n \tag{2.2}$$

where K_c is the voltage constant at the nominal condition of operation (V), E_n is the Nernst voltage (V).

The Nest voltage is determined as follows:

$$E_n = \begin{cases} 1.229 + (T - 298)\dfrac{-44.43}{zF} + \dfrac{RT}{zF}\ln\left(P_{H_2}P_{O_2}^{\frac{1}{2}}\right) & ,T \leq 273^o\,K \\[4ex] 1.229 + (T - 298)\dfrac{-44.43}{zF} + \dfrac{RT}{zF}\ln\left(\dfrac{P_{H_2}P_{O_2}^{\frac{1}{2}}}{P_{H_2O}}\right) & ,T > 273^o\,K \end{cases} \qquad (2.3)$$

where T is the operation temperature (^{0}K), z denotes the number of moving electrons, R is the ideal gas constant (J/(mol ^{0}K)), F is the Faraday constant (A s/mol), P_{H_2} is the partial pressure of hydrogen inside the stack (atm), P_{O_2} is the partial pressure of oxygen inside the stack (atm), and P_{H_2O} is the partial pressure of water vapor (atm).

The partial pressure values are given by equations:

$$P_{H_2} = \left(1 - U_{f_{H_2}}\right)xP_{fuel} \qquad (2.4)$$

$$P_{O_2} = \left(1 - U_{f_{O_2}}\right)yP_{air} \qquad (2.5)$$

$$P_{H_2O} = \left(w + 2yU_{f_{O_2}}\right)yP_{air} \qquad (2.6)$$

where $U_{f_{H_2}}$ is the rate of hydrogen utilization, $U_{f_{O_2}}$ denotes the rate of oxygen utilization, x is the percentage of hydrogen in the fuel (%), y is the percentage of oxygen in the oxidant (%), w is the percentage of water vapor in the oxidant (%), P_{air} is absolute supply pressure of air (bar), and P_{fuel} is absolute supply pressure of fuel (bar). Herein, the terms of $U_{f_{H_2}}$ and $U_{f_{O_2}}$ are defined as follows:

$$U_{f_{H_2}} = \frac{60000RTI_{FC}}{zFP_{fuel}V_{fuel}x} \qquad (2.7)$$

$$U_{f_{O_2}} = \frac{60000RTI_{FC}}{2zFP_{air}V_{air}y} \qquad (2.8)$$

where V_{fuel} is the fuel flow rate (lpm) and V_{air} is the airflow rate (lpm).

The activation voltage loss due to reaction kinetics at low current densities can be calculated as follows:

$$V_{act} = A\ln\left(\frac{I_{FC}}{I_0}\right)\frac{1}{\frac{sT_d}{3} + 1} \qquad (2.9)$$

where A is the Tafel slope (V), I_0 is the exchange current (A), I_{FC} is the PEMFC output current (A), T_d is the cell settling time to a current step (s).

In equation (2.9), the Tafel slope and exchange current are described as follows:

$$I_0 = \frac{zFk\left(P_{H_2} + P_{O_2}\right)}{Rh}\exp\left(\frac{-\Delta G}{RT}\right) \tag{2.10}$$

$$A = \frac{RT}{z\alpha F} \tag{2.11}$$

where k is Boltzmann's constant (J/^{0}K), α is the charge transfer coefficient, h is Planck's constant (J s), and ΔG is the activation energy barrier (J/mol).

The resistive and diffusion voltage loss of PEMFC due to the internal resistance of the electrolyte membrane is expressed as the following equation:

$$V_r = R_i I_{FC} \tag{2.12}$$

where R_i is the combined cell and diffusion resistance (Ω).

The cell voltage is assumed to display a delay that is roughly equivalent to three times the time constant when the cell current change rapidly. Then, the total voltage is generated by combining the number of cells N as follows:

$$V_{FC} = NV_{ce} \tag{2.13}$$

where V_{FC} is the stack output voltage of the PEMFC (V), N is the total number of cells.

During the operation, the output power of PEMFC is not only supplied to the DC bus but also partly used to operate the auxiliary systems such as cooling and temperature management systems. Thus, the supplied power from the PEMFC stack is obtained by:

$$P_{FC} = \eta_{FC}V_{FC}I_{FC} \tag{2.14}$$

where P_{FC} is the supplied power of the PEMFC stack (W), η_{FC} represents the efficiency of the PEMFC power source (%).

Regarding the power fed for auxiliary subsystems (cooling fan, heating system, pumps, and so on), the PEMFC efficiency can be computed by:

$$\eta_{FC} = \frac{V_{ce}I_{FC}}{-\Delta H_{LHV}I_{FC} \times 2F}\left(1 - \frac{P_{aux}}{P_{FC}}\right) = \frac{V_{ce}}{1.254}\left(1 - \frac{P_{aux}}{P_{FC}}\right) \tag{2.15}$$

where F is the Faraday constant, ΔH_{LHV} denotes the lower reaction heating value of hydrogen (241.98 kJ/mol), and P_{aux} is the power required to supply for auxiliary subsystems of the PEMFC system, respectively, that satisfy:

$$P_{tot} = P_{aux} + P_{FC} \tag{2.16}$$

Based on the system modeling and system characteristics, the PEMFC hydrogen consumption can be obtained from the polarization of [54]:

$$m_{H_2} = \int_0^t \frac{P_{FC}(t)}{\eta_{FC}\rho_{H_2}} dt \qquad (2.17)$$

where m_{H_2} denotes the hydrogen consumption (g), P_{FC} is the power of PEMFC (W), ρ_{H_2} is the energy density of hydrogen chemical (MJ/kg).

Based on the technical specification, polarization curves of the specific fuel cell stack, which consists of power-current (P-I) and voltage-current (U-I), can be described in Figure 2.4.
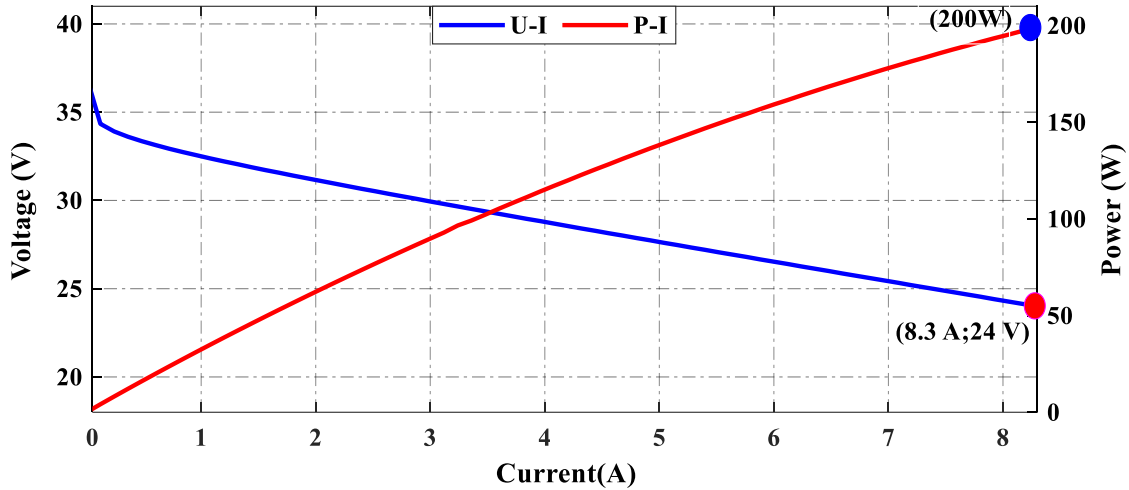
Figure 2.4 The PEMFC polarization curves of voltage-current (U-I) and power-current (P-I).

As the obtained efficiency of the PEMFC system from (2.16), the power-efficiency map [50, 54] can be plotted as shown in Figure 2.5.
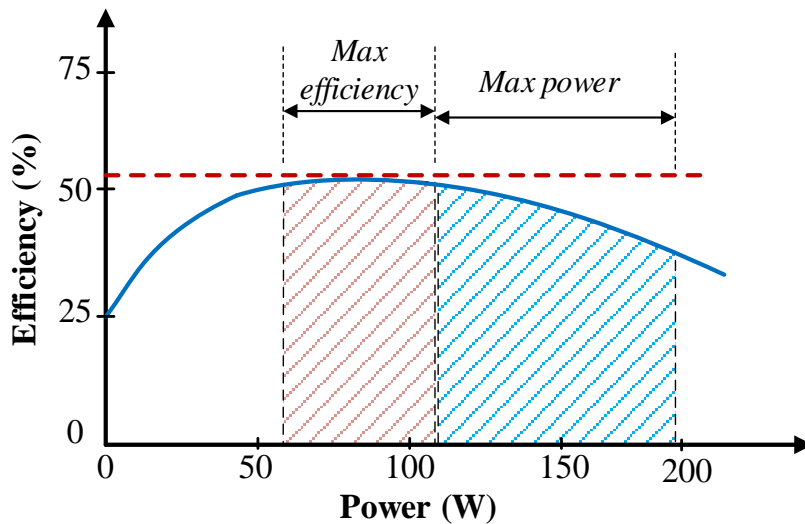
Figure 2.5 Efficiency map of the 200-W PEMFC.

2.2.2 Battery Model

The BAT is used as a secondary power source of the hybrid power system. Due to its high

15

energy density, fast dynamic response, and low self-discharge rate, the lithium-ion battery is a promising device that can be used to compensate for the excess power that PEMFC cannot supply. Besides, it also works as a storage device with a large capacity to store regenerative energy in the hybrid system. To explore its behaviors, an equivalent circuit is employed to construct the simulation model for the BAT as shown in Figure 2.6.
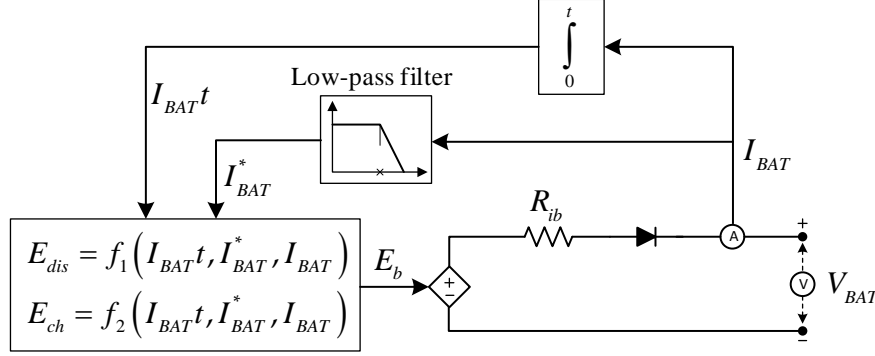
Figure 2.6 BAT equivalent model [55].

Depending on the discharge or charge mode, the nonlinear voltage is regulated to maintain the BAT's capacity in a reasonable performance. The voltage in the discharge mode is calculated as follows:

$$
\begin{aligned}
E_{dis} &= f_1\left(I_{BAT}t, I_{BAT}^*, I_{BAT}\right) \\
&= E_0 - K\frac{Q_b}{Q_b - I_{BAT}t}I_{BAT}^* - K\frac{Q_b}{Q_b - I_{BAT}t}I_{BAT}t + A_b\exp\left(-BI_{BAT}t\right)
\end{aligned}
\tag{2.18}
$$

where E_{dis} is the nonlinear voltage in discharge mode (V), E_0 is the BAT constant voltage (V), Q_b is the maximum BAT capacity (Ah), I_{BAT} is the BAT output current (A), I_{BAT}^* is the low-frequency current dynamics (A), K is the polarization constant (V/Ah), A_b is the exponential voltage (V), and B is the exponential capacity (Ah^{-1}).

For the charging mode, due to the fast-increasing voltage of the BAT, the polarization resistance $K\left(Q_b\big/\left(Q_b - I_{BAT}t\right)\right)$ is regulated to depict the performance at the end of the charging process. Thus, the voltage is given by:

$$
\begin{aligned}
E_{ch} &= f_2\left(I_{BAT}t, I_{BAT}^*, I_{BAT}\right) \\
&= E_0 - K\frac{Q_b}{I_{BAT}t - 0.1Q_b}I_{BAT}^* - K\frac{Q_b}{Q_b - I_{BAT}t}I_{BAT}t + A_b\exp\left(-BI_{BAT}t\right)
\end{aligned}
\tag{2.19}
$$

where E_{ch} is the nonlinear voltage in charge mode (V).

The output voltage of the BAT model is represented as follows:

$$
V_{BAT} = E_b - R_{ib}I_{BAT}
\tag{2.20}
$$

where R_{ib} is the BAT internal resistance (Ω), E_b is the nonlinear voltage (V) that equals E_{dis} in discharge mode and equals E_{ch} in charge mode as defined in equations (2.18) and (2.19).

The SOC of the BAT can be obtained from the relationship between the current charge and the maximum capacity by:

$$SOC_{BAT}(t) = SOC_{BAT}(t_0) - \frac{1}{Q_b} \int_{t_0}^{t} I_{BAT}(\tau) d\tau \tag{2.21}$$

where SOC_{BAT} is the SOC level of the BAT (%), t is the instant time, and t_0 is the initial time.

From the input parameters of the BAT model, the discharge curves of a specific battery is portrayed in Figure 2.7.

(a)

(b)
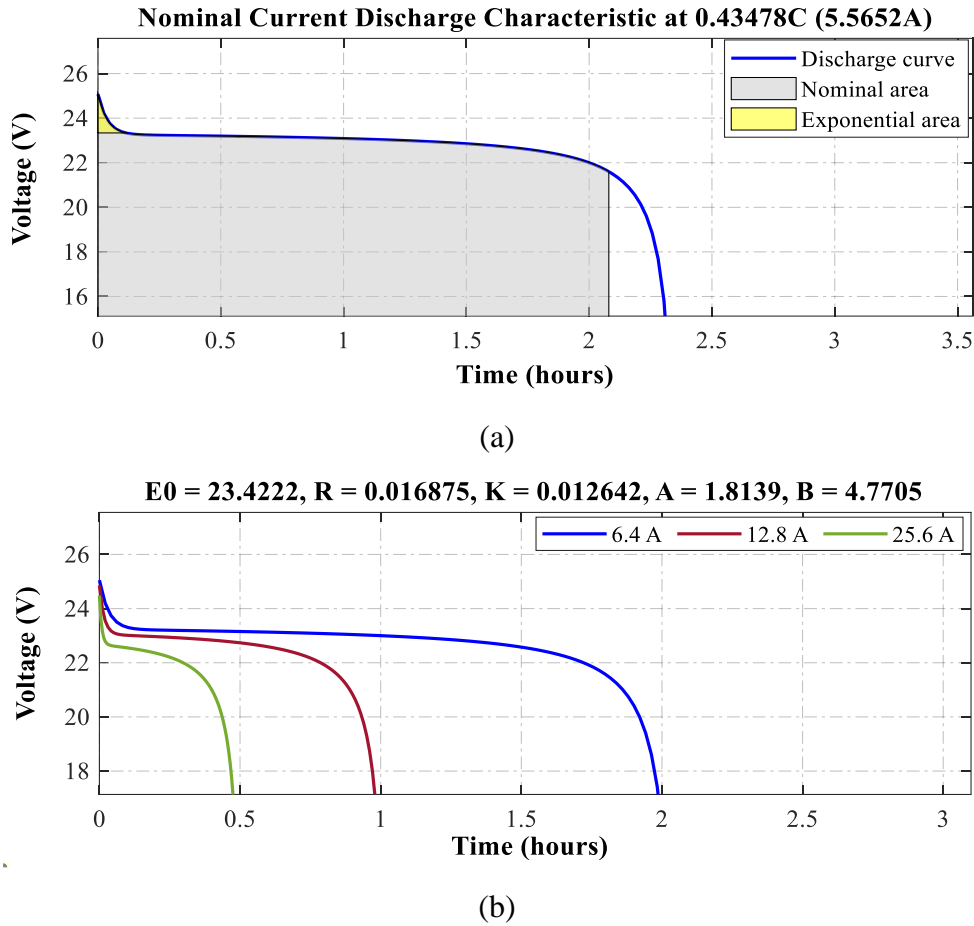
Figure 2.7 Polarization curves of the BAT. (a) Nominal current discharge characteristics. (b) Discharge current.

2.2.3 Supercapacitor Model

The SC is an electric double-layer capacitor that can store and release fast energy due to its high capacitance. In the hybrid system, this component can be used to store the regenerative energy or release more energy to compensate for the PEMFC dynamics during the transient or the peak

power when abrupt load variation. In this study, an SC model is constructed by using the Stern model [56, 57]. The equivalent circuit of the SC model is illustrated in Figure 2.8.
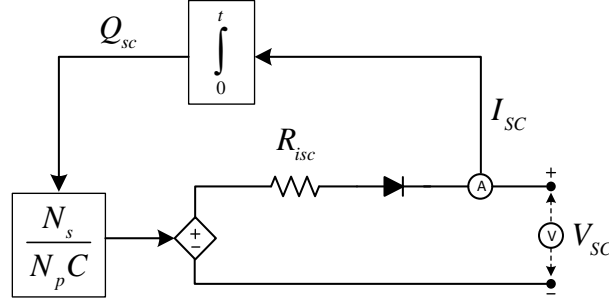
Figure 2.8 SC equivalent model [53].

The output voltage (V) of an elementary SC can be estimated as follows:

$$V_{SC} = \frac{N_s Q_{sc}}{N_p C} - R_{isc} I_{SC} \tag{2.22}$$

where I_{SC} is the SC output current (A), R_{isc} is the SC module resistance (Ω), Q_{sc} is the total electric charge (C), C is the capacitance of an electric double-layer capacitors cell (F), N_s denotes the cells in series, N_p presents cells in parallel.

The capacitance of a cell can be expressed as follows:

$$C = \left(\frac{1}{C_H} + \frac{1}{C_{GC}} \right)^{-1} \tag{2.23}$$

with:

$$C_H = \frac{N_e \varepsilon \varepsilon_0 A_i}{d} \tag{2.24}$$

$$C_{GC} = \frac{F Q_{sc}}{2 N_e RT} \sin \left(\frac{Q_{sc}}{N_e^2 A_i \sqrt{8 RT \varepsilon \varepsilon_0 c}} \right) \tag{2.25}$$

where C_H is the Helmholtz capacitance (F), C_{GC} is the Gouy – Chapman capacitance (F), N_e is the number of layers of electrodes, ε and ε_0 are the permittivity of material and free space (F/m), A_i is the interfacial area between electrodes and electrolyte (m^2), d is the molecular radius (m), F is the Faraday constant (A s/mol), R is the ideal gas constant (J/(mol ^{0}K)), T is the operating temperature (^{0}K), c is the molar concentration (mol/m^{-3}).

Next, the total electric charge is formulated by:

$$Q_{sc} = \int_{t_0}^{t} I_{SC}(\tau) d\tau \tag{2.26}$$

18

The SOC of the SC is estimated as the relationship between the current and the maximum capacity. This SOC value is computed by using the following equation:

$$SOC_{SC}(t) = SOC_{SC}(t_0) - \frac{1}{Q_{sc}} \int_{t_0}^{t} I_{SC}(\tau) d\tau \qquad (2.27)$$

where SOC_{SC} is the SOC level of the SC (%), t is the instant time, and t_0 is the initial time.

2.2.4 DC/DC Converters

DC/DC converters are designed to control the desired current of power sources as well as DC bus voltage. These converters are utilized to connect the PEMFC, BAT, and SC with a DC bus that supplies voltage and current to the load. Depending on the role and function of each energy source, converters will operate to boost or buck the voltage that delivers to the DC bus through discharge or charge mechanisms. In detail, the unidirectional converter is used to convert the lower voltage of the PEMFC to the higher voltage on the DC bus in the boost mode, whereas two bidirectional converters are used to transform the voltage in two directions between BAT/ SC and the DC bus, with the boost mode for discharging and the buck mode for charging.

Generally, there are two types of DC/DC converter models, usually used for simulation activities, which are the average-value model and the switching model. In the first model, the controlled voltage/current sources are used to replace the switching component. The advantage of the average-value model is the neglect of switching harmonics and less time-consuming. However, it cannot observe all the switching actions and converter dynamics. The switching model, on the contrary, regards switching harmonics and losses of switching components. This model is mainly utilized for experimental boards designed with a PWM control strategy. Due to the low sampling time requirement, all the switching actions and the converter dynamics can be investigated. In this study, the switching model of DC/DC converters is used with structures as shown in Figure 2.9.

Both types of converters consist of high-frequency inductor L, two filtering capacitors C_1 and C_2, resistor R, power source V_{in}, one switch S with a diode D for the unidirectional converter, and two switches S_1 and S_2 for the bidirectional converter. For the bidirectional converter, it is noteworthy that when switch S_1 is activated, switch S_2 serves as a diode component and the converter operates with boost mode; thus, increasing the output voltage to meet the load demand. In contrast, if switch S_2 is activated, switch S_1 works as a diode component, the converter acts in buck mode that steps down the voltage in the DC bus and charges for the BAT or SC. These converters are employed to regulate the DC bus voltage and the output net power of each device.

(a)

(b)
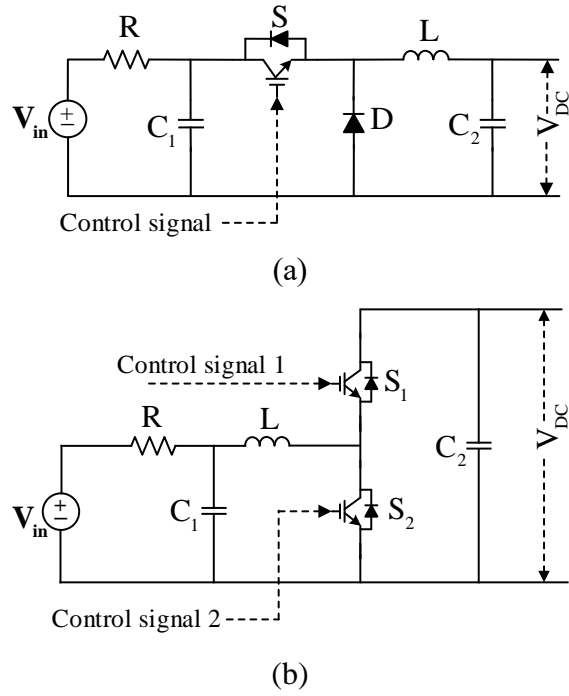
Figure 2.9 The DC/DC converter models. (a) Unidirectional converter with boost mode. (b) Bidirectional converter with buck and boost modes.

When designing a DC/DC converter, the necessary parameters of input voltage range, nominal output voltage, and maximum output current should be defined to calculate the maximum switching current, the range of recommended inductor values, and the capacitance of output capacitors. This calculation is important to select suitable components that match the requirements of the hybrid power system. Besides, a duty cycle plays an important role to control the converter according to the reference current in buck mode or boost mode. This duty cycle can be calculated by:

$$D_{buck} = \frac{V_{out}}{V_{in\_max}\eta_{buck}} \tag{2.28}$$

$$D_{boost} = 1 - \frac{V_{in\_min}\eta_{boost}}{V_{out}} \tag{2.29}$$

where D_{boost} is the duty cycle of boost mode (%), D_{buck} is the duty cycle of buck mode (%), V_{in_min}, V_{in_max}, and V_{out} are the minimum, maximum input voltage and output voltage (V) of the converter, respectively. η_{buck} and η_{boost} are the efficiencies of the converter which are estimated to equal 90% for buck mode and 80 – 90% for boost mode, respectively.

2.2.5 Load Profile Model

In this study, two load profile models are applied to verify and evaluate the effectiveness of energy management strategies that are proposed in the next chapters. Firstly, a step load power profile with several levels [58, 59] is used to describe the different working conditions, particularly

the abrupt load variations. This load power demand is partitioned into three levels: high, medium, and low in which PEMFC will provide respective power levels depending on each load power level. Secondly, a specific driving cycle [18] is used under operating circumstances such as acceleration, deceleration, and regenerative energy in practical applications. Both load profiles are shown in Figure 2.10.

(a)

(b)
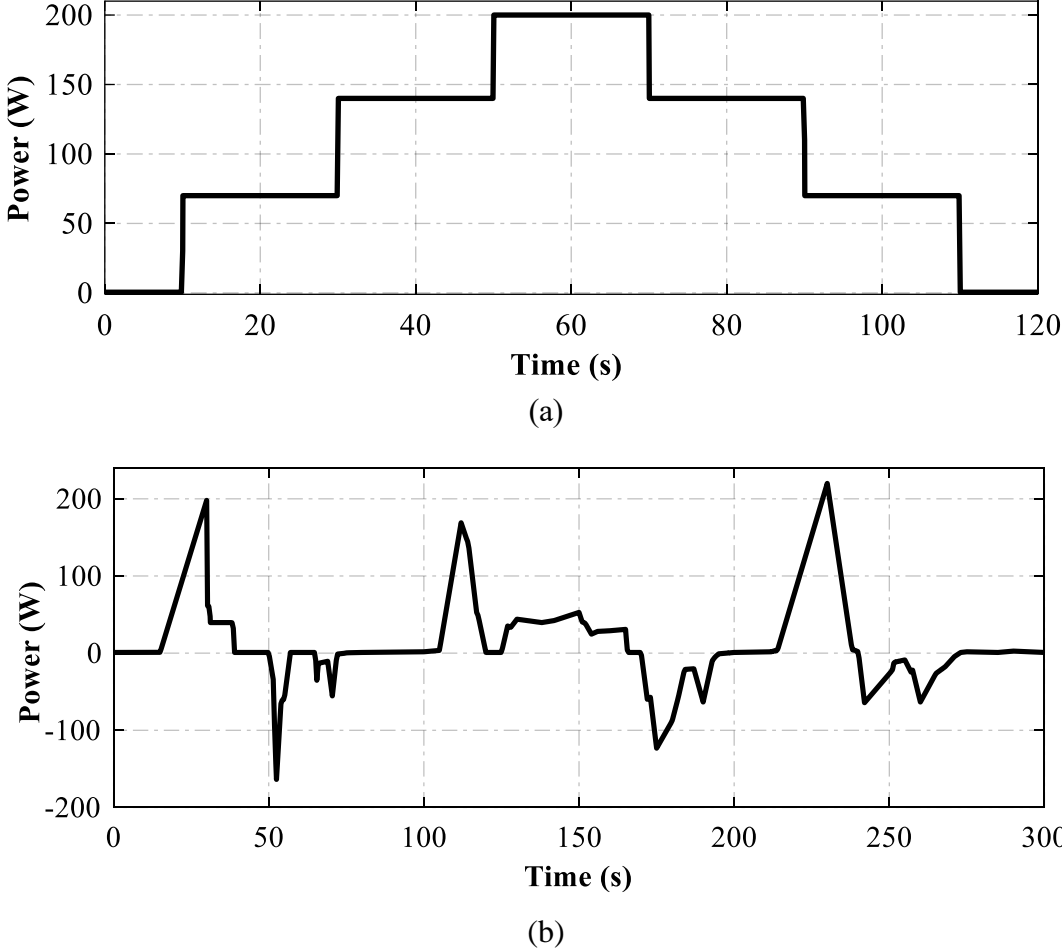
Figure 2.10 Load profile models. (a) Step load power profile. (b) Specific driving cycle.

2.3 Energy Management Strategy

Fuel cells are undoubtedly one of the most powerful and emission-free power sources. Yet, fuel cells alone are inadequate when it comes to a large number of real-world applications. The main reason lies in the fact that the slow dynamic response characteristic of fuel cells prevents them from meeting the fast-changing dynamic of power requirement. It is then necessary to integrate fuel cells with batteries and, or supercapacitors to power a system. However, generally, batteries exhibit higher energy density yet lower power density in comparison with supercapacitors, and both are faster in response compared to fuel cells. Their differences in dynamic characteristics

pose a direct threat to the coordination between them, in turn, the system's performance and safety. Therefore, the implementation of an appropriate energy management strategy (EMS) is crucial to guarantee smooth operation without sacrificing the performance of a system.

EMS for fuel cell hybrid power systems is a vast area of research and can be divided into three major techniques, namely rule-based, optimization-based, and learning-based methods. Each method exhibits specific advantages and disadvantages and is briefly discussed as follows. Also, Table 2.1 and Figure 2.11 are added for easier comparison.

Table 2.1 Advantages and disadvantages of different EMSs

Method		Advantages	Disadvantages
Rule-based	Fuzzy	- Fusion of numerical data and linguistic information - High robustness - Easy to realize	- Long run time - Limited input parameter - Requirement of expert knowledge to determine fuzzy rules
	Deterministic	- Simple and easy control - Low initial cost - Improving hydrogen fuel economy - Minimization energy transmission loss	- Insufficient accuracy - Demand of rule tables with human reasoning under optimal conditions
Optimization-based	Offline	- Able to achieve global optimization	- Requirement of prior knowledge of working cycles
	Online	- Localize global optimization problems - Suitable for real-time implementation	- Solution is often sub-optimal - Need for instantaneous cost function calculation
Learning-based	Learning	- Data-driven - No requirement for absolute models	- Accurate data mining is difficult and time-consuming
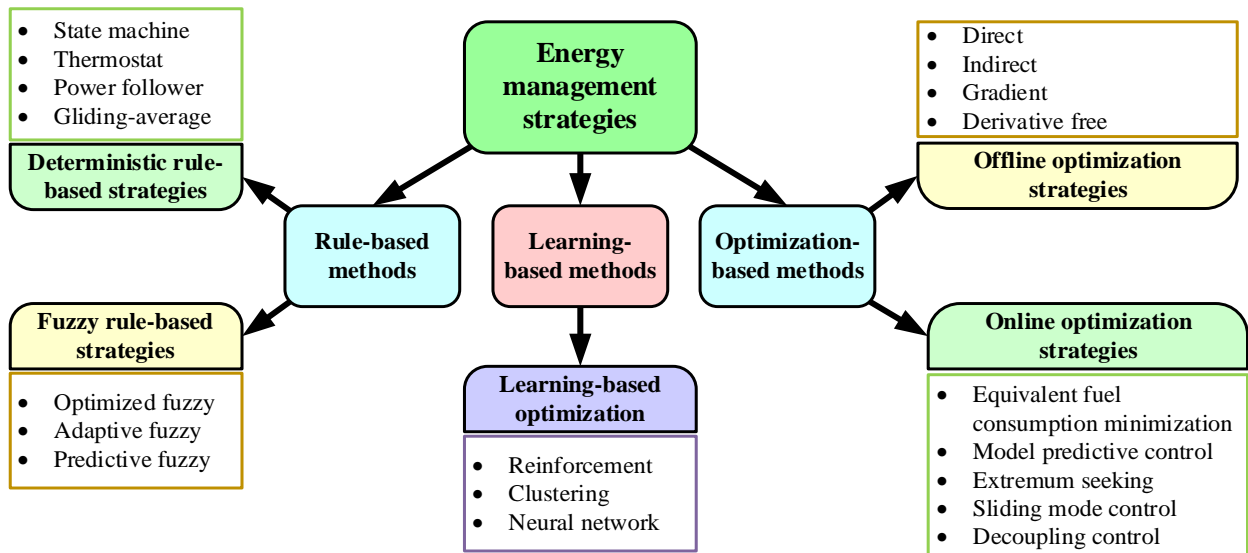
Figure 2.11 Classification of energy management systems.

The rule-based approach is the most popular method to achieve real-time energy management for fuel cell hybrid storage system. Sets of rules are stated heuristically based on mathematical formulation and expert experience. Hence, rule-based approaches are famous for their simplicity, ease of real-time implementation, and robustness against changes in load patterns. However, as they are built on the foundation of expert knowledge, the solution obtained cannot be certainly optimal. Two major types of rule-based methods are fuzzy logic control and deterministic control. The ability to fuse numerical data with linguistic information simultaneously makes fuzzy logic control a unique energy management strategy. Since the main advantages of fuzzy logic control are its robustness to measurement noise and component variability, fuzzy logic control is commonly applied in practice. Nonetheless, some drawbacks of fuzzy logic control can be named as long run time, limited input parameters, or requirement of expert knowledge to determine the fuzzy rules. Three types of fuzzy rule-based strategies are optimized, adaptive and predictive. Whereas, deterministic rules are often achieved through the previously calculated search tables. Their advantage is the simple and straightforward way of designing rules. However, it also exhibits some serious disadvantages such as insufficient accuracy or the demand for rule tables with human reasoning under optimal conditions. Some deterministic rule-based control strategies are state machine control, thermostat, power follower, and gliding-average.

Optimization-based approaches, on the other hand, are developed to achieve better performance. The primary objective of these approaches is to optimize certain prescribed criteria subject to several operational constraints. Therefore, multiple objectives can be achieved simultaneously. Nonetheless, the fact of being sophisticated poses a problem in that the computational load can be heavy and thus hard for real-time implementation. Optimization-based

23

approaches can be categorized as offline and online optimization methods. For offline optimization methods, prior knowledge of working cycles is usually required. Four groups of this type and their representatives are direct optimization methods with dynamic programming, indirect optimization methods with Pontryagin's minimum principle, gradient optimization methods with linear and convex programming, and finally, derivative-free optimization methods with simulated annealing, stochastic control, genetic algorithm and so on. The biggest advantage of this category is the ability to achieve global optimization since the knowledge of working cycles is known in advance. However, the requirement for prior information is also the main reason why these methods are not suitable for real-time applications. On the contrary, online optimization methods, as their name suggests, are designed to be applicable to real-time analyses. Some typical algorithms of this type are equivalent consumption minimization, model predictive control, extremum seeking, sliding mode control, and decoupling strategy. The equivalent consumption minimization approach converts the electrical energy consumption into equivalent hydrogen consumption and minimizes the summation of them. Model predictive control takes advantage of previous and current values and uses a model to predict future output. Extremum-seeking method obtains maximum or minimum values for a nonlinear optimization problem. Sliding mode control is also considered for its simplicity and robustness. While in decoupling control, researchers employ this method to manage the regulation of common dc-bus voltage in FC-battery hybridization, for example. Although each algorithm possesses distinctive characteristics, they are all developed to optimize some cost functions subject to several constraints and physical limitations. As a result, a global optimization problem can be transformed into a local one, but the result is often suboptimal. Also, their computational load and performance should be carefully evaluated.

Learning-based methods exploit data mining arrangements to generate optimum controller performance. While absolute model knowledge is not required to perform system evaluation, creating an accurate database, which has a direct impact on control performance and size, is difficult and time-consuming. Different learning-based methods are implemented to regulate the power flow such as reinforcement learning, clustering learning, and neural network learning.

In general, a proper EMS is required not only to regulate power split among sources but also to minimize hydrogen consumption and to sustain the lifetime of power sources. Fuel consumption estimation to be minimized usually appears inside the cost function, whereas the lifetime criterion can be assessed with constraints on the current and/or state-of-charge of batteries and supercapacitors. An enormous amount of effort has been made by researchers to satisfy these requirements. Consequently, the unceasing study in this field of research enriches the variety of research directions and encourages the development of greater power systems. Regarding the

literature, it is clear that to meet the demanding requirement of real-world applications, a well-designed EMS should possess several essential characteristics. Specifically, they should be globally optimal, real-time, self-adaptive, easy to implement, and of light computational load.

2.4 Conclusion

In this chapter, the configuration of power sources, DC/DC converters, and load profile models is developed to capture the key dynamics of a hybrid power system for the following analysis and energy management algorithm design. Dynamic models of PEMFC, BAT, SC, and DC/DC converter models are described with detailed characteristic functions. The load profile models also are presented as the load power demand for the hybrid power system. The fuel cell serves as the primary power source, with the battery pack and supercapacitors serving to absorb transient loads and protect the fuel cell. Finally, several techniques and requirements of EMS are illustrated as the theoretical background for the next chapters.

Chapter 3

COMPREHENSIVE EMS BASED ON DETERMINISTIC-FREQUENCY DECOUPLING METHOD AND COMPENSATOR DESIGN

In this chapter, a comprehensive energy management strategy with high- and low-level control is proposed to improve the accuracy of power distribution from energy sources to the load demand for a hybrid power system powered by PEMFC, BAT, and SC. Firstly, in the high-level control, a deterministic rule-based strategy is developed to distribute the load power demand optimally to the power sources under different working conditions. Then, according to the different characteristics of energy sources, a frequency decoupling (FD) method is designed to determine three frequency ranges response of required currents based on the different characteristics of PEMFC, BAT, and SC. Next to the low-level control, the dynamics response of converters is analyzed by using the Bode diagram to design correct gains for compensators of current and voltage control loops that maintain the stability of DC bus voltage based on the BAT. Finally, to evaluate the effectiveness of the proposed strategy, the simulation model is implemented in a MATLAB/Simulink environment and an experiment is conducted on the real hybrid power system. The obtained results reveal that the proposed energy management strategy can precisely coordinate energy flows between the three power sources and guarantee the robustness of the DC bus under various load scenarios.

3.1 Introduction

The integration of BATs and SCs with the PEMFC can exhibit better performance, reduce the system size, solve problems of fuel economy, and prolong devices' lifespan than the traditional configuration of one or two power sources. However, problems along with the advantages of the HPS include the design of an EMS for efficient power-sharing as high-level control and maintaining the DC bus voltage at a constant and output performance in low-level control.

The first concern, in the field of designing EMS strategies, has recently become an interesting topic for researchers. Truong et al. [60] employed the fuzzy-based EMS, developed based on rule-based methodology from the previous work [7], to satisfy the power demand, reduce hydrogen consumption and maintain storage devices' SOC for excavators. With the same objective,

Dao et al. [61] developed an EMS with the integration of a backtracking search algorithm and sequential quadratic programming to adjust the fuzzy membership functions (MFs); thus, reducing the fuel consumption and enhancing supplements qualification. Ahmadi et al. constructed a genetic algorithm for integrated PEMFC-BATs-SCs to improve hybrid vehicle behaviors [34]. In [33], Ameur et al. exploited the master-slave model-based fuzzy logic strategy (FLS) to design an EMS for efficient energy management and component lifespan prolonging. Marzougui et al. [62] deployed the flatness control and rule-based methodology towards hybridization of the PEMFC, ultra-capacitor, and BAT for an electric vehicle. Come up with the idea of the HPS's power management, Han et al. developed a strategy for multi-source management of PEMFCs-BATs-SCs on hybrid tramways [63]. The author employed a pair of set PEMFC-BAT-SC systems to generate multiple motor units with self-convergence droop control for power distribution among all devices. Such reports revealed a variety of feasible configurations with certified effectiveness of using the HPS for industrial automation systems.

Following the historical literature of the EMS designs, the main task is to distribute the power flow between the PEMFC and other energy sources by executing the current regulation while maintaining a constant DC bus voltage through a converter. Despite achieving good performance under arbitrary working conditions, most presented works did focus on designing EMSs as high-level concerns without dedicatedly considering the problems of DC/DC converter behaviors and DC bus voltage stabilization due to the variation of the load power and its influence on the whole system. Besides, regarding the physical characteristics of the switching regulator for PWM rectifiers, voltage ripple also occurs [64, 65]; thus, reducing the system efficiency and voltage instability subjected to the load variations. Therefore, it is necessary to investigate the comprehensive control strategy with high-level control and low-level control that improves the overall system qualification's stability and performance.

3.2 Proposed Deterministic-Frequency Decoupling Method and Compensator Design

In order to overcome the drawbacks of the traditional deterministic strategy for power distribution in the fuel cell hybrid system, a deterministic-frequency decoupling control strategy for high-level control combined with the compensator design for low-level control is developed to achieve the required powers, as well as to determine the reference currents of three energy sources.

The overall proposed control strategy is described in Figure 3.1. In this figure, the deterministic rule-based power regulator block is applied to define the required power of the PEMFC based on the magnitude of the load profile and the SOC of BAT and SC. Then, the frequency decoupling method is applied to generate the reference currents for the PEMFC system

and BAT based on the lowpass filter 1 (LPF-1) and lowpass filter 2 (LPF-2). Besides, no matter how the load changes, the compensator design of DC-DC converters is realized to improve the system performance and maintain the stability of DC bus voltage. The adaptation of voltage and current control loops in low-level control is considered to implement operation modes of DC/DC converters.
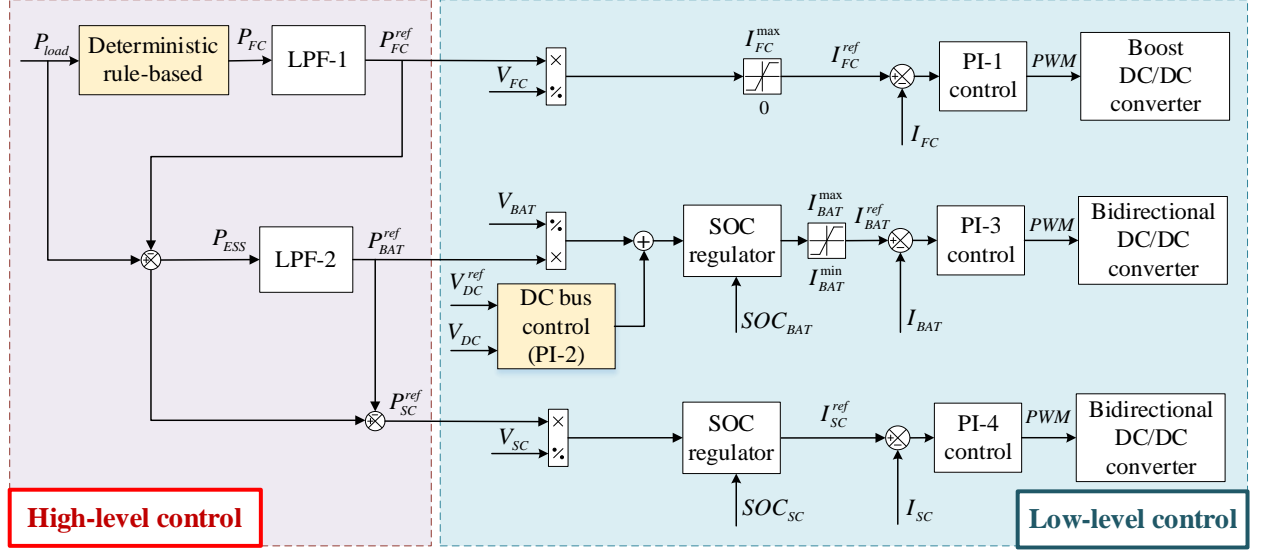
Figure 3.1 The proposed energy management strategy for the hybrid power source.

The load power demand and total power of energy sources should be defined to ensure the balanced power-sharing of the system at all times as in equation (3.1).

$$P_{load} = P_{FC} + P_{ESS} \tag{3.1}$$

where P_{load} is the load power demand (W), P_{ESS} is the power of the energy storage system including BAT and SC (W).

3.3 High-level Control Design

3.3.1 Frequency Decoupling Method

Based on the dynamic characteristics of energy sources, the Rangone diagram [30] is usually used to define the specific power and specific energy of each device. This diagram shows the performance of energy and power density of one specific source as presented in Figure 3.2.
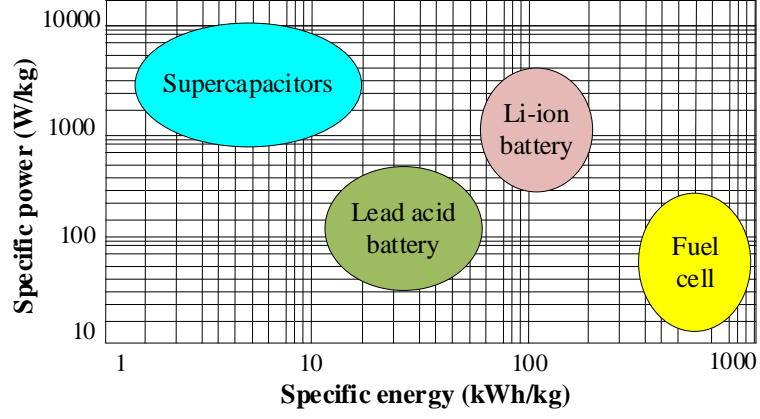
Figure 3.2 Rangone diagram of power sources [30].

According to these two densities, a specific frequency as the ratio between power density and energy density is designed to define the frequency ranges allowed by each power source as follows:

$$f_c = \frac{\rho_{power}}{\rho_{energy}} \tag{3.2}$$

where f_c is the cut-off frequency of each source (Hz), ρ_{power} is the power density of each source (W/kg), ρ_{energy} is the energy density of each source (J/kg).

From the Rangone diagram, the fuel cell has the lowest-frequency range, the BAT can adapt to the faster frequency range than the fuel cell, and the SC can deal with the highest-frequency range. Therefore, the frequency decoupling (FD) method is used to decompose the load power demand into three frequency bands. This method has the advantages of short-time calculation and a simple design for experimental applications. To implement the FD algorithm, the low-pass filter (LPF) is chosen as a transfer function as follows:

$$G(s) = \frac{2\pi f_c}{2\pi f_c + s} \tag{3.3}$$

In this proposed strategy, two LPFs are designed with two different cut-off frequencies (f_{c1}, f_{c2}). The LPF-1 is used to generate the lower frequency power of the PEMFC (P_{FC}^{ref}) which is fed to the low-level control to derive the desired fuel cell current. The LPF-2 is applied to achieve the faster frequency of BAT power (P_{BAT}^{ref}) and then is used to define the reference current of the BAT. Because the PEMFC is a primary source in the HPS, the fuel cell power distribution is regulated to match the load power demand as well as ensure the working point of PEMFC in the high-efficiency range following the U-I polarization curves.

3.3.2 Deterministic Rule-Based Method

The working principle of the deterministic rule-based power regulator is portrayed in Figure

3.3. In this flow chart, the required power of the PEMFC is defined depending on the levels of power load. Firstly, the load's voltage and current are measured to calculate the power demand from the system. In the case of a low level, where the load power is lower than the nominal PEMFC power $(P_{load} < P_{FC}^{nom})$, the PEMFC is a primary source that sufficiently provides power to satisfy the load demand $(P_{FC} = P_{load})$, while BAT and SC are only used to compensate for the PEMFC dynamics in the transient state when an abrupt change of load power occurs. Besides, extra power generated from PEMFC can also be used to charge the BAT or SC if needed. The medium level is determined when the load power demand exceeds the nominal value but is still less than the maximum power of the PEMFC $P_{FC}^{nom} \le P_{load} \le P_{FC}^{max}$. In this case, the PEMFC output power is regulated at the nominal value $(P_{FC} = P_{FC}^{nom})$, and the BAT and SC are enabled to complement the residual induced from insufficient power of the PEMFC via the converters as discharging and charging processes. At the high level, if the load power demand is greater than the maximum power of the fuel cell $(P_{load} \ge P_{FC}^{max})$, the PEMFC releases the maximum value $(P_{FC} = P_{FC}^{max})$, and the remaining load power will be provided by the BAT and SC, depending on the status of these devices and the particular working conditions.
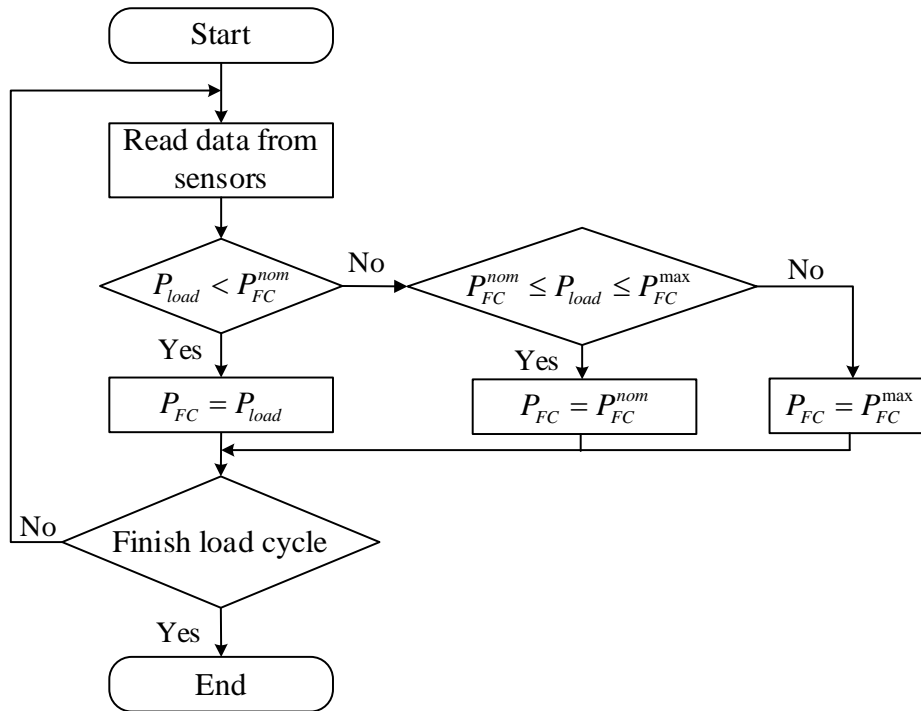
Figure 3.3 The flowchart of deterministic rule-based for fuel cell power distribution.

In order to match the characteristic of the PEMFC, the low-pass filter 1 is applied to decompose the low-frequency and high-frequency power of the PEMFC. Thus, the reference power of the PEMFC can be determined from the required PEMFC power as follows:

30

$$P_{FC}^{ref} = G_1(s).P_{FC} \tag{3.4}$$

$$G_1(s) = \frac{2\pi f_{c1}}{2\pi f_{c1} + s} \tag{3.5}$$

where P_{FC} and P_{FC}^{ref} describe the required power and reference power of the PEMFC (W), respectively; $G_1(s)$ is a transfer function of LPF-1, f_{c1} is the cut-off frequency to define the reference PEMFC power (Hz).

Based on the reference power of PEMFC, the power of the energy storage system can be defined as follows:

$$P_{ESS} = P_{load} - P_{FC}^{ref} \tag{3.6}$$

Similarly for the BAT, the low-pass filter 2 is also utilized to separate the low- and high-frequency BAT power which obtains the reference BAT power. This power can be defined as follows:

$$P_{BAT}^{ref} = G_2(s)P_{ESS} \tag{3.7}$$

$$G_2(s) = \frac{2\pi f_{c2}}{2\pi f_{c2} + s} \tag{3.8}$$

where $G_2(s)$ is the transfer function of LPF-2, f_{c2} is the cut-off frequency to define the reference BAT power (Hz).

Due to the slow dynamic, the PEMFC and BAT cannot adapt to the high-frequency power of load demand instantly. Fortunately, the SC, with the high power density and fast dynamic response, is combined to compensate for the load fluctuation and high-frequency powers of PEMFC and BAT. The reference SC power can be calculated by

$$P_{SC}^{ref} = P_{ESS} - P_{BAT}^{ref} \tag{3.9}$$

As a result, the obtained reference powers of PEMFC, BAT, and SC are used in the low-level control to define the required currents of power sources, which will be discussed in the next section.

3.4 Low-Level Control Design

In this work, four PI controllers are designed to generate the PWM signals for DC/DC converters and regulate the DC bus voltage. The current control loop of the PEMFC boost converter is controlled by the PI-1 controller. The PI-2 controller is the outer voltage control loop to maintain the DC bus voltage, while the PI-3 controller is the inner current control loop for the BAT's bidirectional buck-boost converter. Meanwhile, the PI-4 controller is designed for use in the current control loop of the SC's bidirectional buck-boost converter. In the bidirectional converter, because both buck (charge direction) and boost (discharge direction) modes employ the

similar transfer function of control loops, the operating characteristics of boost mode are taken into account while designing the controller.

In the control parameters design process, the controller gains of the SC converter are designed first because the SC has a fast dynamic response than the BAT and PEMFC. Besides, the current control loop bandwidth (BW) of the PI-4 controller is selected higher than the BW of other controllers. Similarly, the current control loop BW of the PI-3 controller is chosen as lesser than the PI-4 controller but higher than the PI-1 controller because the BAT charge/discharge rates are slower than the SC but faster than the PEMFC. Besides, the BW of the BAT and PEMFC current controller is designed such that high-frequency components are transferred to the SC for power or current compensation. In this work, the current control loop BW of the PI-4, PI-3, and PI-1 controllers is limited to equal 1/6, 1/10, and 1/14 of the switching frequency (f_{sw}) of the DC/DC converters, respectively [66]. Furthermore, to regulate the DC bus voltage, the voltage control loop (PI-2 control) BW is chosen smaller than the current control loop (PI-3 control) of the BAT because the current control loop has a faster response than the voltage control loop.

3.4.1 Design of SC Current Controller (PI-4 Controller)

In the control strategy, SC is used as the ESS to compensate for the response of BAT and PEMFC. The controller of the SC converter is designed by using the reference and measured SC current. Thus, the characteristics of the current control loop are considered to guarantee the stability of the current controller. The block diagram of the SC current control loop is presented in Figure 3.4.
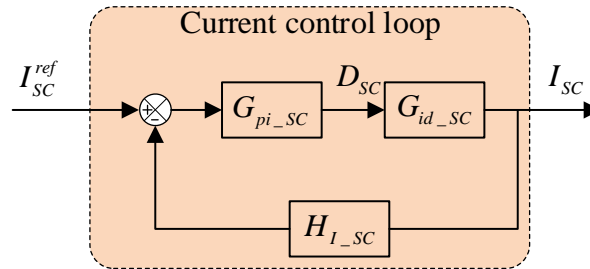
Figure 3.4 Current controller diagram of the SC converter.

The duty-cycle-to-current transfer function of the SC converter is given by [67]

$$G_{id\_SC}(s) = \frac{2V_o}{(1-D_{SC})^2 R} \frac{\left(1 + \frac{RC_2}{2}s\right)}{1 + \frac{L}{(1-D_{SC})^2 R}s + \frac{LC_2}{(1-D_{SC})^2}s^2} \tag{3.10}$$

where V_0 is the output voltage of the converter (V), D_{SC} is the duty cycle of the SC bidirectional converter (%), $R, L,$ and C_2 are the values of the resistor, inductor, and capacitor of the bidirectional converter, respectively.

To achieve the desired crossover frequency and stability margin of the transfer function (3.10), the PI compensator (PI-4 controller) is designed as follows:

$$G_{pi\_SC}(s) = K_{p\_SC} + K_{i\_SC}\frac{1}{s} \tag{3.11}$$

where K_{p_SC} and K_{i_SC} are the PI compensator gains.

The transfer function of the compensated current control loop of the SC converter is defined as follows:

$$T_{i\_SC}(s) = G_{pi\_SC}(s).G_{id\_SC}(s).H_{I\_SC} \tag{3.12}$$

where H_{I_SC} is the current sensor gain.

The parameters of electronic components used in the SC converter are given in Table 3.1. The Bode diagram of the SC current control loop with and without using the PI compensator is shown in Figure 3.5. It can be seen that the phase margin (PM) decreases from 90^0 to 60.1^0 at 2.09×10^4 rad/sec when using the PI compensator. Thus, this compensator can ensure the stability of the current control loop for the SC converter. As a result, the PI-4 controller parameters are defined with $K_{p\_SC} = 0.0257$ and $K_{i\_SC} = 307.3101$.
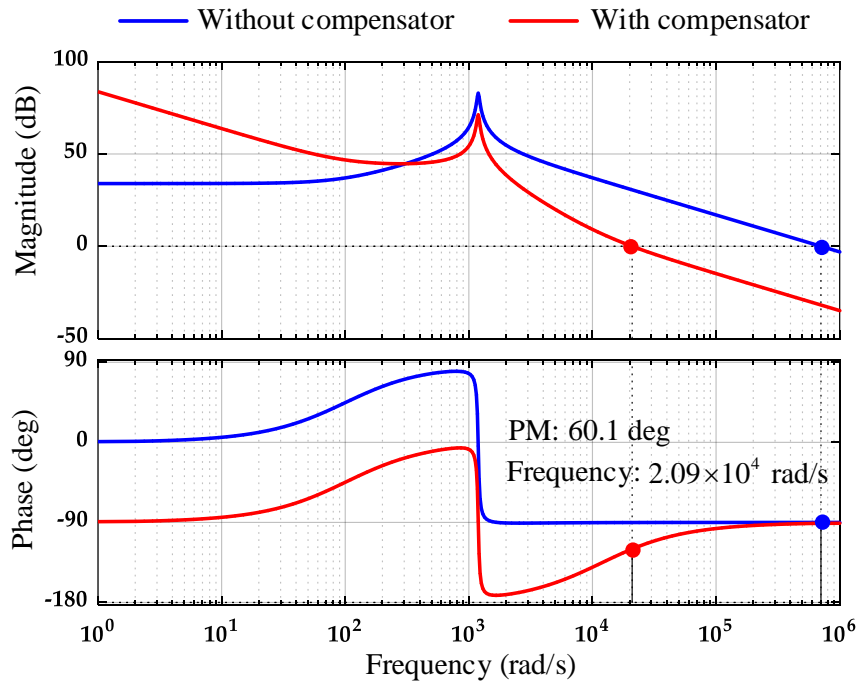
Figure 3.5 Bode diagram of the SC current control loop.

Table 3.1 Parameters of the SC bidirectional converter.

Parameter	Value	Parameter	Value
V_o	48 (V)	C_2	3.2 (mF)
V_{in_SC}	24 (V)	D_{SC}	0.5
H_{I_SC}	1	L	140 (uH)
R	50 (mΩ)	f_{sw}	20 (kHz)

3.4.2 Design of BAT Current Controller (PI-3 Controller)

In the control strategy, the BAT is used to guarantee the DC bus voltage. Thus, two control loops are applied in which the inner loop is the current control and the outer loop is the voltage control. The block diagram of the BAT controllers is shown in Figure 3.6.
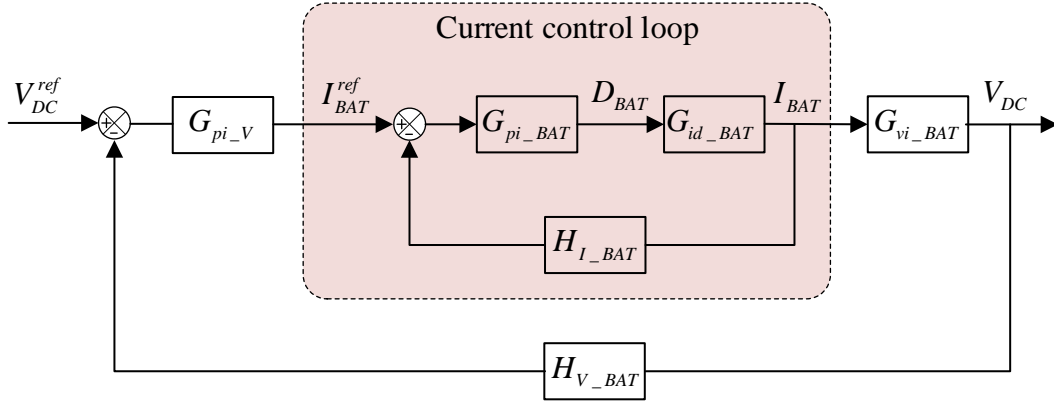
Figure 3.6 Block diagram of the controllers for BAT converter.

The voltage control loop produces the reference current to the BAT (I_{BAT}^{ref}) that is then compared to the measured BAT current to generate the input signal in the current control loop. The transfer function of duty-cycle-to-current is described as follows [67]

$$G_{id\_BAT}(s) = \frac{2V_o}{(1-D_{BAT})^2 R} \frac{\left(1 + \frac{RC_2}{2}s\right)}{1 + \frac{L}{(1-D_{BAT})^2 R}s + \frac{LC_2}{(1-D_{BAT})^2}s^2} \tag{3.13}$$

where V_0 is the output voltage of the converter (V) and D_{BAT} is the duty cycle of the BAT converter (%).

The PI compensator of the BAT current control loop (PI-3 controller) is given as

$$G_{pi\_BAT}(s) = K_{P\_BAT} + K_{i\_BAT}\frac{1}{s} \tag{3.14}$$

where K_{P_BAT} and K_{i_BAT} are the gains of the PI controller.

The transfer function of the current control loop is described as

$$T_{i\_BAT}(s) = G_{pi\_BAT}(s).G_{id\_BAT}(s).H_{I\_BAT} \tag{3.15}$$

where H_{I_BAT} is the current sensor gain.

The parameters of the BAT converter are given in Table 3.2. The Bode plot of the BAT current control loop with and without the PI compensator is shown in Figure 3.7. The PM with PI compensator is 60^0 which achieves the stability of the current control loop at 1.26×10^4 rad/sec. Then, the PI-3 controller parameters are determined with $K_{p\_BAT} = 0.0153$ and $K_{p\_BAT} = 110.1810$.
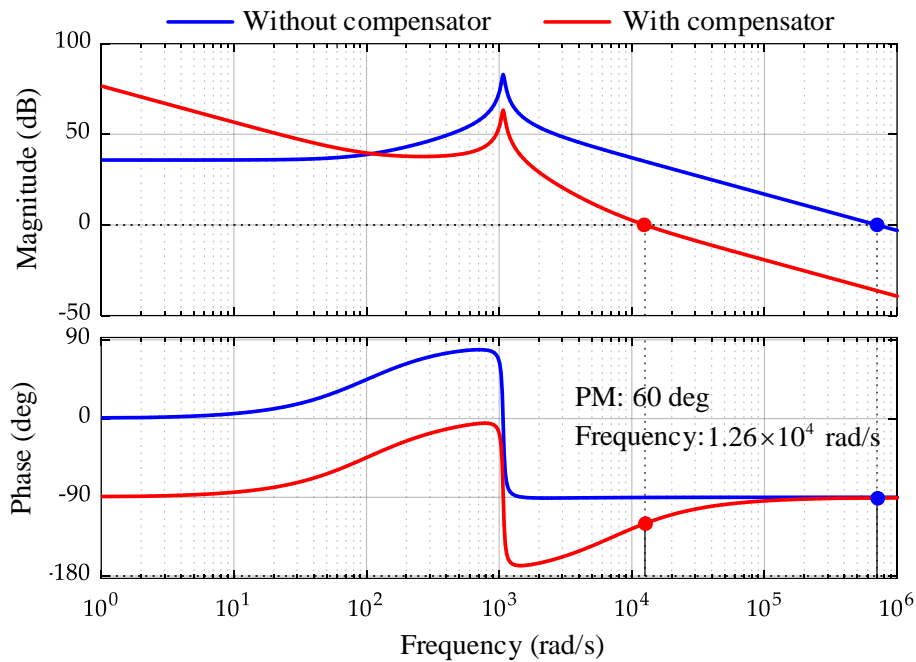
Figure 3.7 Bode diagram of the BAT current control loop.

Table 3.2 Parameters of the BAT bidirectional converter.

Parameter	Value	Parameter	Value
V_o	48 (V)	C_2	3.2 (mF)
V_{in_BAT}	21.6 (V)	D_{BAT}	0.55
H_{I_BAT}	1	L	140 (uH)
R	50 (mΩ)	f_{sw}	20 (kHz)

3.4.3 Design of DC Bus Voltage Controller (PI-2 Controller)

In the HPS, the DC bus voltage decreases when load power demand increases rapidly, whereas this voltage will boost if the power load declines. A bus regulation, thus, is necessary to

obtain the stability of DC bus voltage. In this study, the BAT is employed to keep the DC bus voltage at the desired value. As a result, the DC bus voltage controller is based on the outer voltage control loop of the BAT bidirectional converter as presented in Figure 3.6. The transfer function of the voltage control loop is given as [67]

$$G_{vi\_BAT}(s) = \frac{R(1-D_{BAT})\left(1 - \frac{L}{R(1-D_{BAT})^2}s\right)}{2 + RC_2 s} \tag{3.16}$$

Due to the slower response than the inner current control loop, the outer voltage control loop has a lesser bandwidth than the current control loop. The PI compensator transfer function of the voltage control loop (PI-2 controller) is given as

$$G_{pi\_V}(s) = K_{p\_V} + K_{i\_V}\frac{1}{s} \tag{3.17}$$

where K_{p_V} and K_{i_V} are the gains of PI-2 controller.

The transfer function of the voltage control loop is described as

$$T_v(s) = G_{pi\_V}(s).G_{vi\_BAT}(s).H_{V\_BAT} \tag{3.18}$$

where H_{V_BAT} is the voltage sensor gain.

The Bode plot of the voltage control loop with and without the PI compensator is shown in Figure 3.8. The DC bus voltage controller is designed such that the PM of 59.4^0 at 1.24×10^3 rad/sec. As a result, the PI-2 controller parameters are defined with $K_{p\_V} = 6.1436$ and $K_{i\_V} = 482.52$.
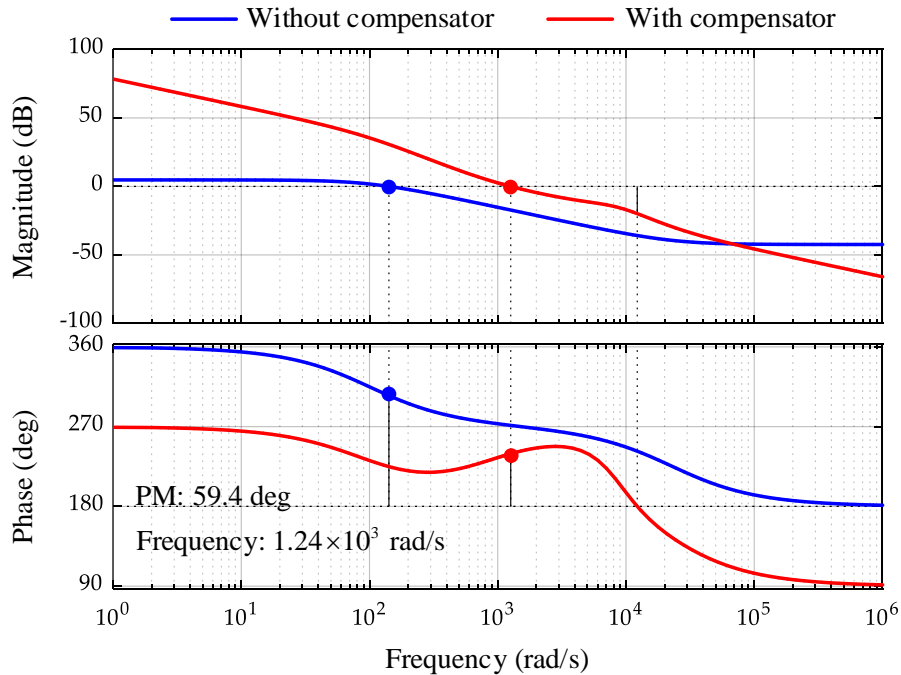
Figure 3.8 Bode diagram of the DC bus voltage control loop.

3.4.4 Design of PEMFC Current Controller (PI-1 Controller)

In this hybrid system, the PEMFC is used as the primary source to supply the power for load power demand. The block diagram of the current controller for PEMFC is presented in Figure 3.9.
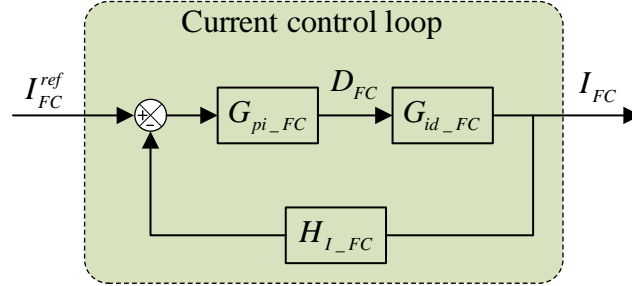
Figure 3.9 Current controller diagram of the PEMFC converter.

The duty-cycle-to-current transfer function of the PEMFC converter is given by [67]

$$G_{id\_FC}(s) = \frac{2V_o}{(1-D_{FC})^2 R} \frac{\left(1+\frac{RC_2}{2}s\right)}{1+\frac{L}{(1-D_{FC})^2 R}s+\frac{LC_2}{(1-D_{FC})^2}s^2} \tag{3.19}$$

where V_o is the output voltage of the converter (V) and D_{FC} is the duty cycle of the FC boost converter (%).

The PI compensator (PI-1 controller) is designed as follows:

$$G_{pi\_FC}(s) = K_{p\_FC} + K_{i\_FC}\frac{1}{s} \tag{3.20}$$

where K_{p_FC} and K_{i_FC} are the PI compensator gains.

The compensated current control loop of the PEMFC converter is given by

$$T_{i\_FC}(s) = G_{pi\_FC}(s).G_{id\_FC}(s).H_{I\_FC} \tag{3.21}$$

where H_{I_FC} is the current sensor gain.

The parameters of the PEMFC converter are given in Table 3.3. The Bode diagram of the SC current control loop with and without using the PI compensator is shown in Figure 3.10. The result of PM with PI compensator is 60^0 at 8.98×10^3 rad/sec, which can achieve the stability of the current control loop for the PEMFC boost converter. Therefore, the PI-1 controller parameters are achieved with $K_{p\_FC} = 0.0104$ and $K_{i\_FC} = 23.3103$.
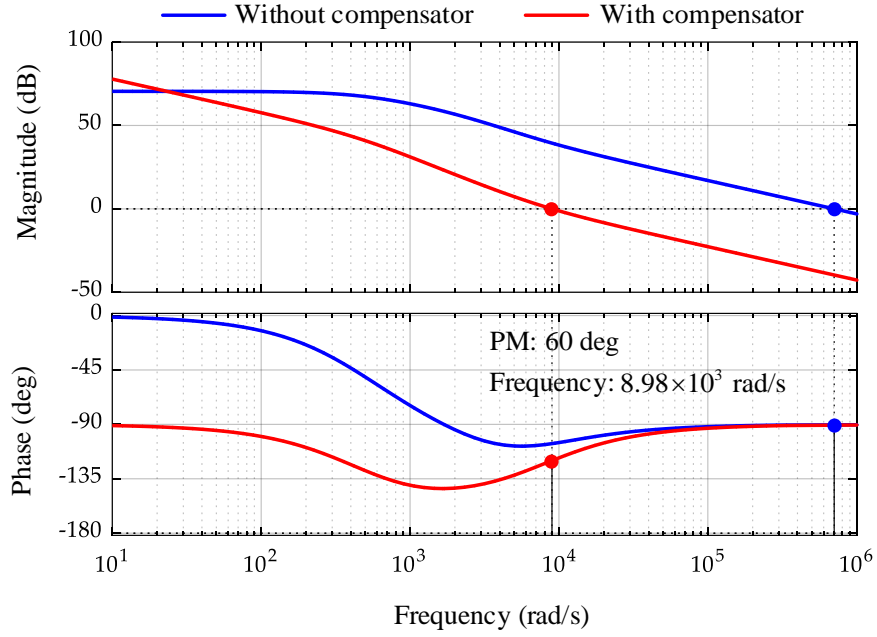
Figure 3.10 Bode diagram of the PEMFC current control loop.

Table 3.3 Parameters of the PEMFC converter.

Parameter	Value	Parameter	Value
V_o	48 (V)	C_2	3.2 (mF)
V_{in_FC}	24.3 (V)	D_{FC}	0.51
H_{I_FC}	1	L	140 (uH)
R	50 (mΩ)	f_{sw}	20 (kHz)

3.4.5 SOC Regulators

In order to maintain the SOC of BAT and SC in the limited range $SOC_{\min} < SOC < SOC_{\max}$, two SOC regulators are designed in the low-level control as shown in Figure 3.1. For the BAT, a SOC regulator scheme is proposed to maintain the battery SOC level of the BAT in a limited range $SOC_{BAT\_\min} < SOC_{BAT} < SOC_{BAT\_\max}$. The value of SOC status is compared with $SOC_{BAT\_\min}$ and $SOC_{BAT\_\max}$ to decide the reference current of the BAT [68] as follows:

$$I_{BAT}^{ref} = \begin{cases} \alpha_1 \left| I_{BAT}^{cmd} \right| & if & SOC_{BAT} \le SOC_{BAT}^{\min} \\ I_{BAT}^{cmd} & if & SOC_{BAT}^{\min} < SOC_{BAT} < SOC_{BAT}^{\max} \\ \beta_1 \left| I_{BAT}^{cmd} \right| & if & SOC_{BAT} \ge SOC_{BAT}^{\max} \end{cases} \quad (3.22)$$

38

where I_{BAT}^{ref} is the reference current of the BAT (A), I_{BAT}^{cmd} is the required BAT current (A), SOC_{BAT} is the BAT status (%), SOC_{BAT}^{min} and SOC_{BAT}^{max} are the minimum and maximum allowable SOC level of the BAT (%), α_1 and β_1 are the tuning parameters.

Based on the SOC conditions of the BAT, the above tuning parameters are defined below:

$$\alpha_1 = -\frac{\gamma_1 \left| SOC_{BAT} - SOC_{BAT}^{min} \right|}{SOC_{BAT}^{min}} \tag{3.23}$$

$$\beta_1 = \frac{\delta_1 \left| SOC_{BAT} - SOC_{BAT}^{max} \right|}{SOC_{BAT}^{max}} \tag{3.24}$$

where γ_1 and δ_1 are the positive constants depending on the charge/discharge characteristics of the BAT.

The same as BAT, a SOC regulator is also considered to guarantee the SC SOC in the limited ranges. Hence, the reference current for the SC can be considered as follows:

$$I_{SC}^{ref} = \begin{cases} \alpha_2 \left| I_{SC}^{cmd} \right| & if & SOC_{SC} \leq SOC_{SC}^{min} \\ I_{SC}^{cmd} & if & SOC_{SC}^{min} < SOC_{SC} < SOC_{SC}^{max} \\ \beta_2 \left| I_{SC}^{cmd} \right| & if & SOC_{SC} \geq SOC_{SC}^{max} \end{cases} \tag{3.25}$$

where I_{SC}^{ref} is the reference current of the SC (A), I_{SC}^{cmd} is the required SC current (A), SOC_{SC} is the SC status (%), SOC_{SC}^{min} and SOC_{SC}^{max} are the minimum and maximum allowable SOC of the SC (%), respectively; α_2 and β_2 are the tuning parameters.

Based on the SOC_{SC} conditions, the value of α_2 and β_2 is governed by:

$$\alpha_2 = -\frac{\gamma_2 \left| SOC_{SC} - SOC_{SC}^{min} \right|}{SOC_{SC}^{min}} \tag{3.26}$$

$$\beta_2 = \frac{\delta_2 \left| SOC_{SC} - SOC_{SC}^{max} \right|}{SOC_{SC}^{max}} \tag{3.27}$$

where γ_2 and δ_2 are the positive constants depending on the charge/discharge characteristics of the SC.

During the operation, the EMS appropriately distributes power to each power supply to not only sufficiently satisfy the workload demand but also maintain the supplements' SOCs. These parameters should be properly determined to avoid the state of overcharging or deep discharging. For the charging process, if a certain storage device has higher SOC, the injected power is lower, and vice versa. Meanwhile, in the discharging process, the output power is higher with higher SOC

and is lower with lower SOC. Furthermore, if the SOC of the BAT or SC reaches its upper bound, or lower bound, disconnected action is executed and this device will wait for the next discharging or charging process, respectively.

3.5 Simulation Results

In the following simulations and experimental tests, two load power profiles in Fig 2.8 are chosen to evaluate the effectiveness of the proposed control strategy. In the first case study, a step-changing load is utilized with abrupt variations of power load, which can describe the different working conditions. For the second case study, a specific driving cycle is used under operating circumstances such as acceleration, deceleration, and regenerative energy in practical applications. The component characteristics of PEMFC, BAT, and SC were chosen from commercially available devices which could satisfy the load power demand and verify the proposed approach as listed in Tables 3.4 – 3.7. In addition, appropriate cut-off frequencies were also determined such that they could produce the smooth reference current for the FC and BAT converters.

Table 3.4 Specifications of PEMFC Horizon (H-200)

Parameter	Symbol	Value
Number of cells	N	40
Voltage range	V_{FC}	20 – 37 (V)
Rated power	P_{FC}	200 (W)
Maximum current	I_{FC}^{max}	8.3 (A)
Maximum operating point	U_{max}, I_{max}	24V – 8.3A
Hydrogen pressure	P_{fuel}	0.45 – 0.55 (bar)
Nominal air pressure	P_{air}	2 (bar)
Air flow rate	V_{air}	2.6 (lpm)
Hydrogen fuel flow rate	V_{fuel}	6.452 (lpm)
Operating temperature	T	318 (ºK)
Response time	T_d	7 (s)
Faraday constant	F	96485 (A s/mol)
Ideal gas constant	R	8.3145 (J/(mol ^{0}K))
Percentage of hydrogen in the fuel	x	99.95 (%)

Percentage of oxygen in the oxidant	y	50 (%)
Boltzmann's constant	k	1.38×10^{-23} (J/^{0}K)
Charge transfer coefficient	α	1.2518
Planck's constant	h	6.626×10^{-34} (J s)
Internal resistance	R_i	1.0375 (Ω)
Number of moving electrons,	z	2
Cooling		Air

Table 3.5 SC bank parameters of DLCAP

Parameter	Symbol	Value
Number of cells in series	N_s	9
Number of cells in parallel	N_p	1
Internal resistance	R_{SC}	2.8 (mΩ)
Helmholtz capacitance	C_H	18 (μF/cm^2)
Operating temperature	T	298 (^{0}K)
Number of layers of electrodes	N_e	1
Molecular radius	d	10^{-9} (m)
Cell electric charge	Q_c	9 (C)
Molar concentration	c	208 (mol/m^{-3})
Permittivity of material	ε	6.0208×10^{-10} (F/m)
Permittivity of free space	ε_0	8.85×10^{-12} (F/m)
Rated voltage	V_{SC}	24.3 (V)
Capacitance	C	50 (F)

Table 3.6 BAT parameters of Panasonic NCR18650BF

Parameter	Symbol	Value
Capacity	Q	13 (Ah)
Rated voltage	V_{SC}	21.6 (V)

BAT constant voltage	E_0	23.4222 (V)	
Internal resistance	R_{i_SC}	16.875 (mΩ)	
Polarization constant	K	0.012642 (V/Ah)	
Exponential voltage	A_b	1.8139 (V)	
Exponential capacity	B	4.7705 (Ah^{-1})	
Number of series cells		6	
Number of parallel cells		4	

Table 3.7 EMS and controller parameters

Parameter	Value	Parameter	Value
SOC_{BAT}^{min}	0.5	γ_2	0.01
SOC_{BAT}^{max}	0.9	δ_2	0.085
SOC_{SC}^{min}	0.5	K_{p_FC}	0.0104
SOC_{SC}^{max}	0.9	K_{i_FC}	23.3103
f_{c1}	5 (Hz)	K_{p_BAT}	0.0153
f_{c2}	32 (Hz)	K_{i_BAT}	110.1810
V_{DC}^{ref}	40 (V)	K_{p_V}	6.1436
γ_1	0.007	K_{i_V}	482.52
δ_1	0.05	K_{p_SC}	0.0257
		K_{i_SC}	307.3101

3.5.1 Case Study 1: Step-Changing Load

The system performance and effectiveness of EMSs are described in Figures 3.11 – 3.16. It is noteworthy that for this investigated scenario, all devices' signals for processing, i.e., voltage and current, were measured on the low-voltage side of the DC/DC converters. First of all, Figure 3.11 presents load power adaptation in the HPS based on three EMSs, with a continuous black line representing the reference power of the load, a dashed-dot blue line indicating the power of the deterministic rule without using the frequency decoupling method (without FD), a dashed-dot green line showing the load power adaptation without compensator design consideration (without CD), and a dashed-dot red line displaying the load power adaptation of the proposed deterministic-

frequency decoupling EMS (proposed DFD-EMS), which takes into account the deterministic-frequency decoupling method and compensator design for voltage and current control loops.
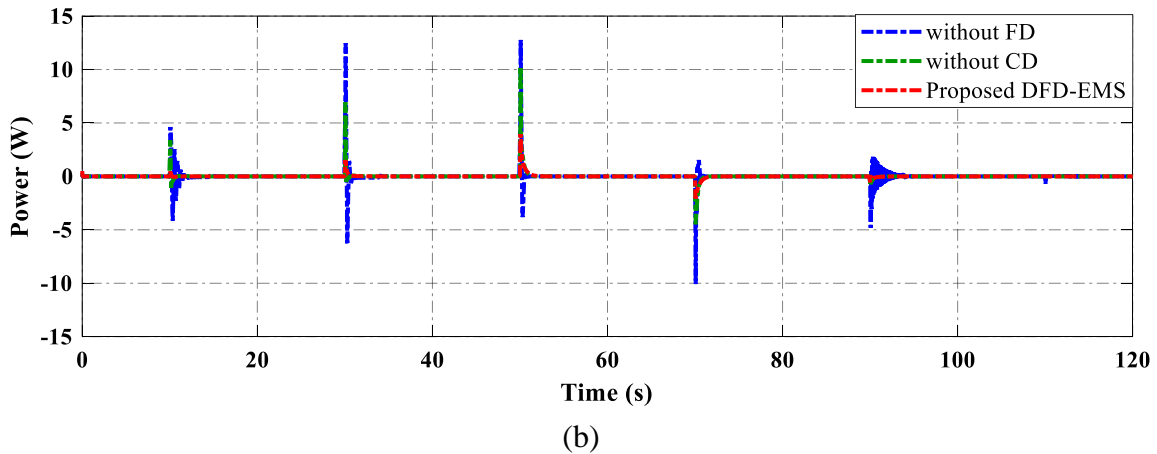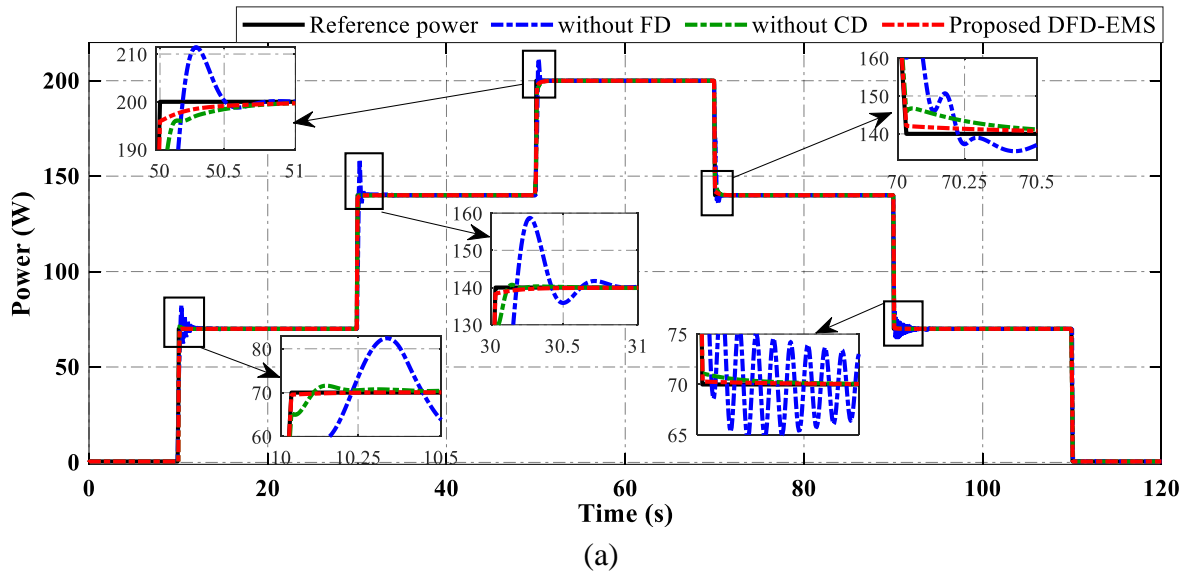
Figure 3.11 The comparison of load power adaptation based on three EMSs. (a) The load power adaptation. (b) The power tracking error.

As shown in Figure 3.11 (a), the proposed strategy achieves a better power adaptation to the load power demand than strategies without FD and without CD under different working conditions. When the load power is abruptly changed at the time of the 10th, 30th, 50th, 70th, 90th, and 110th, the without FD strategy can not satisfy the fast transient state of power load causing the overshoot power, while the released power of the proposed-EMS shows a good tracking performance to meet the load requirements. In the case without FD, the HPS operates based on the released power of the PEMFC and BAT because the high-frequency powers are not decomposed and compensated by SC. Hence, the system adaptation has more fluctuation in the transient state of abrupt load change. In the case without CD, because the dynamics characteristics are not considered comprehensively, the trial-error method is used to tune the parameters of voltage and current control loops. As a result, the dynamics

43

response of controllers is not stable to ensure load power adaptation and system performance. Due to using the FD technique regarding each device's characteristics and consideration of low-level control design, the power command is appropriately distributed from the requirement into each component. In addition, the power tracking error of three EMSs was presented in Figure 3.11 (b). The proposed EMS gets the optimum distributed accuracy with the error in the range of $(-2 \rightarrow 4)$ W, while the without CD strategy has an inadequate power approximated $(-5 \rightarrow 10)$ W, and the without FD strategy takes the inaccuracy power up to $(-10 \rightarrow 12)$ W. The obtained results show that the proposed EMS has the best power adaptation with the smallest power fluctuations.
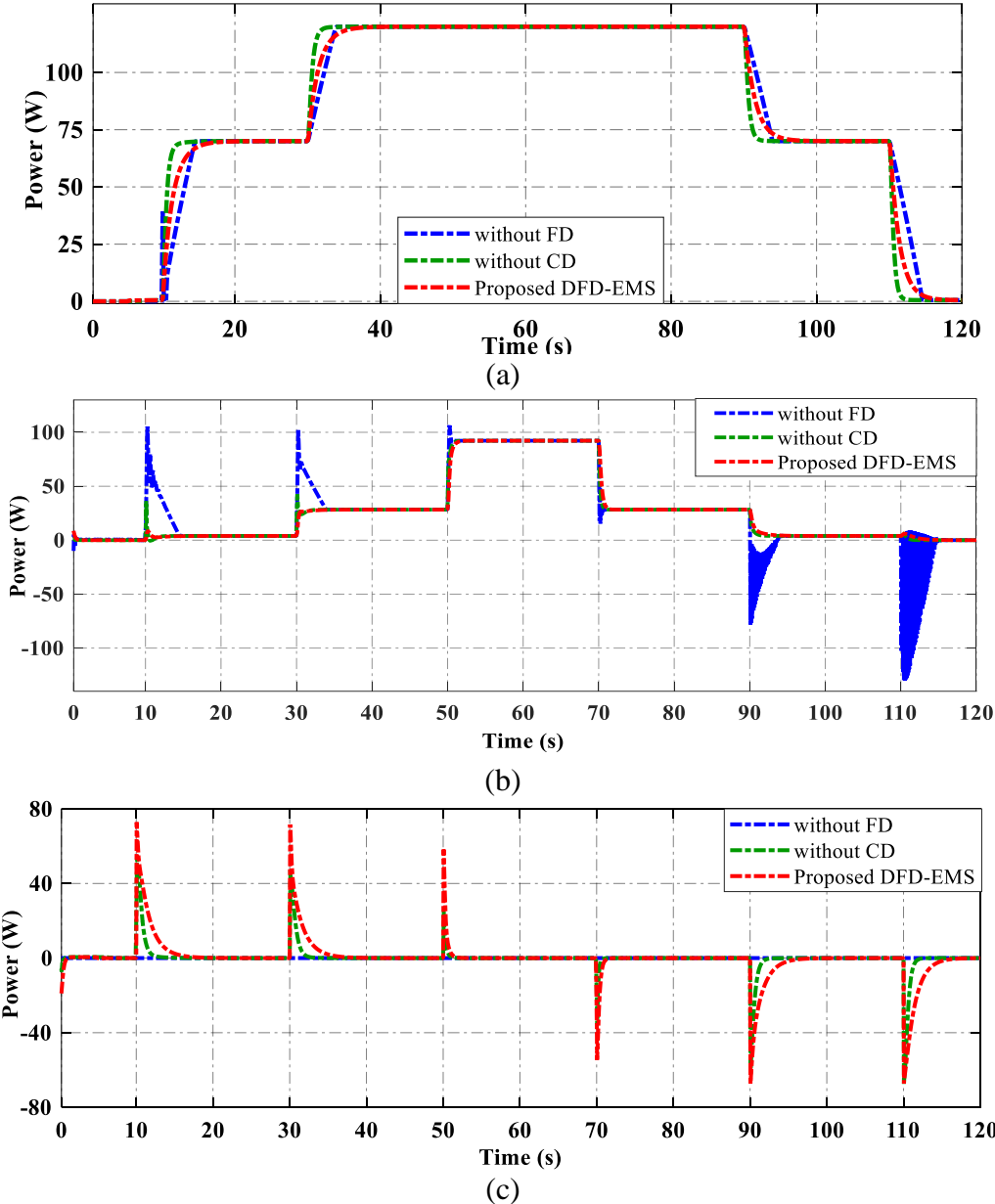
Figure 3.12 The power distribution of energy sources. (a) PEMFC. (b) BAT. (c) SC.

Next, the power distributions of the PEMFC, BAT, and SC in the hybrid system are shown in Figure 3.12. Due to a primary power source, the PEMFC supplies the majority of the load power

demand and has a power distribution higher than the BAT and SC. For the proposed and without CD strategies, SC bank not only supplied the peak power when the load changed abruptly at the moment of transient peak power but also delivered the fast response of required power and minimizes the fluctuating power on PEMFC and BAT. Conversely, PEMFC provided a base portion of the load power without satisfying the required power in the transient state. In addition, BAT supported the PEMFC to provide power in a steady state to reduce the PEMFC's power fluctuation. Although the PEMFC, with the lowest dynamics, could not instantly react to the load change, the load tracking effort could still be ensured due to the power compensation from the BAT and SC at each time of transient peak power. Meanwhile, in the case without FD strategy, the BAT will provide more energy to compensate for the PEMFC system, resulting in more fluctuation in the dynamics response of the BAT when the load changes abruptly.
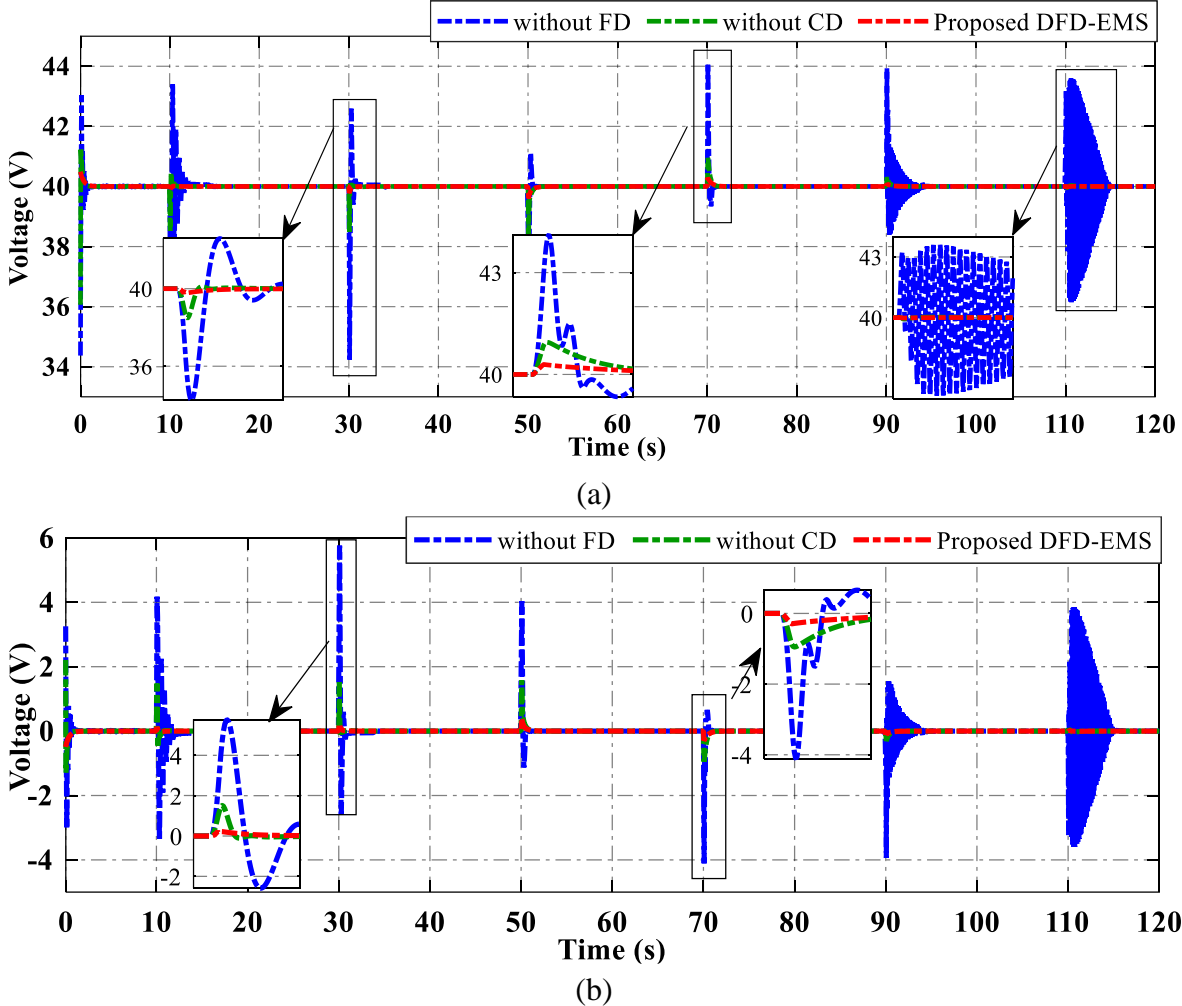
Figure 3.13 The DC bus voltage regulation. (a) Voltage tracking. (b) Tracking error.

The comparison of DC bus voltage regulation of three EMSs under different working load conditions is shown in Figure 3.13. Because the PEMFC, the SC bank, and the BAT were connected in parallel to the DC bus, the output voltage of these sources was the same as the DC bus voltage.

By using the proposed strategy, the DC bus voltage is steadily maintained at around 40 V with a very small fluctuation, despite the abrupt change of the load. In particular, the peak voltage of the DC bus by using the proposed EMS is in the range of $(39.6 \rightarrow 40.3)$ V, which was approximated by a 1.75 % voltage ripple. Conversely, the DC bus voltages fluctuate in the range of $(38.4 \rightarrow 41)$ V and $(34.2 \rightarrow 44)$ V corresponding to 6.5 % and 24.5 % ripples for the cases without CD and without FD, respectively.

(a)

(b)
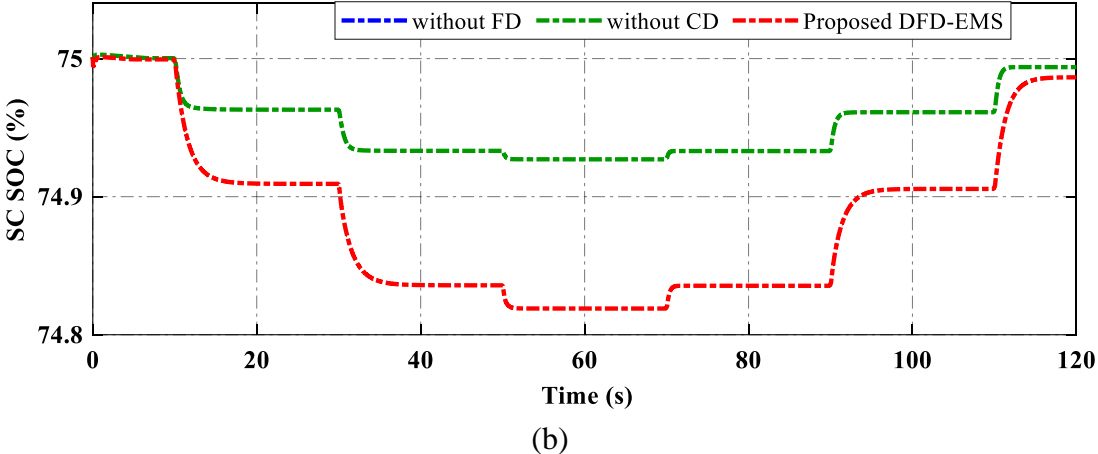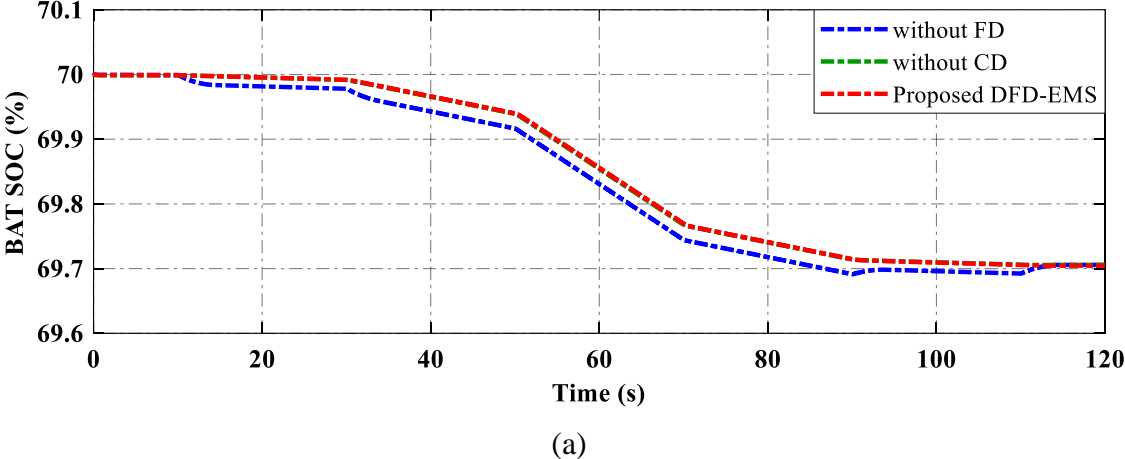
Figure 3.14 The SOC status. (a) BAT SOC. (b) SC SOC.

The SOC levels of both BAT and SC are performed in Figure 3.14, which describes the charged and discharged status at each timeline when the load changes. As shown in Figure 3.14 (a), the proposed EMS can hold the SOC BAT level better than the without FD and without CD. The proposed approach could maintain the fluctuation of BAT SOC level in the range of $(69.7 \rightarrow 70)$ %. However, for the SC, the proposed EMS shows faster SOC degradation than the without CD because the PEMFC works at an appropriate adaptive power rate for improving efficiency and reducing fuel consumption. SC is used to compensate for high-frequency power in the transient state. The without CD strategy has a SOC varying range within $(74.93 \rightarrow 75)$ % which is stable and lower than the proposed EMS with the range of $(74.82 \rightarrow 75)$ %, In addition, because the SC does not operate in

the case without FD, the SOC status is zero.
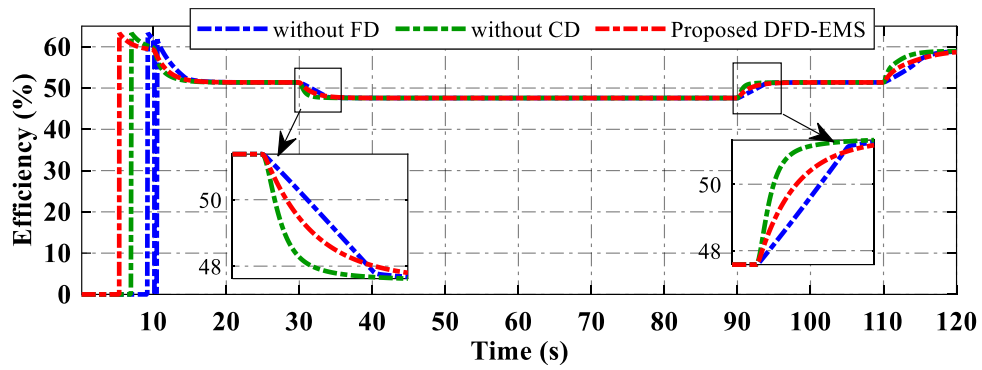
(a)
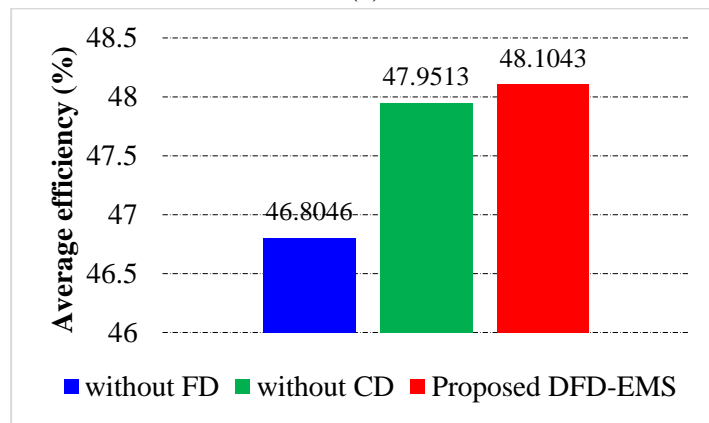
(b)

Figure 3.15 The comparison of PEMFC stack efficiency. (a) Efficiency status. (b) Average efficiency.

The PEMFC stack efficiency is investigated to evaluate the effectiveness of three EMSs as depicted in Figure 3.15. The efficiency status corresponding to levels of PEMFC power is depicted in Figure 3.15 (a). In addition, the average efficiency of the PEMFC stack is presented in Figure 3.15 (b). It can be seen that the PEMFC stack achieves the highest average efficiency at 48.1043 (%) by using the proposed DFD-EMS while the without CD strategy has an average efficiency of 47.9513 (%) and the without FD strategy is the lowest efficiency of 46.8046 (%).

(a)
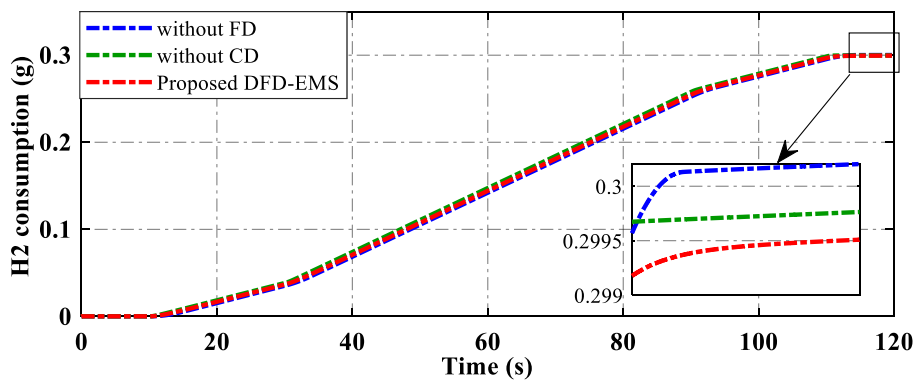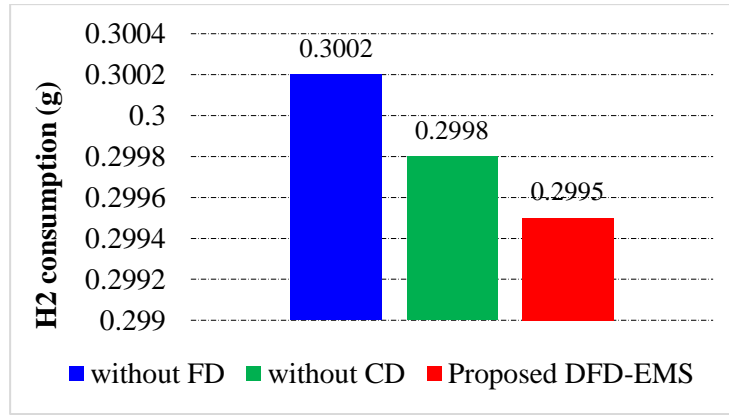
Fig 3.16 The comparison of hydrogen (H2) consumption. (a) H2 consumption status. (b) Total H2 consumption.

Finally, Figure 3.16 illustrates the fuel consumption of three EMSs. As a result, the proposed EMS consumes less hydrogen fuel than the without CD and without FD strategies based on the amount of fuel consumption. The without FD and without CD strategies consume high hydrogen fuel with 0.3002 (g) and 0.2998 (g) in comparable operating conditions, respectively. In contrast, in the case of the proposed approach, hydrogen consumption is 0.2995 (g). With hydrogen consuming less than compared to other ways, it demonstrates that the proposed strategy delivers superior fuel efficiency.

3.5.2 Case Study 2: Specific Driving Cycle

The system qualification in the case of the specific driving cycle, which is inherited from section 2.2.5, is described in Figures 3.17 – 3.22. Parameters for simulation are presented from Table 3.4 to Table 3.7. Here in this simulation, examined specific driving cycle is shown in Figure 3.17, along with the workability of load satisfaction under three control strategies in which the black line is the required load power, the load satisfaction under the without FD, without CD, and proposed DFD-EMS are presented by the dashed-dot blue line, dashed-dot green line, and dashed-dot red line, respectively. The behaviors of PEMFC, BAT, and SC devices are displayed in Figure 3.18. The DC bus regulation is depicted in Figure 3.19. The SOC status of BAT and SC are described in Figure 3.20. In addition, the PEMFC stack efficiency and hydrogen fuel consumption are depicted in Figure 3.21 and Figure 3.22, respectively. Generally, the use of the BAT could help maintain the DC bus voltage to meet the desired one at 40 V.
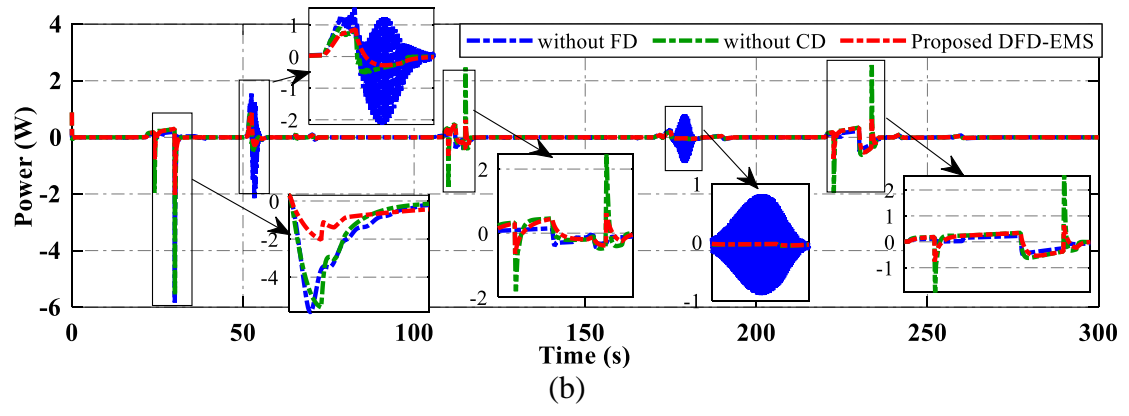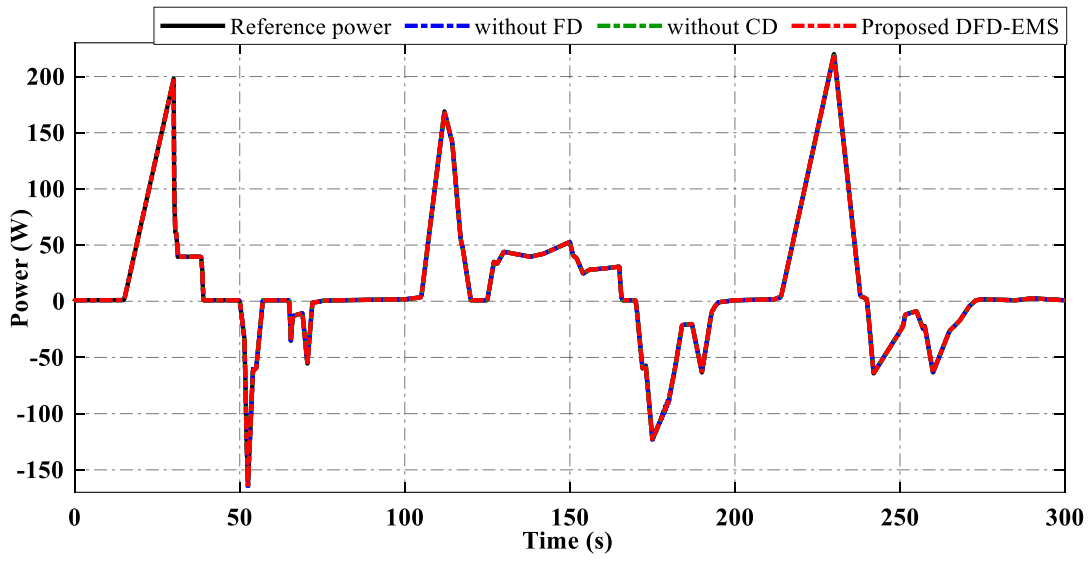
Figure 3.17 The comparison of load power adaptation based on three EMSs. (a) The load power adaptation. (b) The power tracking error.

Firstly, the load power adaptation of three EMSs is presented in Figure 3.17. In general, all three algorithms could satisfy the load requirement as shown in Figure 3.17 (a). However, Figure 3.17 (b) will describe detailed the power tracking error. The without CD strategy takes an insufficient power in the range of $(-5.5 \rightarrow 2.5)$ W, while the without FD strategy obtains a smaller error approximated $(-5.6 \rightarrow 1.8)$ W, and the proposed DFD-EMS achieves the highest distributed accuracy within $(-2 \rightarrow 0.6)$ W. This result reveals that the suggested methodology is able to guarantee the load power demand under different operating conditions.
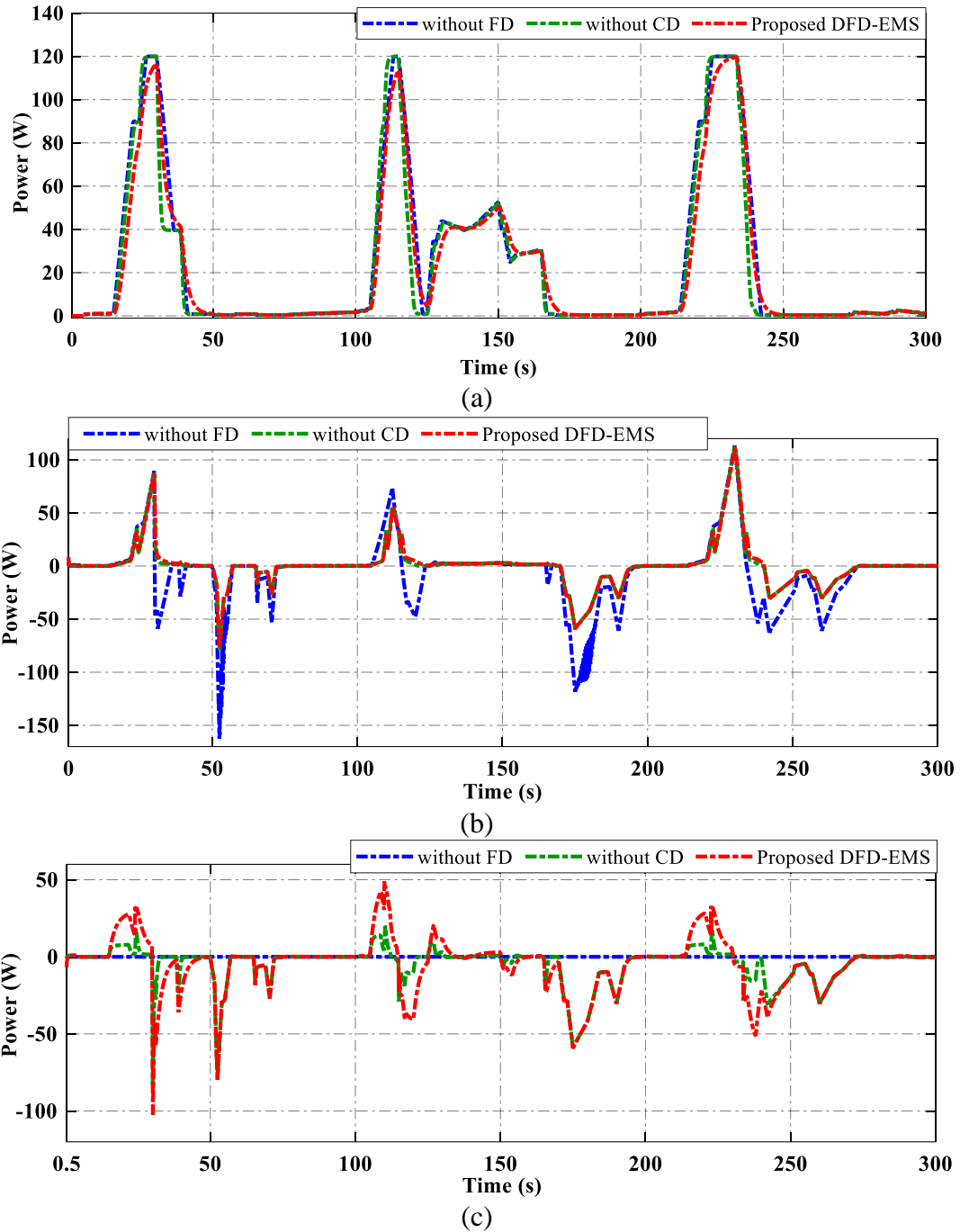
Figure 3.18 The power distribution of energy sources. (a) PEMFC. (b) BAT. (c) SC.

Next, the power distributions of the PEMFC, BAT, and SC in the hybrid system are shown in Figure 3.18. As expressed in Figure 3.18 (a), the PEMFC powers of the without FD and without CD strategies have a high power level that can diminish the aging and performance of the PEMFC system. Meanwhile, the proposed DFD-EMS provides a better performance indicator with a suitable change rate of PEMFC power and smaller power fluctuation, which can improve the fuel economy and durability of the PEMFC system. The power capability of the BAT under three EMSs is depicted in Figure 3.18 (b). It can be seen that the BAT power of the without FD strategy is higher than others

during the period of acceleration. This is because the SC does not work when using the without FD strategy, thus the BAT power must be more discharged to compensate for the lacking power from the fuel cell source to match the load power demand. However, in the regenerative mode, the proposed strategy can provide a smooth power response to charge the redundant power from the DC bus to the BAT. The comparative result of the SC power distribution is illustrated in Figure 3.18 (c). Due to the fast power response, the SC is employed to supplement the slow power response of the PEMFC and BAT to power the load. As a result, the proposed algorithm regulates the SC power in a suitable range that can accommodate the abrupt power of load and reduce power fluctuation of the PEMFC and BAT despite the rapid load change.
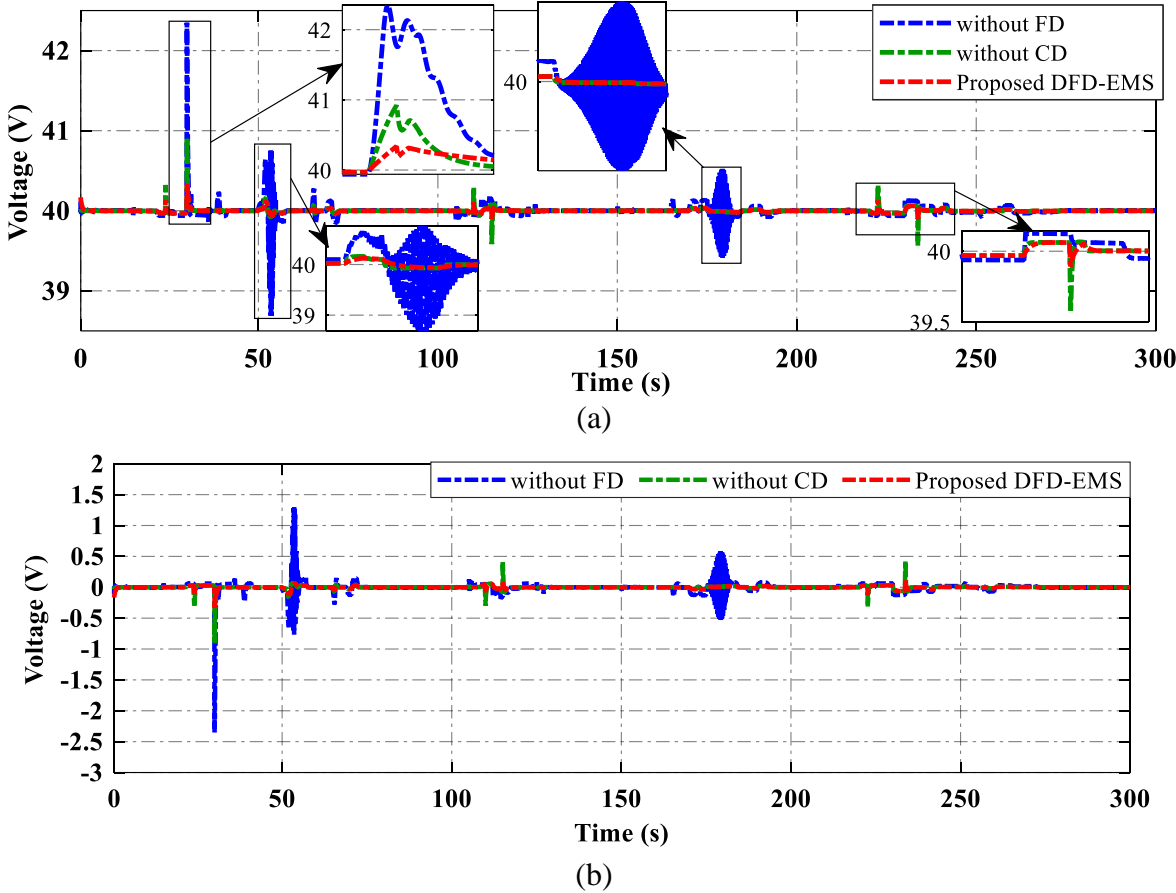
Figure 3.19 The DC bus voltage regulation. (a) Voltage tracking. (b) Tracking error.

Figure 3.19 shows the DC bus voltage regulation of three EMSs under different working load conditions. By using the proposed DFD-EMS, the DC bus voltage is steadily maintained at around 40 V with a smaller fluctuation than using the two other strategies. In the change interval of the load, the DC bus peak voltage is in the range of $(39.75 \rightarrow 40.42)$ V, approximated by a 1.68 % voltage ripple, by using the proposed strategy. This result is better than the ones under the without CD with the range of $(39.5 \rightarrow 41)$ V and the without FD with the range of $(38.7 \rightarrow 42.3)$ V corresponding to 3.75% and 9% voltage ripple.
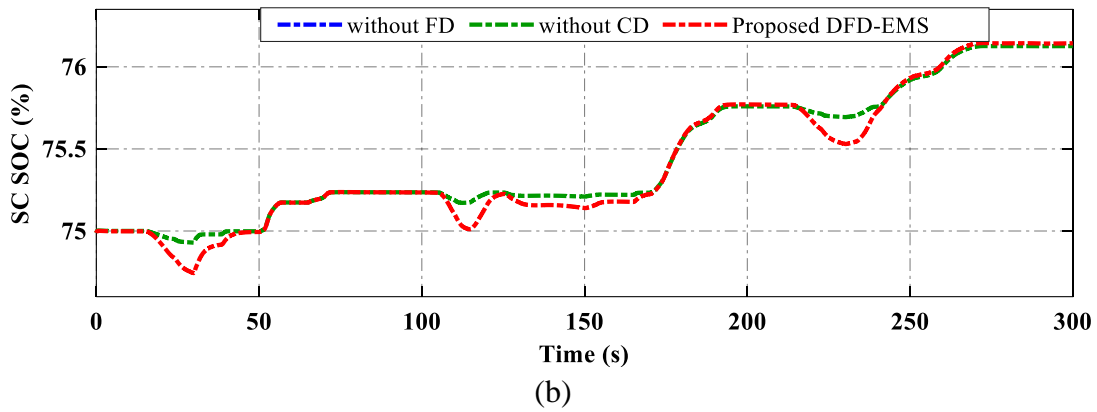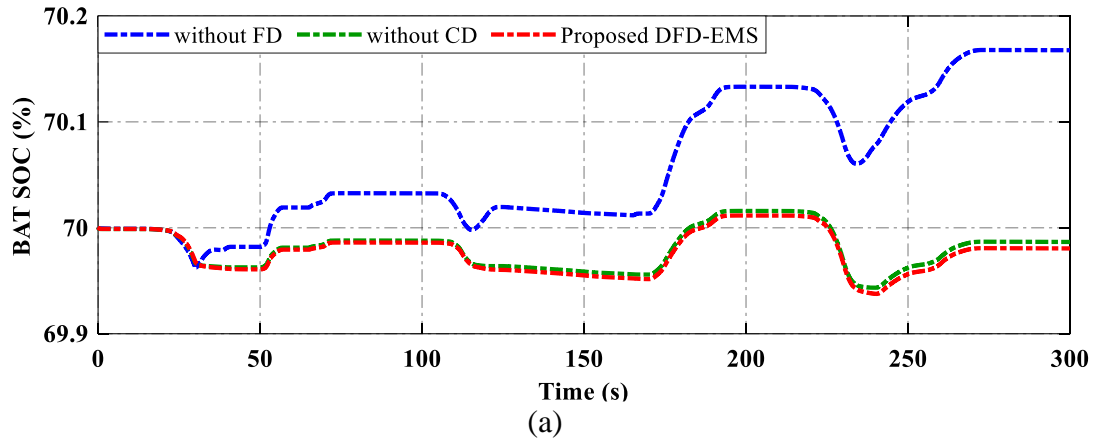
Figure 3.20 The SOC status. (a) BAT SOC. (b) SC SOC.

The SOC levels of both BAT and SC bank are performed in Figure 3.20, which describe the charged and discharged status at each timeline when the load changes. In Figure 3.20 (a), for the BAT SOC, the suggested DFD-EMS and the without CD strategy can maintain the fluctuated range of (69.95 → 70) % lower than the without FD strategy. For the SC, Figure 3.20 (b) shows that the SOC level of the proposed EMS and the without CD strategy varies from (74.9 → 76.2) %.

(a)
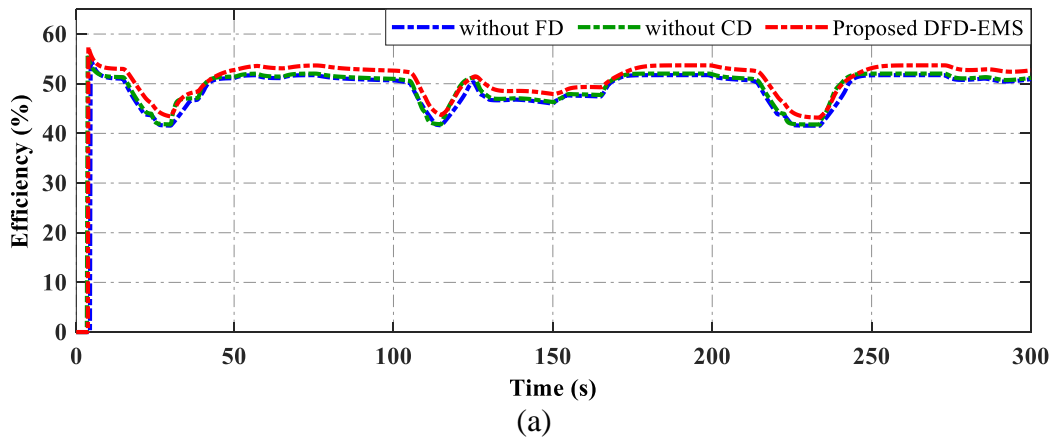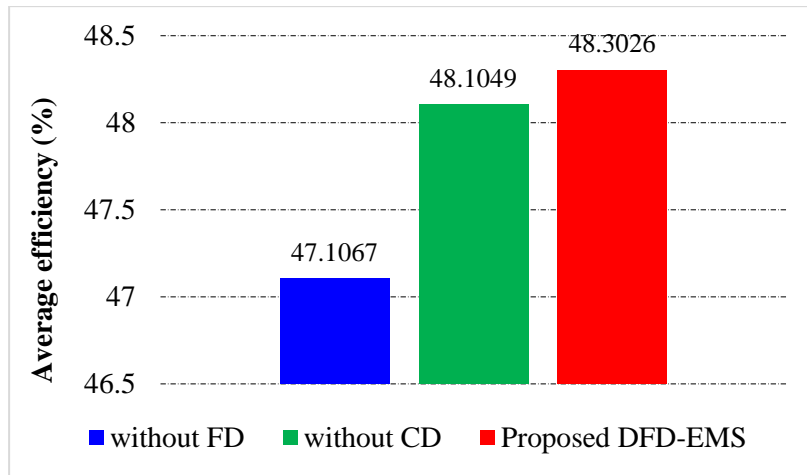
(b)

Figure 3.21 The comparison of PEMFC stack efficiency. (a) Efficiency status. (b) Average stack efficiency.

The comparative simulation results of the PEMFC stack efficiency are illustrated in Figure 3.21. As a result, the PEMFC stack achieves an average efficiency of 48.3026 % by conducting with the proposed strategy, while this efficiency is 48.1049 % and 47.1067 % if using the without CD and the without FD strategies, respectively.
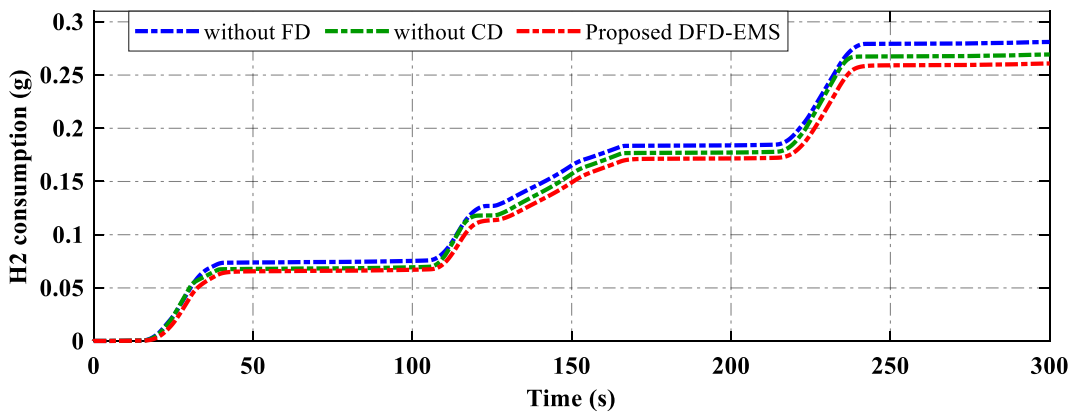
(a)
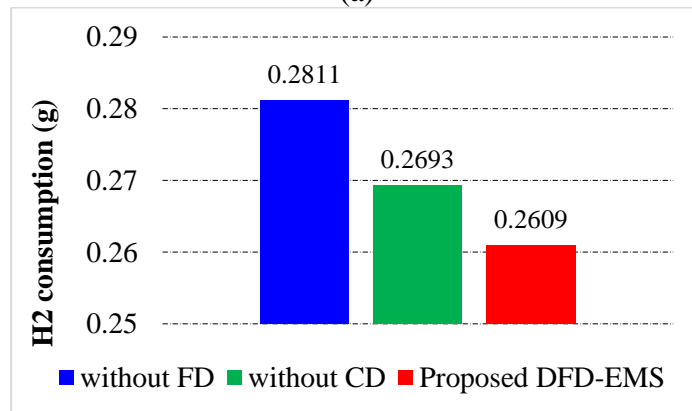
(b)

Figure 3.22 The comparison of H2 consumption. (a) H2 consumption status. (b) Total H2 consumption.

Furthermore, with the same driving cycle, the fuel consumption of three EMSs is evaluated as well in Figure 3.22. In the case of the proposed strategy, the total amount of hydrogen consumption is 0.2609 g during the time of the driving cycle, whereas the total fuel consumption of the without CD and the without FD strategies reaches 0.2693 g and 0.2811 g in the same working conditions, respectively. It proves that the proposed approach gives better fuel economy with hydrogen consuming less than 7.18 % in comparison with other approaches. The aforementioned results show that the proposed DFD-EMS is a better effective strategy than other strategies for saving fuel consumption and enhancing efficiency for the PEMFC stack.

3.6 Experimental Results

In this section, an HPS test bench is implemented with three power sources (PEMFC/BAT/SC), a unidirectional DC/DC converter, two bidirectional DC/DC converters, a controller board, a DC load simulator, a power supply, measurement device, and PC monitor as shown in Figure 3.21.
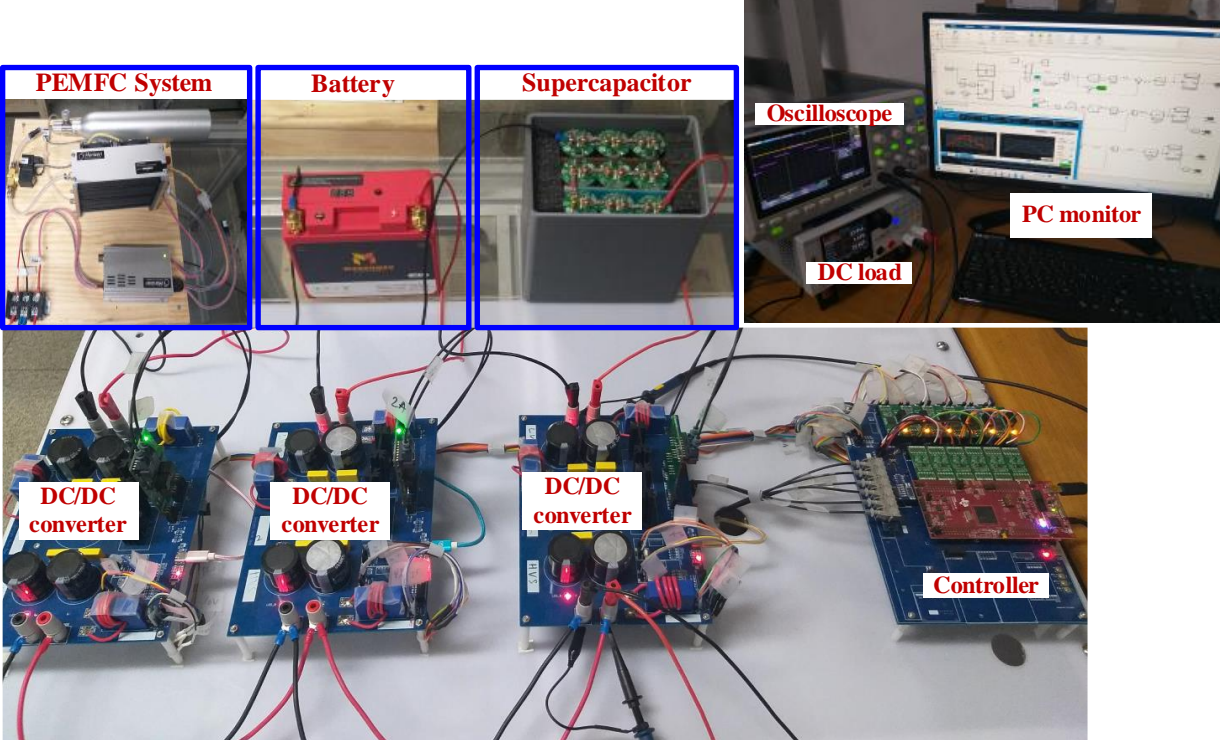
Figure 3.21 The hybrid power system test bench.

The used test bench is designed with PEMFC, as a primary power source, integrated with BAT and SC bank, as an auxiliary power system, to compensate for the PEMFC dynamics. The parameters and characteristics of PEMFC, BAT, and SC are shown in Tables 3.4 – 3.7. Besides, the DC/DC converter for the PEMFC is unidirectional with a boost mode topology, whereas the BAT and SC converters are bidirectional with buck/boost topology. Three DC/DC converters are connected in parallel and the output voltage side is integrated into the DC bus. These converters are composed of

a high-frequency inductor (L = 140 μH), capacitors on two sides of the converter ($C_1 = C_2 = 3.2$ mF), a resistor (R = 0.05 Ω), a diode (D), and MOSFET switches (S, S_1, S_2). The control loops of three DC/DC converters are executed in real-time by using the DSP TMS320F28379D controller board and Matlab/Simulink. The switching frequency is generated to drive the MOSFET switching gates of each converter using a PWM control signal at 20 kHz. The measured values of DC bus voltage, voltage, and current of the PEMFC, BATs, and SC bank were acquired by the LEM transducer sensors with the Hall effect. A controllable DC load simulator is used to set up the step-changing load scenario. The characteristics of this DC load simulator are described in Table 3.8.

Table 3.8 DC load simulator characteristics

Parameter	Value
Voltage range	0 – 150 (V)
Current range	0 – 60 (A)
Maximum power	350 (W)
Constant current range	2/6/60 (A)
Constant voltage range	16/80/150 (V)
Constant power range	7/35/350 (W)
Constant resistance range	0.05 – 250 (Ω)

The experiment is carried out to increase the persuasion of the proposed EMS. The experiment is conducted using the step-changing load profile. The experimental result of load power adaptation, power distribution, and DC bus voltage is presented from Figure 3.22 to Figure 3.24.

(a)
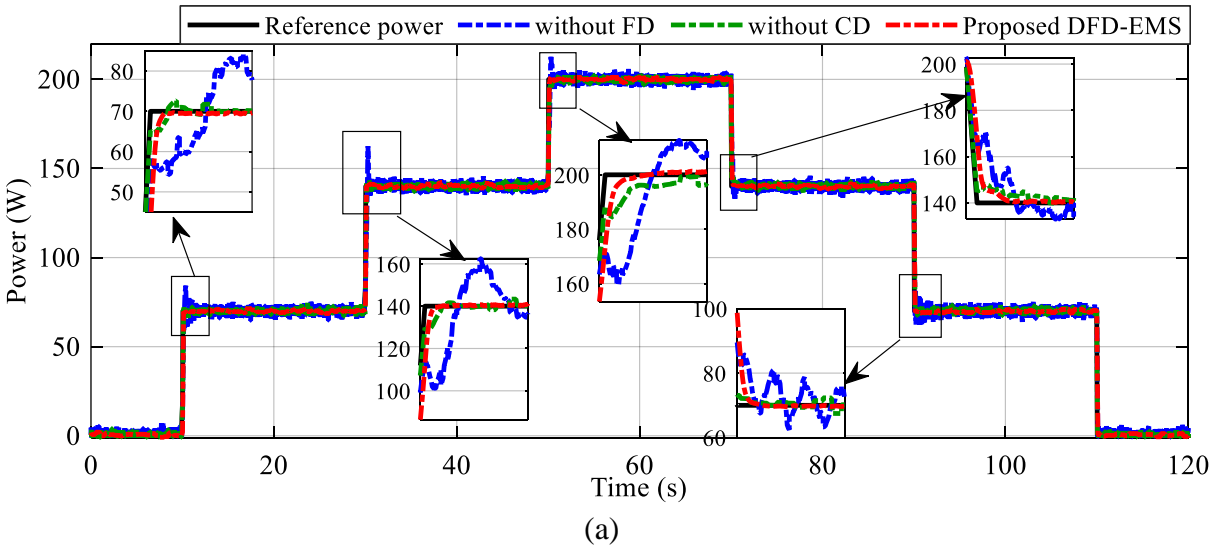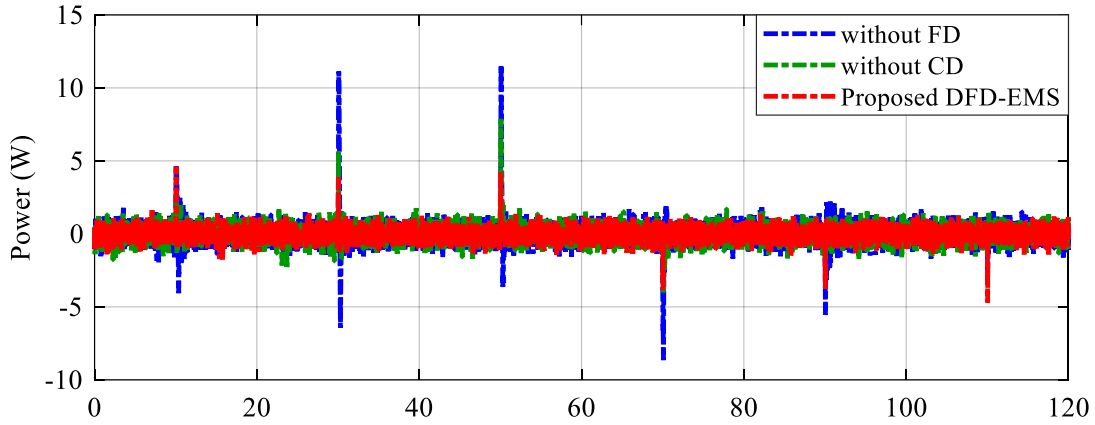
(b)

Figure 3.22 The load power adaptation of three EMSs. (a) The tracking performance. (b) The power tracking error.

Firstly, the load power adaptation of three EMSs with the same initial conditions is compared in Figure 3.22(a). It can be seen that the proposed strategy shows a good working performance with the closely same response of load demand satisfaction. As a result, the experiment's power of the proposed DFD-EMS has the smallest ripple approximated ±0.5 W and the peak power tracking error in the range of (-3.5 → 4.5) W in comparison to the required load power, while the power tracking error of strategies without FD and without CD is in a range of (-4 → 7.5) W and (-8 → 12) W, respectively, as described in Figure 3.22 (b).
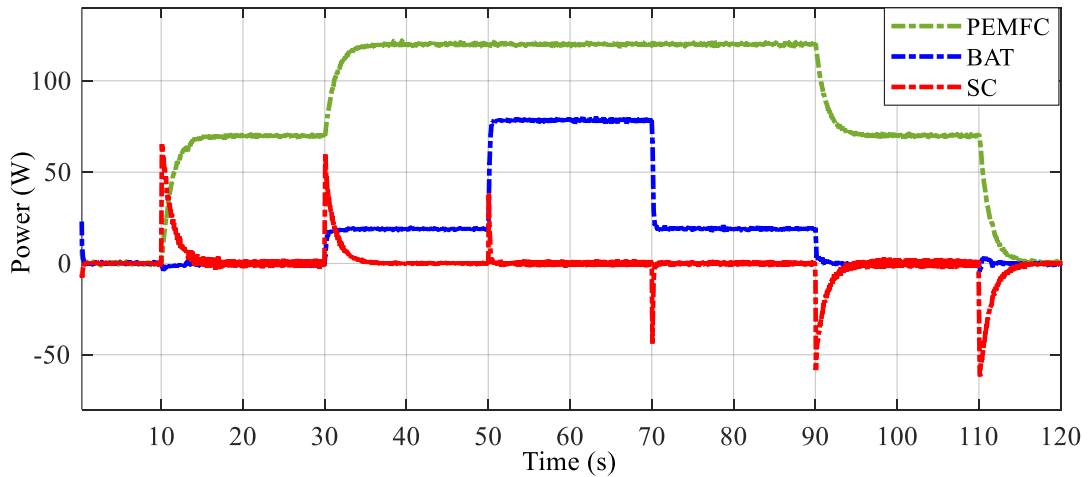
Figure 3.23 The power distribution of PEMFC, BAT, and SC by using the proposed EMS.

Based on the good tracking performance of the proposed strategy, the power distribution of three energy sources is shown in Figure 3.23. It can be observed that the PEMFC supplied energy as a primary power source and increases slowly until reaching the required power of the load. The lacking power was provided by the BAT in the steady-state and the SC in the transient state. In order

56

to reduce the power fluctuation of the PEMFC, the BAT provided supplemental power to the PEMFC with a faster power response than the PEMFC's power response. Meanwhile, the SC bank delivered the highest power response to deal with the peak power demand of load at the transient states, which also compensated for the total insufficient power of PEMFC and BAT to meet the requirement of load at a slow rate.
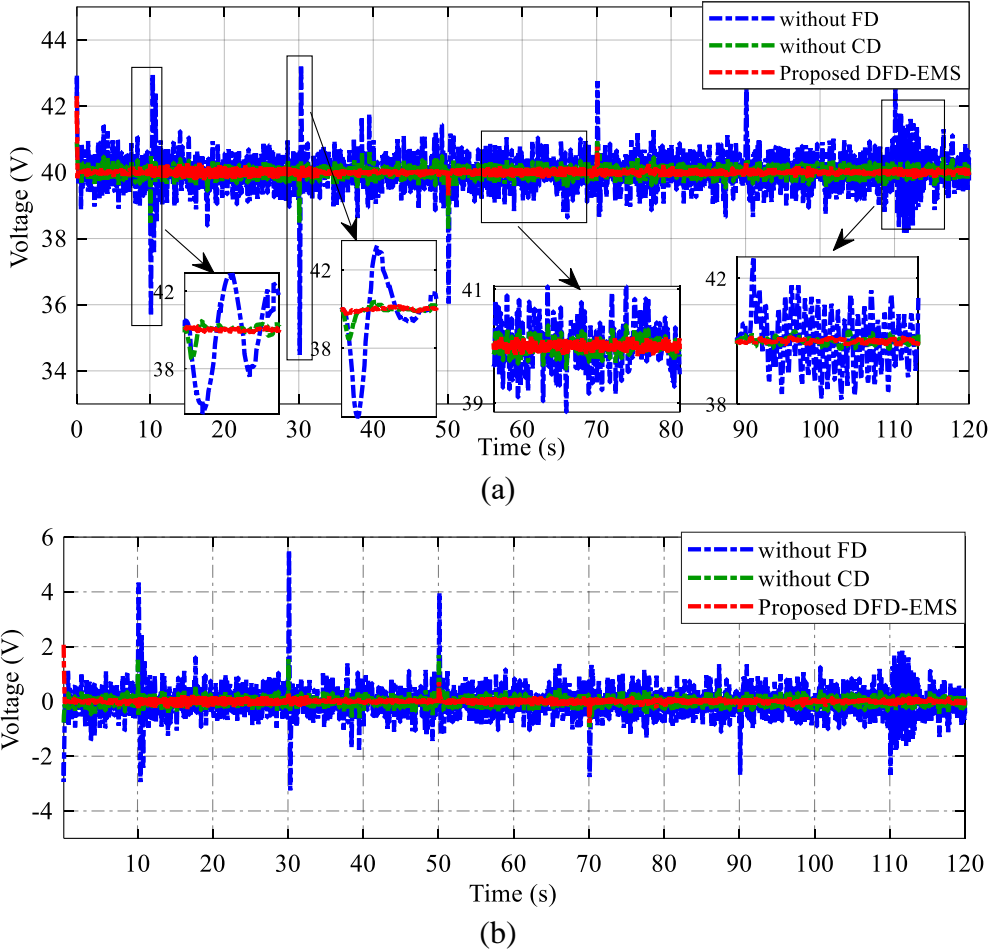
Figure 3.24 The comparison results of DC bus voltage by using three EMSs. (a) Voltage tracking. (b) Tracking error.

The comparison of DC bus voltage by using three EMSs is described in Figure 3.24. It is easily observed that the experimental DC bus voltage of the proposed strategy is steadily maintained at around the desirable value (40 V) with a small voltage ripple and the overshoot voltage in a range of (39.3 → 40.7) V, approximated by 3.5 %. This result shows the effectiveness of the proposed adaptive DC bus voltage controller that could maintain the stable bus voltage despite the load power variation.

3.7 Conclusion

In this chapter, a comprehensive EMS is proposed with high- and low-level control to guarantee the load power adaptation, determine the power-sharing between energy sources, and regulate the stable DC bus voltage. In high-level control, the combination of deterministic rules and the FD method is used to control the power-sharing of energy sources. According to the different characteristics of energy sources, the FD decomposes the load power demand into three frequency power ranges which involved the PEMFC, BAT, and SC behaviors. In addition, the low-level control is designed to maintain the stability of DC bus voltage based on the analysis of the dynamics response of converters through the Bode diagram to guarantee the operation modes of converters. Finally, the simulation and experiment on the real hybrid power system test bench are implemented to evaluate the effectiveness of the proposed strategy. The obtained simulation results with the step-changing load reveal that the proposed strategy achieves the DC bus voltage with 1.75% ripple, 48.1043% of PEMFC stack efficiency, and 0.2995 (g) hydrogen consumption, while the specific driving cycle has a DC bus voltage ripple of 1.98 %, PEMFC stack efficiency, and hydrogen consumption get 48.3026 % and 0.2609 (g) respectively. For the experiment performance, the proposed strategy maintains the DC bus voltage ripple at 3.5 % in the case of a step-changing load.

Simulation and experimental results are summarized as follows:

		Step-changing load			Specific driving cycle			Experiments		
		without FD	without CD	Proposed	without FD	without CD	Proposed	without FD	without CD	Proposed
Power tracking error	*RMSE*	0.628	0.341	**0.176**	0.163	0.158	**0.107**	0.749	0.629	**0.484**
	Me	12.768	7.279	**3.955**	5.833	5.58	**2.029**	11.586	7.879	**4.706**
	SD	0.63	0.342	**0.176**	0.162	0.157	**0.106**	0.748	0.628	**0.484**
DCbus voltage ripple (%)		24.5	6.5	**1.75**	9	3.75	**1.68**	25.3	6.92	**3.5**
FC stack efficiency (%)		46.8046	47.9513	**48.1043**	47.1067	48.1049	**48.3026**			
H2 consumption (g)		0.3002	0.2998	**0.2995**	0.2811	0.2693	**0.2609**			

Chapter 4

FUZZY LOGIC-BASED EMS

In this chapter, a control strategy in high-level control based on fuzzy logic rules (FLRs) and a frequency decoupling (FD) approach is proposed to improve model uncertainty and complex decisions of deterministic rules. Firstly, FLRs are designed to determine an appropriate reference PEMFC power to supply traction load by using the BAT SOC and load power demand. Secondly, the combination of FLRs and FD method is mainly utilized to ensure the proper power distribution of each energy source based on their dynamic characteristics and operating frequency ranges. Next, current and voltage control loops are designed to provide the appropriate gains for compensators that can maintain a stable voltage on the DC bus. Finally, simulation and experiment are conducted in two case studies of step-changing load and specific driving cycle load to validate and compare the effectiveness of the proposed strategy compared to the deterministic rules. Obtained results present that the proposed EMS achieves the highest distributed power accuracy while reducing the DC bus voltage ripple under various load working conditions in comparison to the other approach.

4.1 Introduction

In order to deal with model uncertainty and complex decisions, FLRs have been applied in several studies for HPS's control strategies and energy management to determine the power distribution between the primary source and the ESS while guaranteeing the system operated in a high-efficiency or fuel economy mode. In [8], Fagundes et al. proposed a fuzzy controller for energy management in the hybrid system of fuel cells and energy storage units. This approach was suitable for compensating/absorbing power during load transients, minimizing fuel cell stack damages, and balancing the SOC status of ESS through the charging/discharging process. For FCEV, in [62, 69], FLRs and flatness control were combined to split the energy flow between three electrical sources. This strategy gained high efficiency in power-sharing from energy sources to satisfy the load power demand in different operating modes. To protect BAT from overcharging, a real-time fuzzy logic was described by Hemi et al. in [70] for three configurations of FCEV. The simulation results confirmed that the proposed strategy could satisfy the load power demand with the unknown driving cycles and achieve power distribution among energy sources. In [33, 34], fuzzy-based EMSs were exploited for integrated PEMFC-BATs-SCs to improve the hybrid vehicle behaviors, enhance system efficiency, and prolong the component lifespan. For the fuel cell

excavator system, Truong et al. [60] used the fuzzy-based EMS to maintain the load power demand, minimize fuel economy and ensure the SOC of ESS. Using the same object, Dao et al. [61] introduced a combination of fuzzy-based EMS and optimal techniques to update the fuzzy membership functions (MFs) to save fuel consumption while improving system performance. Besides, depending on the different characteristics of power sources, the frequency decomposition techniques were applied to regulate the dynamic response, improve the power-sharing accuracy, and extend the lifetime of devices. Based on the Ragone diagram, LPFs were used in [71] to decompose the frequency ranges allowed by each power source, and improve the power performance of HPS while reducing stress and power fluctuation on the PEMFC and ESS. To achieve the optimum distribution of energy between the sources, Snoussi et al. [31] proposed an adaptive filtering-based EMS for minimizing hydrogen consumption and maintaining the constraints of each device such as permissible limitation of storage system capacities and battery current variation. According to the presented studies, the fuzzy logic technique and frequency decomposition approach performed well for power distribution between the PEMFC and ESS in the hybrid system. In [59, 72], an EMS with the combination of FLRs and frequency decoupling method using FPFs was proposed for HPS to achieve the appropriate power distribution and maintain a stable DC output voltage. However, the controllers of DC-DC converters in HPS are designed by the trial and error method without investigating the dynamic characteristics of these converters. As a result, it is difficult to identify suitable compensator gains. This can result in a shortage of supplied power for the load, especially if the required power varies abruptly. Therefore, the development of EMS considering the design of controller gains for DC-DC converters is required to achieve overall system qualification and improve the stable DC bus voltage delivered to the load under different working conditions.

4.2 Proposed Fuzzy Logic Rules-Based EMS

In this work, the proposed control strategy is designed to determine the power distribution of three electrical sources based on the load power demand and SOC of ESS. Additionally, the control scheme of DC bus voltage regulation is considered to guarantee stable voltage during power fluctuation and track the speed limitation of the power converter. The block diagram of the proposed control strategy is described in Figure 4.1.

In this hybrid system, the PEMFC is utilized as a primary source that not only supplies power for the traction load but also ensures the SOC level of the BAT within the desired range. As a result, the load power demand (P_{load}) and the BAT SOC (SOC_{BAT}) are taken as two inputs for the FLRs [72] to generate the reference PEMFC power (P_{FC}). This power is passed to the low-pass

filter (LPF-1) to decompose into low- and high-frequency powers. Then, the reference PEMFC power (P_{FC}^{ref}) is obtained as the low-frequency power of the PEMFC that is used to calculate the energy storage system power (P_{ESS}). Next, the low-pass filter (LPF-2) is used to decompose the P_{ESS} into low and high-frequency powers, which are defined as the BAT's reference power (P_{BAT}^{ref}) and reference supercapacitor power (P_{SC}^{ref}). In addition, the BAT is used to keep the DC bus voltage at the reference value through the voltage control loop. The reference (V_{DC}^{ref}) and measured DC bus voltage (V_{DC}) are compared with each other, and the difference voltage then is provided to the PI controller (PI-2 control) to produce the DC bus current. Due to the fast dynamic response, the SC will take care of the uncompensated power of the PEMFC and BAT. Thus, the SC reference power consists of high-frequency elements of the PEMFC and BAT power.
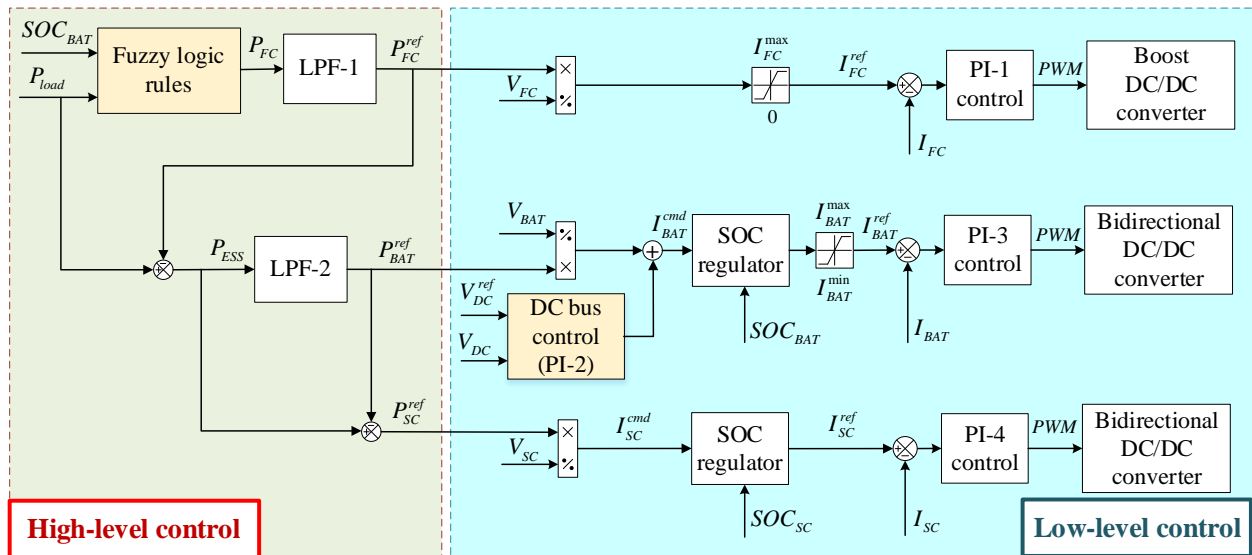
Figure 4.1 Proposed energy control strategy.

4.3 High-Level Control Design

In this strategy, the FLRs are inherited from our previous papers in [59, 72] to calculate the reference power of the PEMFC based on the load power demand and SOC level of BAT. These rules have two input variables (P_{load}, SOC_{BAT}) and one output variable (P_{FC}). Seven membership functions (MFs) are used to characterize the input variable P_{load} including NH (Negative High), NM (Negative Medium), NL (Negative Low), Z (Zero), PL (Positive Low), PM (Positive Medium), PH (Positive High) within the range of (-1,1). For the input variable SOC_{BAT}, five MFs divided into VL (Very Low), L (Low), M (Medium), H (high), and VH (Very High) with the scope as (0.4,

0.9). The output P_{FC} is characterized by five MFs: Min (Minimum), ML (Medium-Low), M (Medium), MH (Medium-High), and Max (Maximum). The inhomogeneous MFs of the inputs and output are depicted in Figure 4.2 and the fuzzy rules are described in Table 4.1.

(a)

(b)

(c)
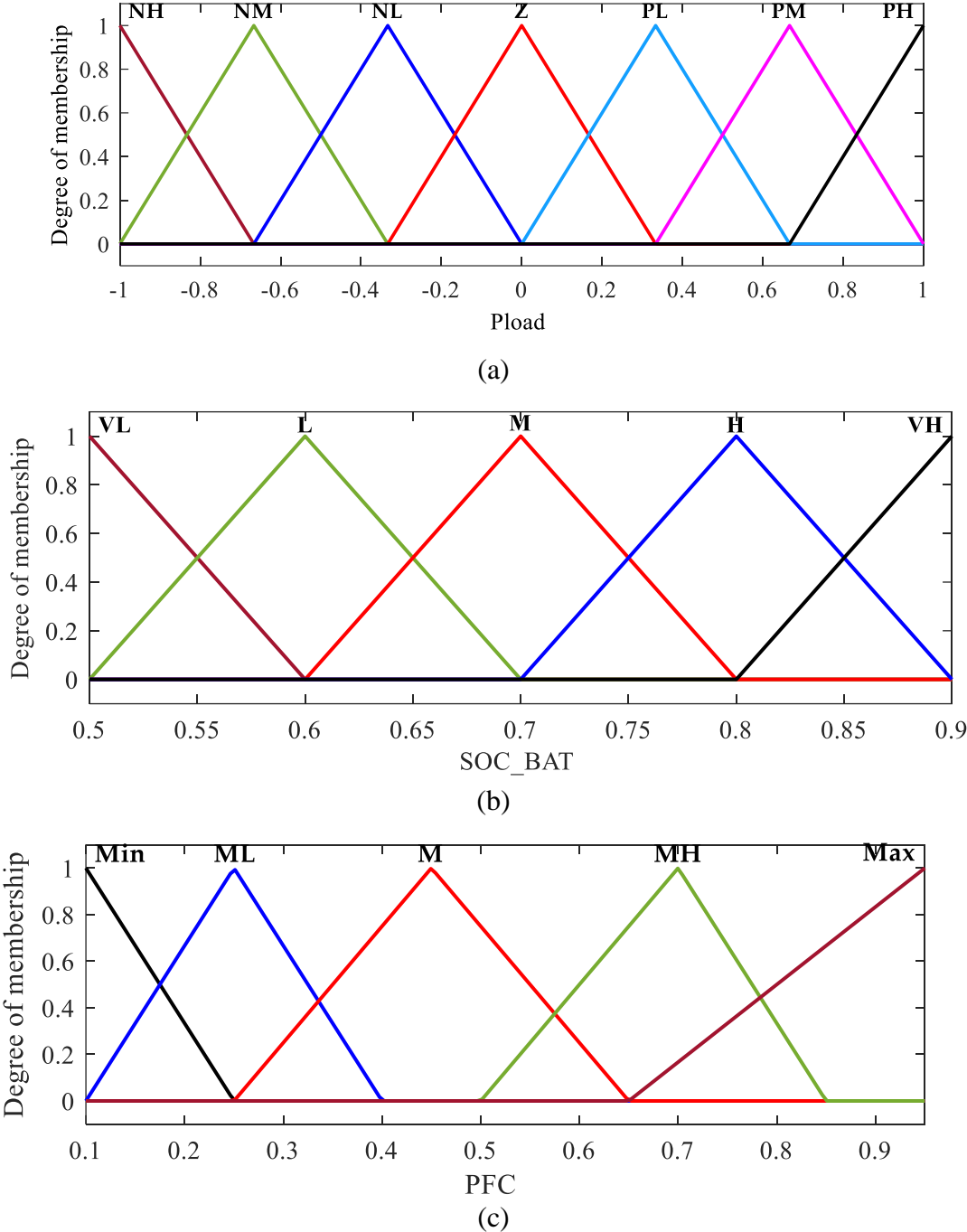
Figure 4.2 Inputs and output membership functions of the FLRs. (a) Input variable P_{load}. (b) Input variable SOC_{BAT}. (c) Output variable P_{FC}.

Table 4.1 Fuzzy rules for the inputs and output membership functions [18].

P_{FC}		P_{load}						
		NH	NM	NL	Z	PL	PM	PH
SOC_{BAT}	VL	Min	Min	ML	M	M	MH	Max
	L	Min	Min	Min	ML	ML	M	MH
	M	Min	Min	Min	Min	ML	M	MH
	H	Min	Min	Min	Min	Min	M	MH
	VH	Min	Min	Min	Min	Min	ML	M

The suggested fuzzy rules distribute the needed power to the PEMFC source in order to not only supply the workload requirement but also maintain the SOC supplement of the BAT. For instance, during the charging process, if the BAT SOC is high level, the injected power is lower, and vice versa. Meanwhile, during the discharging process, if the BAT SOC is at a high level, the BAT will release more output power and vice versa.

Furthermore, low-pass filters are applied to decompose the demand power that corresponds to the operating ranges and power changing rate of the PEMFC, BAT, and SC, using the Rangone diagram theory [30] and the dynamic features of energy sources. This approach is advantageous for experimental applications because of its rapid computation time and simple design. For the PEMFC, the low-frequency or reference power is derived from the required PEMFC power as follows:

$$P_{FC}^{ref} = G_1(s)P_{FC} \tag{4.1}$$

$$G_1(s) = \frac{2\pi f_{c1}}{2\pi f_{c1} + s} \tag{4.2}$$

where P_{FC}^{ref} is the reference PEMFC power (W), P_{FC} is the required PEMFC power (W), $G_1(s)$ is the function of the low pass filter (LPF-1), and f_{c1} is the cut-off frequency to define the reference PEMFC power (Hz).

Based on the PEMFC reference power, the ESS power is determined as given

$$P_{ESS} = P_{load} - P_{FC}^{ref} \tag{4.3}$$

where P_{ESS} is the energy storage system power (W), P_{load} is load power demand (W).

For the BAT, the reference BAT power is obtained by using the low-pass filter 2 to separate the low- and high-frequency BAT power. This power can be defined as follows:

$$P_{BAT}^{ref} = G_2(s).P_{ESS} \tag{4.4}$$

$$G_2(s) = \frac{2\pi f_{c2}}{2\pi f_{c2} + s} \tag{4.5}$$

where $G_2(s)$ is the transfer function of LPF-2, f_{c2} is the cut-off frequency of the reference BAT power (Hz).

The reference SC power is defined based on the high-frequency powers of PEMFC and BAT because the fast dynamic response of SC can be used to compensate for the abrupt load fluctuation that cannot adapt by PEMFC and BAT.

$$P_{SC}^{ref} = P_{ESS} - P_{BAT}^{ref} \tag{4.6}$$

The reference powers of PEMFC, BAT, and SC are used to determine the reference currents of these power sources, which are compared with measured currents to generate input signals for control loops of converters.

4.4 Low-Level Control Design

Similar to chapter 3, compensators of voltage and current control loops are analyzed and designed to guarantee the adaptation of DC/DC converters for required power of energy sources and DC bus voltage regulation. The detailed procedure of the four PI controllers designed in low-level control can be referred to in section 3.4.

The reference PEMFC current can be given by

$$I_{FC}^{ref} = \frac{P_{FC}^{ref}}{V_{FC}} \tag{4.7}$$

where I_{FC}^{ref} is the reference PEMFC current (A), V_{FC} is the measured PEMFC voltage (V).

The reference BAT current can be obtained as the output of the SOC regulator block as follows:

$$I_{BAT}^{ref} = \begin{cases} \alpha_1 \left| I_{BAT}^{cmd} \right| & if & SOC_{BAT} \leq SOC_{BAT}^{\min} \\ I_{BAT}^{cmd} & if & SOC_{BAT}^{\min} < SOC_{BAT} < SOC_{BAT}^{\max} \\ \beta_1 \left| I_{BAT}^{cmd} \right| & if & SOC_{BAT} \geq SOC_{BAT}^{\max} \end{cases} \tag{4.8}$$

where I_{BAT}^{ref} is the reference current of the BAT (A), I_{BAT}^{cmd} is the required BAT current (A), SOC_{BAT} is the BAT status (%), $SOC_{BAT}^{\min}$ and $SOC_{BAT}^{\max}$ are the minimum and maximum allowable SOC level of the BAT (%), α_1 and β_1 are the tuning parameters that can be referred in Chapter 3.

The same as BAT, the reference current for the SC can be considered as follows:

$$I_{SC}^{ref} = \begin{cases} \alpha_2 \left| I_{SC}^{cmd} \right| & if & SOC_{SC} \leq SOC_{SC}^{min} \\ I_{SC}^{cmd} & if & SOC_{SC}^{min} < SOC_{SC} < SOC_{SC}^{max} \\ \beta_2 \left| I_{SC}^{cmd} \right| & if & SOC_{SC} \geq SOC_{SC}^{max} \end{cases} \qquad (4.9)$$

where I_{SC}^{ref} is the reference current of the SC (A), I_{SC}^{cmd} is the required SC current (A), SOC_{SC} is the SC status (%), SOC_{SC}^{min} and SOC_{SC}^{max} are the minimum and maximum allowable SC SOC (%), respectively; α_2 and β_2 are the tuning parameters that can be referred in Chapter 3.

4.5 Simulation Results

In this section, simulation results are conducted with two types of load profiles: step-changing load and specific driving cycle load as presented in Figure 2.8. The proposed fuzzy strategy (proposed fuzzy-EMS) is compared with the deterministic-frequency decoupling method (DFD-EMS) in Chapter 3 to demonstrate the system performance during the fluctuation of load power demand. In addition, the modeling of the HPS is carried out in MATLAB/Simulink environment, with a sampling time of 0.05 ms set up for displaying simulation results. Specifications of energy sources and parameters of the proposed EMS are referred to in Tables 3.4 – 3.7 of section 3.5.

4.5.1 Case Study 1: Step-Changing Load

The hybrid system performance and control strategy effectiveness are described from Figure 4.3 to Figure 4.8 in which a continuous black line represents the reference power of the load, a dashed-dot blue line indicates the power of the DFD-EMS, and a dashed-dot red line displays the output power of the proposed fuzzy-EMS.

(a)

65

(b)
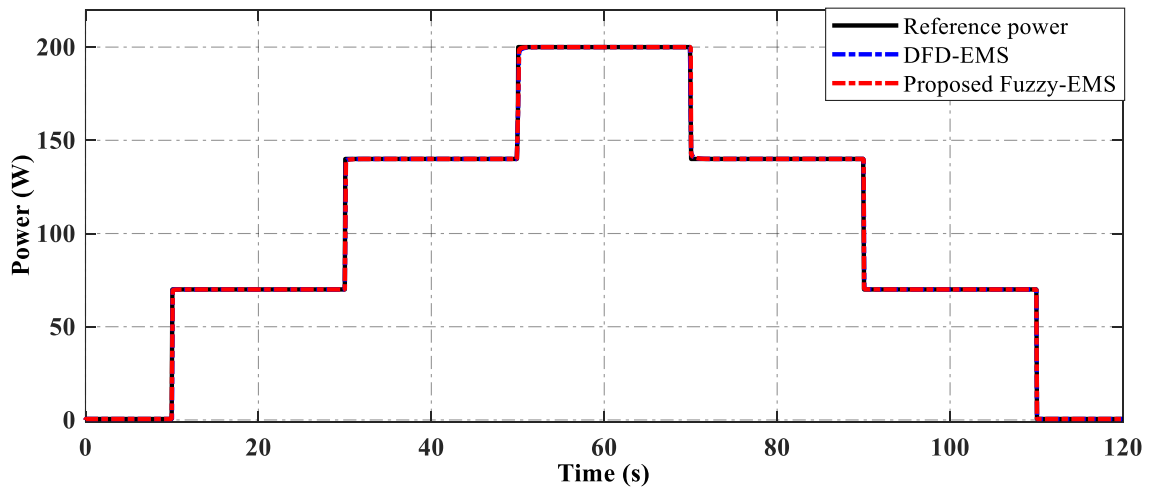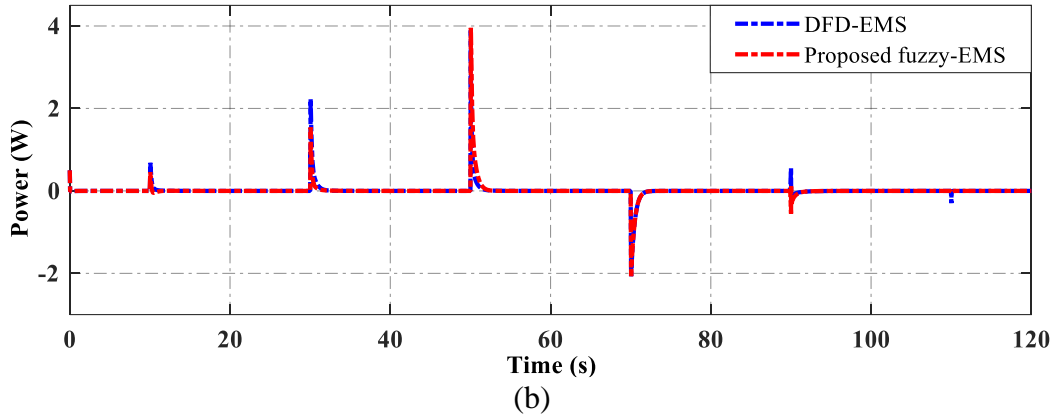
Figure 4.3 The comparison of power adaptation of two EMSs. (a) The adaptation of load power. (b) The tracking error power.

First of all, Figure 4.3 depicts the adaptation of load power using two EMSs. As shown in Figure 4.3 (a), the total power supplied by the HPS could completely fulfill the load requirement, even when an abrupt change occurred. However, the power tracking error in Figure 4.3 (b) presented that the released power of the proposed strategy adapts the load requirements better than the DFD-EMS at the moment of transient peak power of the 10th, 30th, 90th, and 110th. This demonstrates that the proposed approach can absolutely assure the load power demand during different operational situations.

(a)

(b)

66
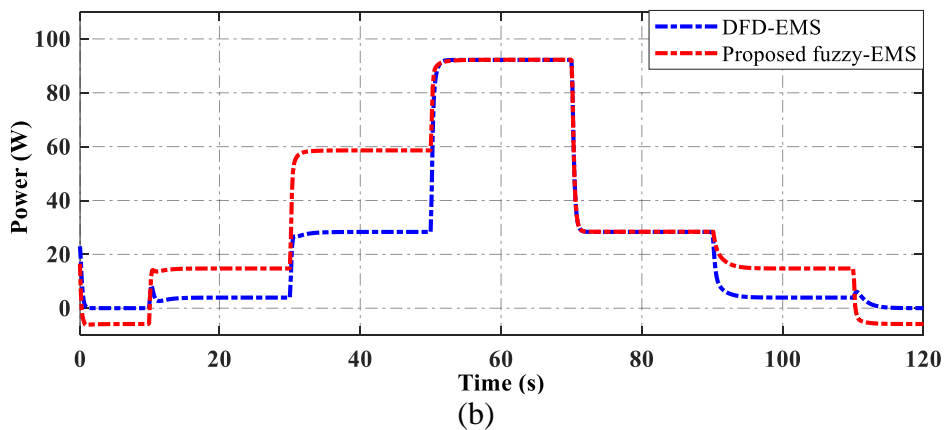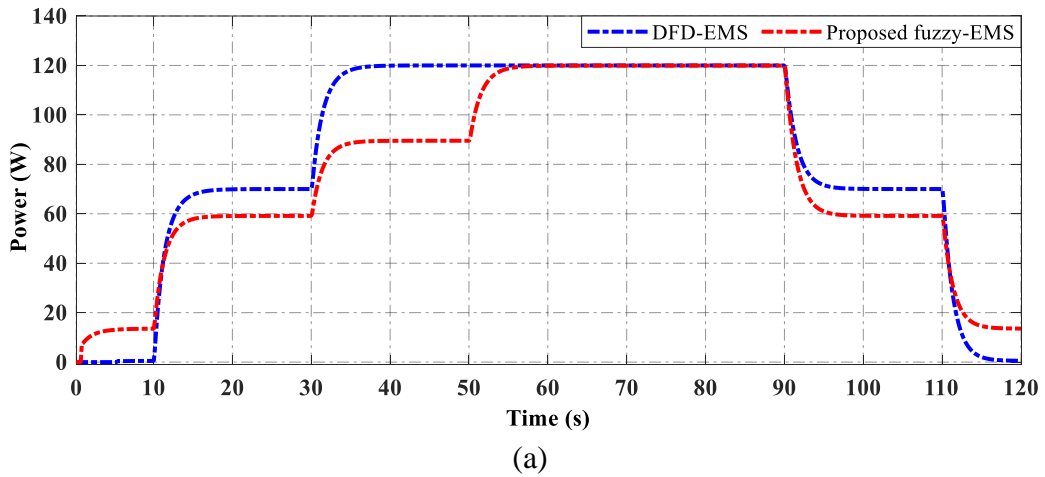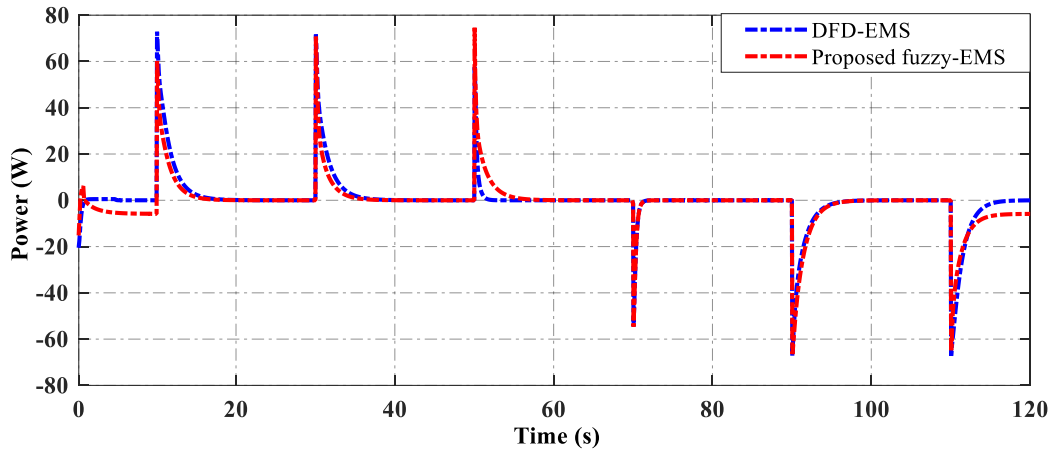
(c)

Figure 4.4 The power distribution from energy sources. (a) PEMFC. (b)BAT. (c) SC.

Next, the power distributions of the PEMFC, BAT, and SC in the hybrid system are shown in Figure 4.4. It can be seen that the EPMFC power distribution is more flexible corresponding to the load power variation by using the proposed fuzzy-EMS than the power distribution of DFD-EMS as shown in Figure 4.4 (a). This will help PEMFC system optimal working performance, improve efficiency, and save fuel economy. Meanwhile, BAT by using the proposed strategy provides more energy to support the PEMFC in a steady state to reduce the PEMFC's power fluctuation as presented in Figure 4.4 (b). In addition, SC is used to compensate for the peak power when the load changes abruptly at the moment of transient peak power and delivered the fast response of required power, and minimizes the fluctuating power on PEMFC and BAT. The power compensation from the BAT and SC maintains the load-tracking performance at each moment of transient peak power even if the PEMFC, with the lowest dynamics, can not react to the change in load right away.

(a)

67

(b)
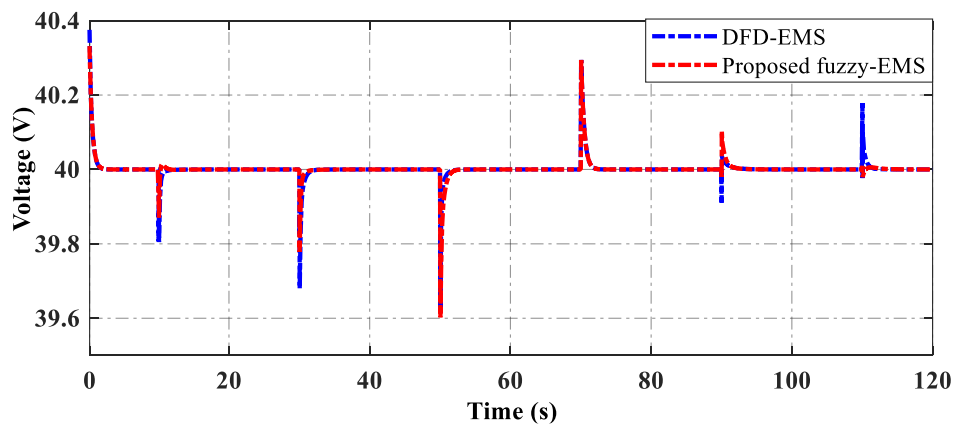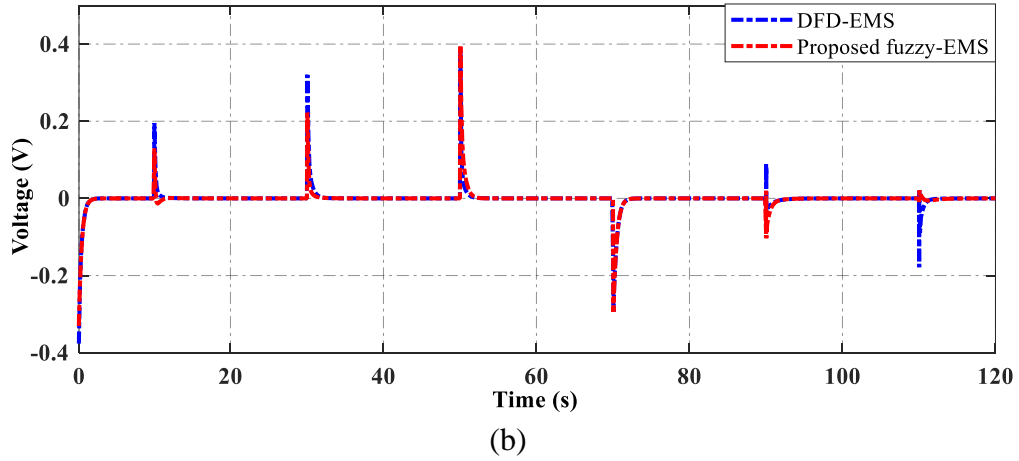
Figure 4.5 The comparison of the DC bus voltage. (a) Voltage tracking. (b) Voltage tracking error.

The comparison of DC bus voltage by using two EMSs is depicted in Figure 4.5. The proposed fuzzy-EMS and DFD-EMS maintain the DC bus voltage stably at around 40 V with small fluctuation. In particular, two strategies produce a DC bus peak voltage in the range of $(39.6 \rightarrow 40.3)$ V, which is approximated by a 1.75 % voltage ripple during the step-change interval of the load. However, in several transient points of 10th, 30th, 90th, and 110th, the voltage tracking error of DFD-EMS is higher than the proposed strategy. This result illustrated that the time response of the proposed strategy is better than the ones by using the DFD-EMS.

(a)

(b)
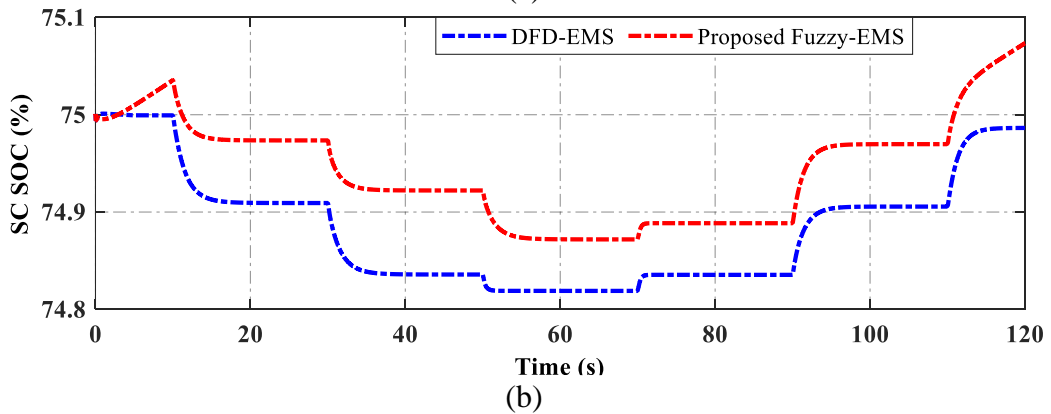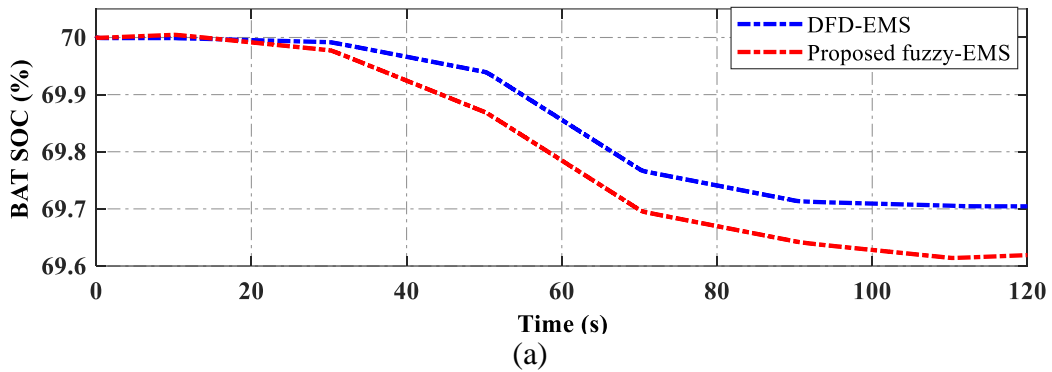
Figure 4.6 The SOC comparison. (a) BAT SOC. (b) SC SOC.

68

Fig 4.6 depicts the simulation results for both BAT and SC SOC, which characterize the charge and discharge state at each timeline when the load changes. As shown in Figure 4.6 (a), the proposed EMS can hold the SOC BAT level better than the DFD-EMS in the first 20 seconds of low load power demand. However, the proposed strategy shows faster SOC degradation than DFD-EMS after 20 seconds under high load power consumption. In contrast, for the SC, the proposed strategy and DFD-EMS achieve a stable SOC varying range with $\Delta SOC = 0.2 \%$ as presented in Figure 4.6 (b).

(a)

(b)
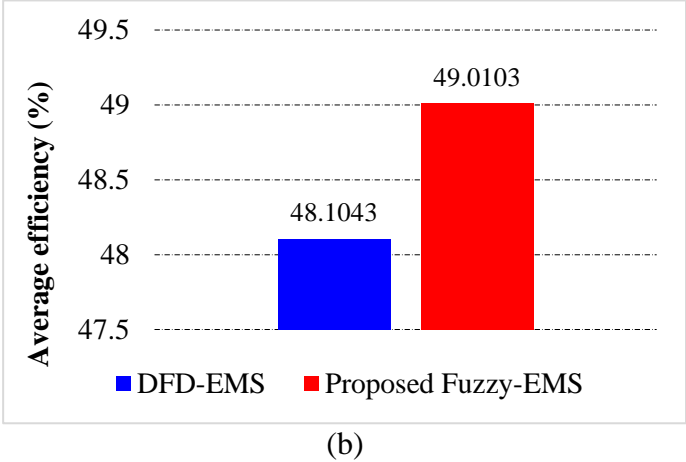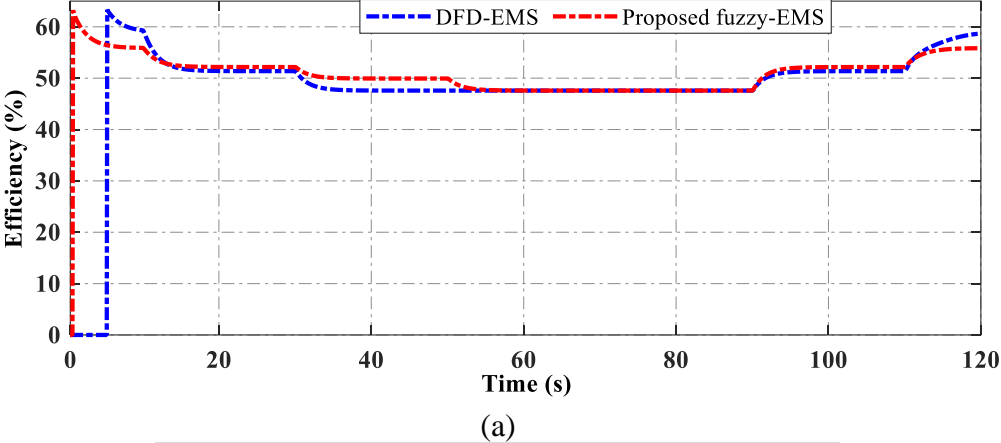
Figure 4.7 The PEMFC stack efficiency. (a) Efficiency status. (b) Average efficiency.

The comparative efficiency of the PEMFC stack is described in Figure 4.7. The efficiency status corresponding to levels of PEMFC power is depicted in Figure 4.7 (a). In addition, the average efficiency of the PEMFC stack is presented in Figure 4.7 (b). It can be seen that the PEMFC stack improves the average efficiency reached 49.0103 (%) by using the proposed strategy-EMS while the DFD-EMS has an average efficiency of 48.1043 (%).
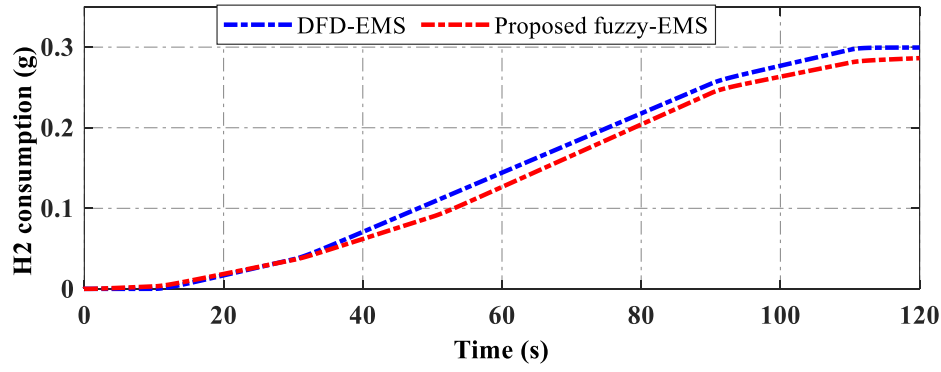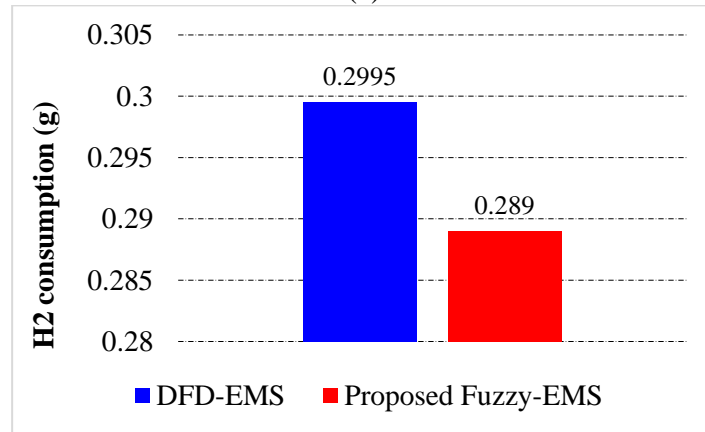
Figure 4.8 The comparison of fuel consumption. (a) H2 consumption status. (b) Total H2 consumption.

Figure 4.8 illustrates the comparison of hydrogen consumption by using two EMSs. As a result, the proposed EMS reduces hydrogen fuel consumption more than using the DFD-EMS. The total hydrogen fuel consumed by the proposed strategy is 0.289 (g), which is less than the DFD-EMS with 0.2995 (g). Because hydrogen consumes less energy than other methods, the proposed strategy saves fuel economy.

4.5.2 Case Study 2: Specific Driving Cycle

The effectiveness of two EMSs is verified by using the specific driving cycle as described in Figures 4.9 – 4.12. Parameters for simulation are inherited from section 3.5. These figures illustrate the workability of load satisfaction under two control strategies in which the black line is the required load power, and the load satisfaction under the DFD-EMS and the proposed fuzzy-EMS are presented by the dashed-dot blue line and dashed-dot red line, respectively. The behaviors of electrical devices, the DC bus voltage regulation, and the SOC status of BAT and SC are described in Figures 4.10, 4.11, and 4.12, respectively. Then, the PEMFC stack efficiency and hydrogen fuel consumption are depicted in Figure 3.21 and Figure 3.22, respectively.
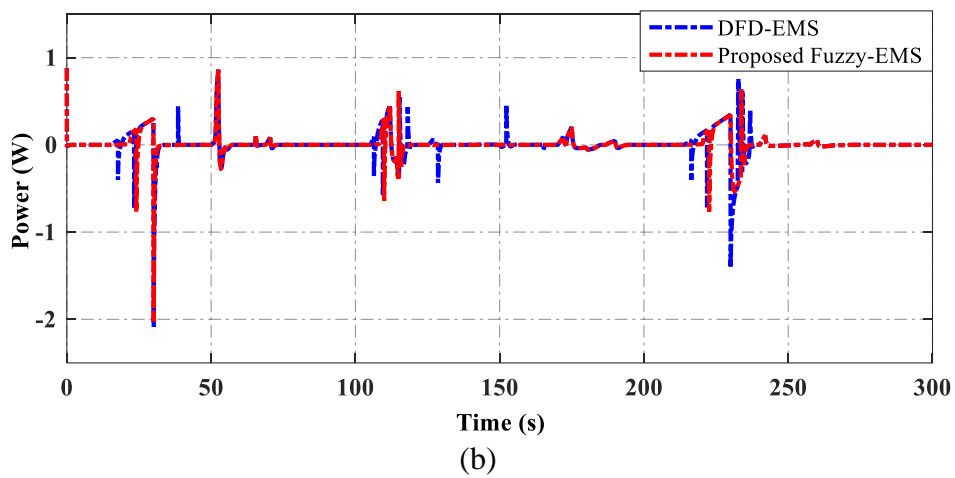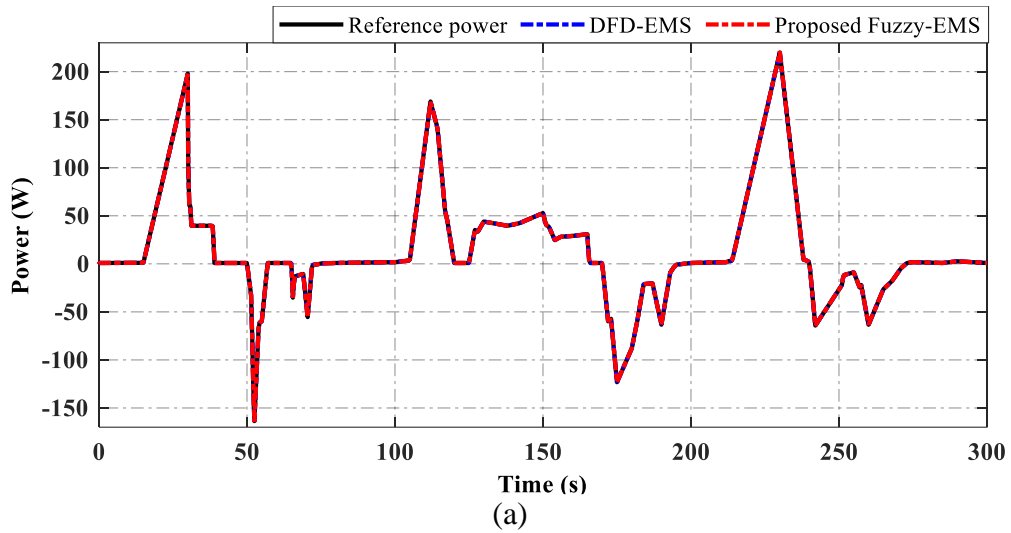
Figure 4.9 The comparison of load power adaptation based on three EMSs. (a) The load power adaptation. (b) The power tracking error.

The comparison of load power performance is presented in Figure 4.9. Firstly, it can be seen that two strategies can adapt to the load requirement as shown in Figure 4.9 (a). In addition, the detailed power tracking error is presented in Figure 4.9 (b). This figure shows that the proposed strategy obtains a better power tracking performance than the DFD-EMS with smaller insufficient power adaptation.

(a)
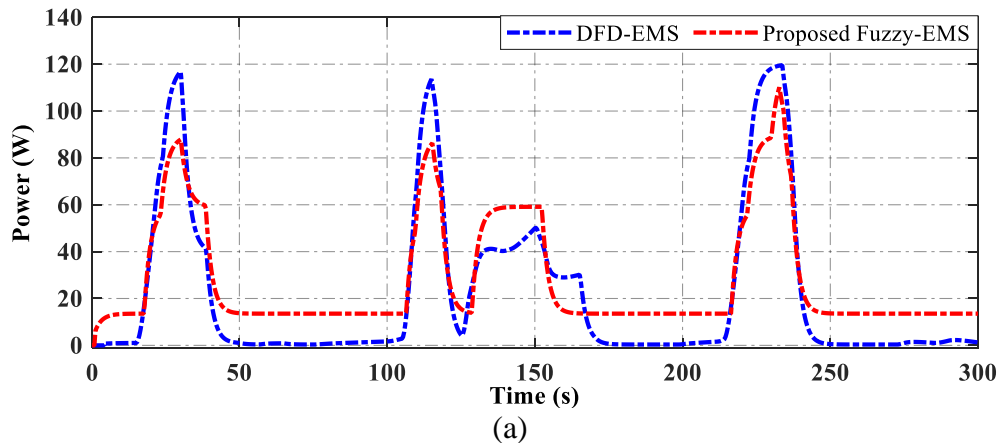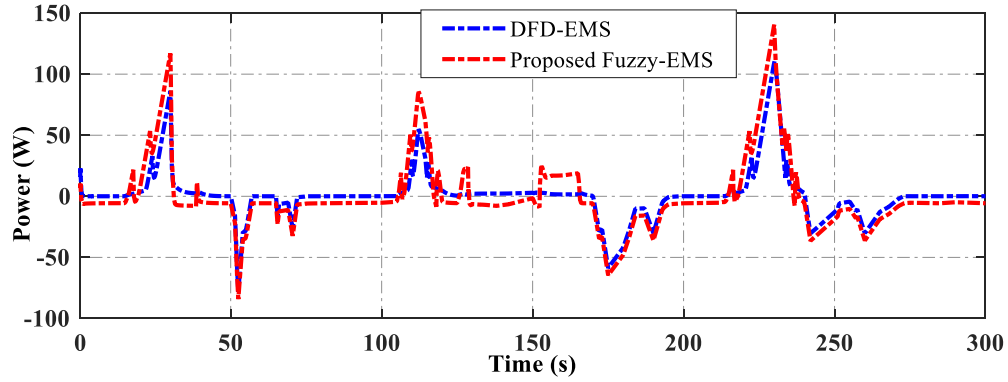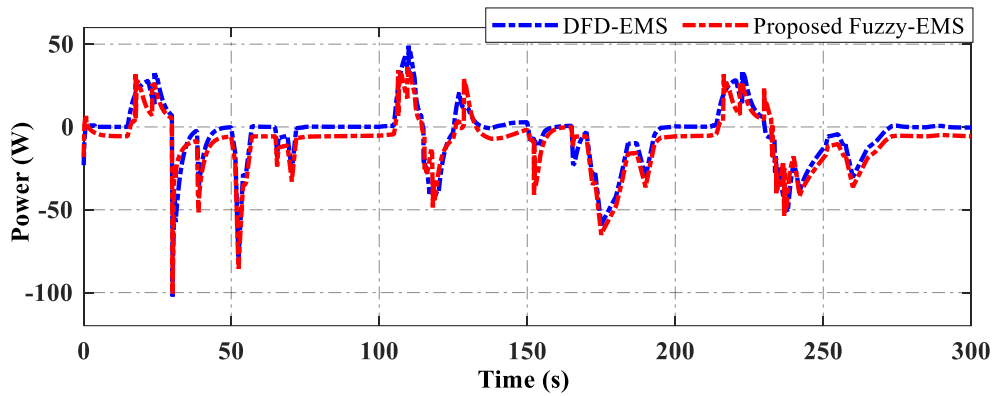
Figure 4.10 The power distribution of energy sources. (a) PEMFC. (b) BAT. (c) SC.

The power distributions of the PEMFC, BAT, and SC in the hybrid system are shown in Figure 4.10. It can be seen that the PEMFC power of the proposed fuzzy-EMS has an appropriate power level and smaller power fluctuation, which can improve the aging and performance of the PEMFC system. Meanwhile, the DFD-EMS provides a higher amplitude that can influence the PEMFC system performance. The power capability of the BAT and SC under two EMSs is presented in Figure 4.10 (b) and (c), respectively. Due to a lower released PEMFC power, the BAT and SC of the proposed strategy operate at a higher working power range to support the PEMFC power for adapting load power demand. As a result, the proposed algorithm can regulate the BAT and SC power in a suitable amplitude that can accommodate the load power fluctuation.

72

(b)
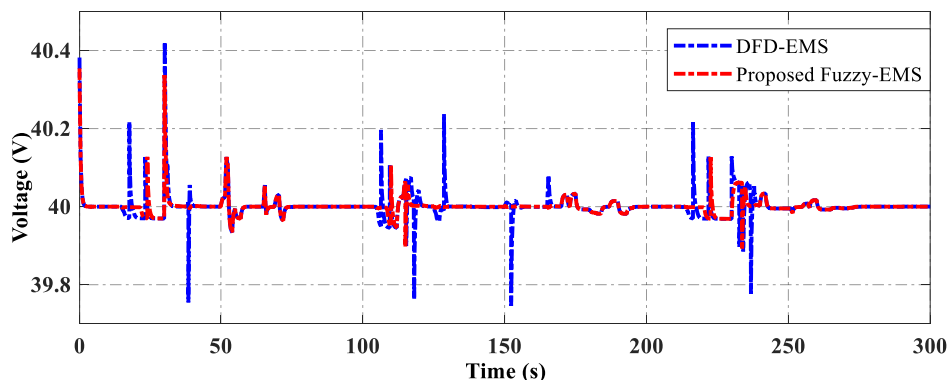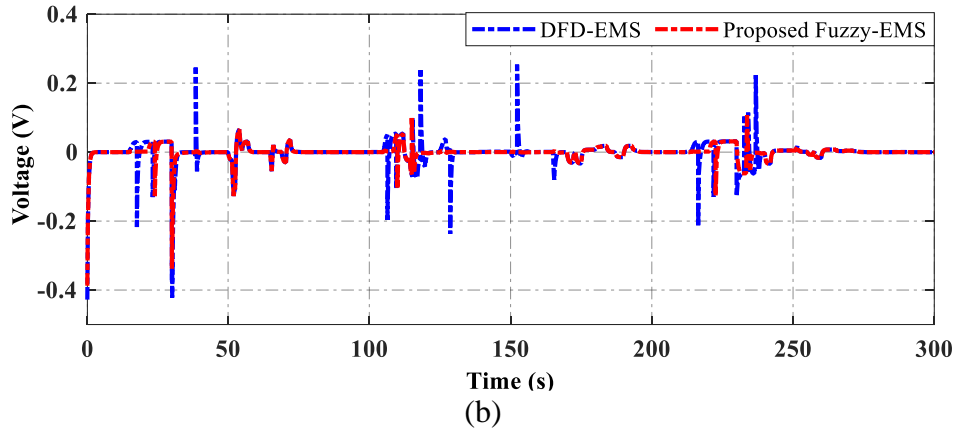
Figure 4.11 The DC bus voltage regulation. (a) Voltage tracking. (b) Tracking error.

Next, Figure 4.11 presents the DC bus voltage regulation of two EMSs. Generally, the DC bus voltage is steadily maintained at around 40 V with a small fluctuation. As described in Figure 4.11 (a) and (b), the proposed fuzzy-EMS guarantees the DC bus peak voltage in the range of (39.9 → 40.35) V with the tracking error of 0.45 V, approximated by a 1.13 % voltage ripple. Meanwhile, the DFD-EMS has a tracking error of 0.67 V, which takes the voltage ripple by 1.68%.

(a)

(b)
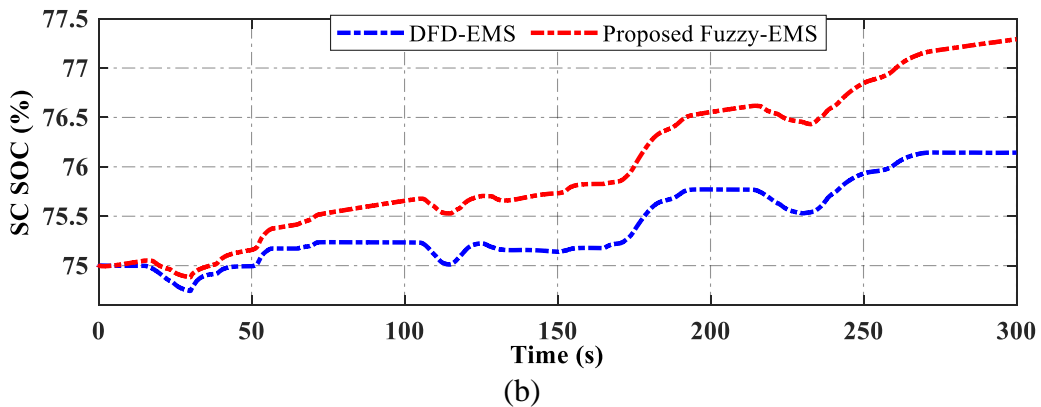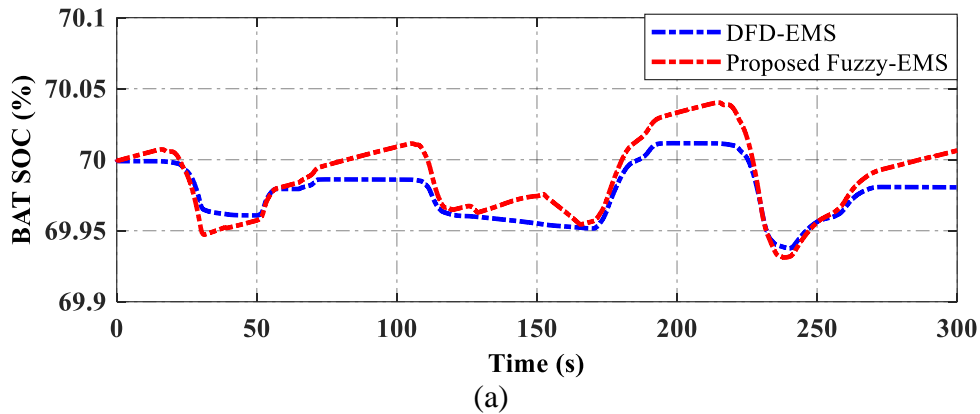
Figure 4.12 The SOC status. (a) BAT SOC. (b) SC SOC.

The SOC levels of both BAT and SC are depicted in Figure 4.12. In detail, Figure 4.12 (a) describes that the BAT SOC of the two strategies can maintain the low fluctuated range of (69.9 → 70.05) %. For the SC, Figure 4.12 (b) shows that the SOC level of the proposed EMS has a higher

73

increasing range of (74.95 → 77.3) % than the DFD-EMS varies from (74.9 → 76.2) %.
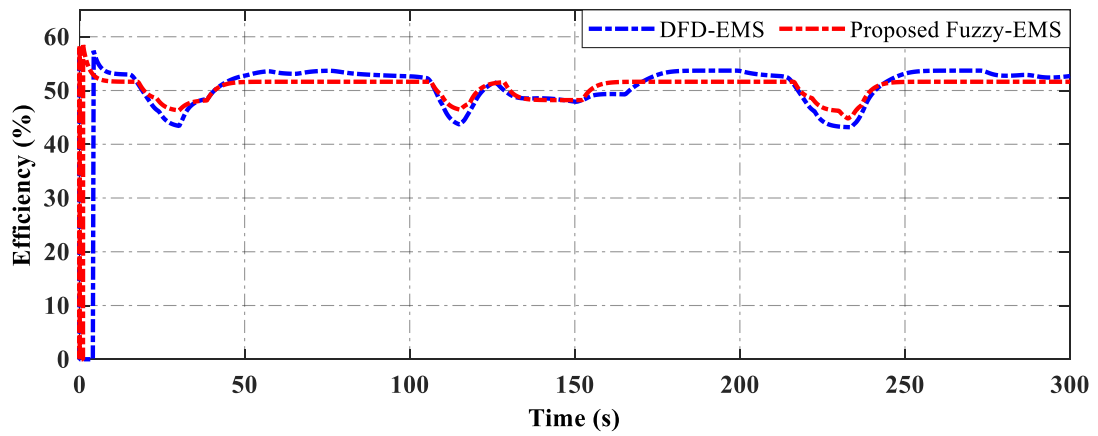
(a)
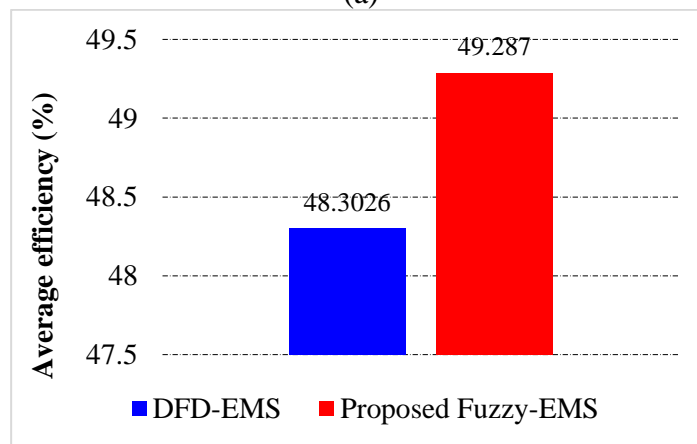
(b)

Figure 4.13 The comparison of PEMFC stack efficiency of PEMFC stack. (a) Efficiency status. (b) Average stack efficiency.

The PEMFC stack efficiency of two EMSs is described in Figure 4.13. As a result, the PEMFC stack of the proposed fuzzy-EMS has a higher average efficiency of 49.287 % than DFD-EMS with an efficiency of 48.3026 %.
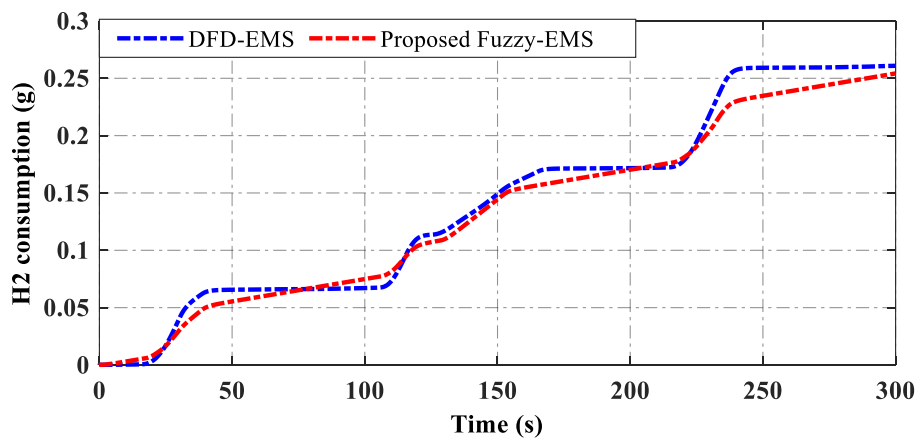
(a)
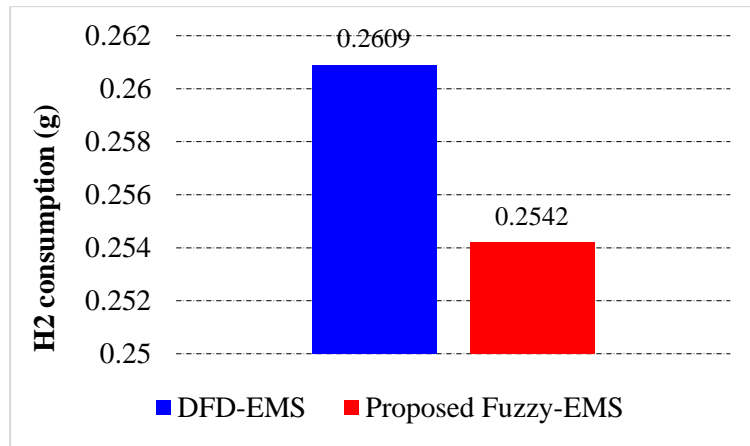
(b)

Figure 4.14 The comparison of hydrogen consumption. (a) H2 consumption status. (b) Total H2 consumption.

Finally, the hydrogen consumption is evaluated in Figure 4.14. In the case of the proposed strategy, the total hydrogen consumption is 0.2542 g during the time of the driving cycle, whereas the total fuel consumption of DFD-EMS is 0.2609 g. It can be seen that the proposed strategy has reduced the total fuel consumption with hydrogen consuming less than 2.57 % in comparison with the DFD-EMS.

4.6 Experimental Results

In this section, an HPS test bench, which is presented in section 3.6, is used to verify the effectiveness of the proposed strategy. The experiment is conducted using the step-changing load profile. The experimental result is presented in Figures 4.15 – 4.17.

(a)

(b)
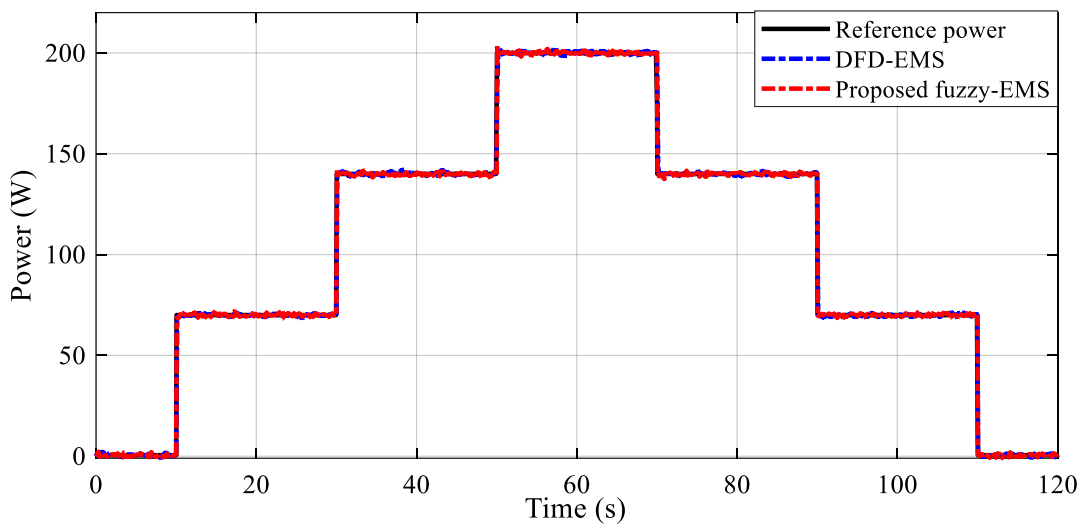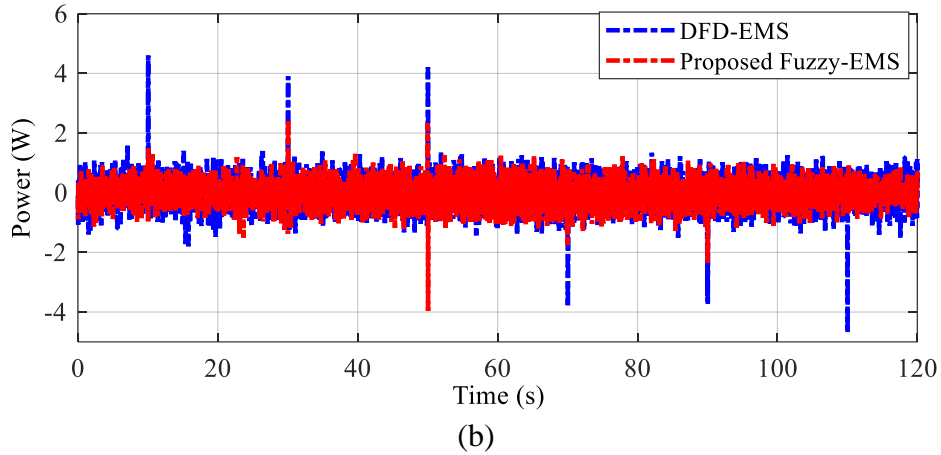
Figure 4.15 The load power adaptation of three EMSs. (a) The tracking performance. (b) The power tracking error.

Firstly, the load power adaptation of two EMSs is depicted in Figure 4.15. As shown in Figure 4.15 (a), the proposed fuzzy-EMS and the DFD-EMS have a good tracking performance and can adapt to load power demand under different working conditions. However, the power tracking error of the proposed strategy achieves a smaller tracking error. In detail, he proposed EMS gets the optimum distributed accuracy with the error in the range of $(-4 \rightarrow 2)$ W and the ripple around ± 0.5 W, while the DFD-EMS strategy has an inadequate power approximated $(-3.5 \rightarrow 4.5)$ W. The obtained results show that the proposed EMS has the best power adaptation with the smallest power fluctuations.
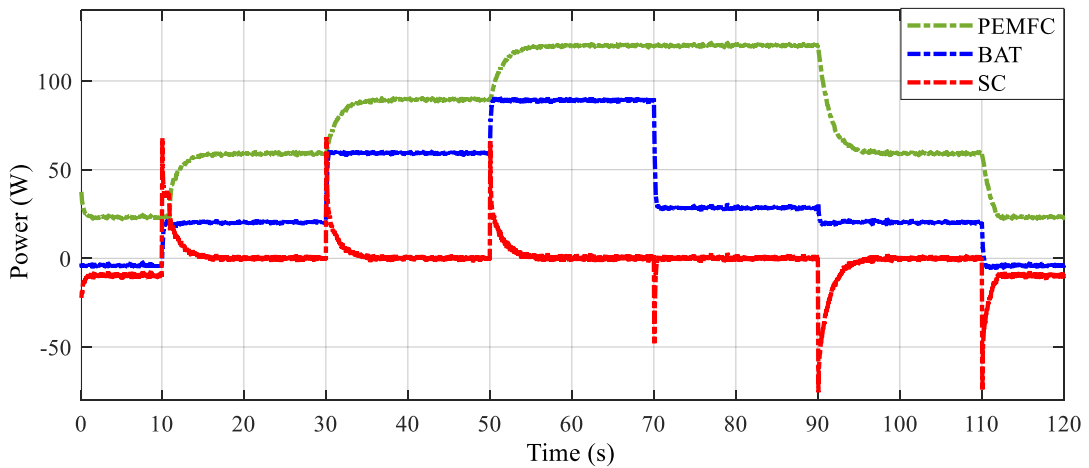
Figure 4.16 The power distribution of PEMFC, BAT, and SC by using the proposed EMS.

The power distribution of three energy sources based on the proposed EMS is shown in Figure 4.16. It can be seen that the PEMFC power distribution has a flexible power that can satisfy the load power demand by using fuzzy rules. The BAT and SC have a function to compensate for the lacked PEMFC power during the abrupt load change.

76
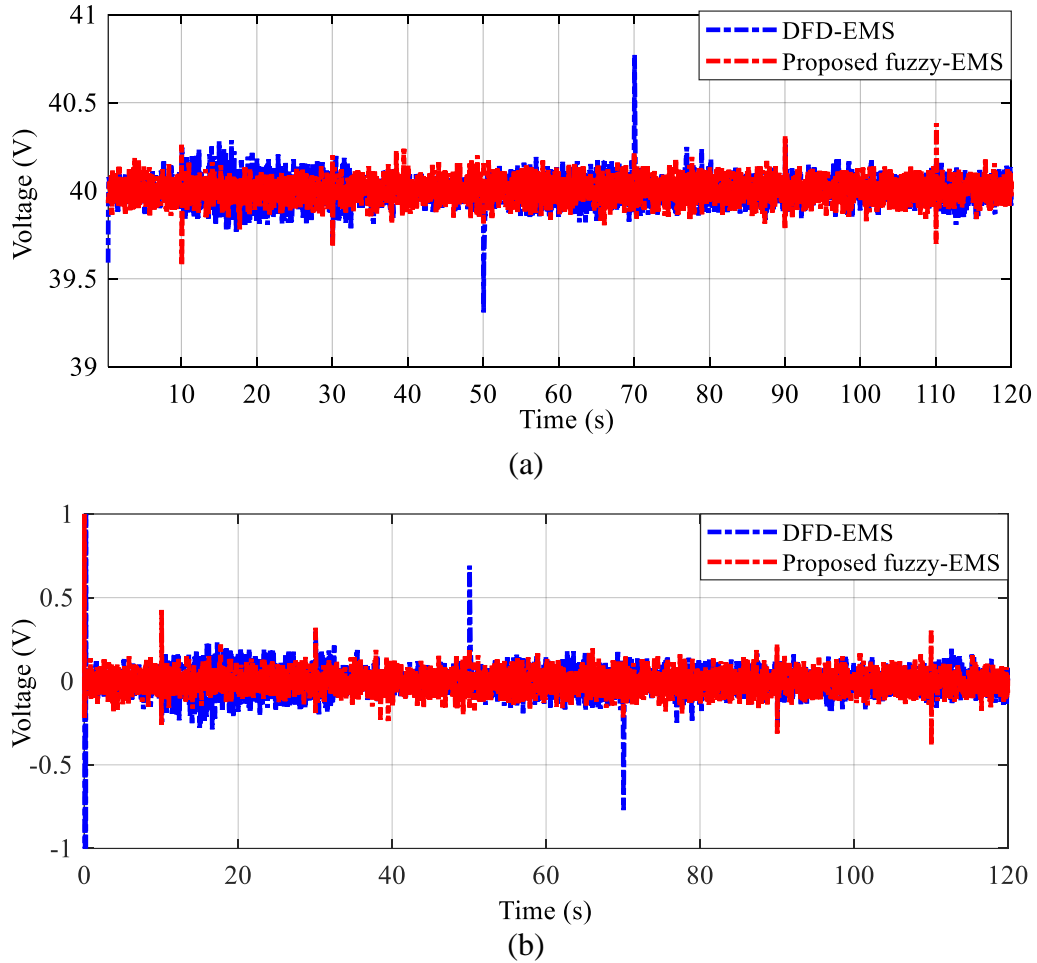
Figure 4.17 The comparison results of DC bus voltage by using three EMSs.

The comparison of DC bus voltage by using two EMSs is described in Figure 4.17. By using the proposed strategy, the DC bus voltage is steadily maintained at around 40 V with a small fluctuation around ±0.2 V and the peak overshoot voltage is smaller than the DFD-EMS despite the abrupt change of the load. In particular, the peak voltage of the DC bus by using the proposed EMS is in the range of (39.55 → 40.4) V, which was approximated by a 2.125 % voltage ripple. Conversely, the DC bus voltages fluctuate in the range of (39.3 → 40.7) V corresponding to 3.5 % ripples for the cases of DFD-EMS.

4.7 Conclusion

This study proposed a new hierarchical approaches-based EMS considering DC bus voltage regulation to correctly distribute energy from the load power demand to the PEMFC, BAT, and SC while also maintaining DC bus voltage stability. In detail, the FLRs and FD are used to determine the reference powers of energy sources based on their dynamic response. In addition, the controller design approach for DC/DC converters is proposed based on the dynamic characteristics and response of converters to guarantee the system performance and maintain the

stability of the DC bus voltage. Simulation and experiment results are employed to evaluate the effectiveness of the proposed strategy. For the simulation, the proposed technique achieves a voltage ripple of approximately 1.68 % and 1.13 % under the step-changing load and specific driving cycle, respectively. Furthermore, the PEMFC stack efficiency and hydrogen consumption obtain by 49.01903 % and 0.2890 (g) for the step-changing load, and 49.287 % and 0.2542 (g) for the specific driving cycle, respectively. For the experiment, the proposed strategy achieves better stability of the DC bus with a 2.125 % voltage ripple.

Simulation and experimental results are summarized as follows:

		Step-changing load		Specific driving cycle		Experiments	
		DFD-EMS	Fuzzy-EMS	DFD-EMS	Fuzzy-EMS	DFD-EMS	Fuzzy-EMS
Power tracking error	*RMSE*	0.176	**0.147**	0.107	**0.103**	0.484	**0.373**
	Me	3.955	**3.89**	2.029	**2.0854**	4.706	**3.96**
	SD	0.176	**0.146**	0.106	**0.102**	0.484	**0.372**
DCbus voltage ripple (%)		1.75	**1.75**	1.68	**1.13**	3.5	**2.125**
FC stack efficiency (%)		48.1043	**49.0103**	48.3026	**49.287**		
H2 consumption (g)		0.2995	**0.289**	0.2609	**0.2542**		

Chapter 5

EXTREMUM SEEKING-BASED OPTIMIZATION FOR ENERGY MANAGEMENT STRATEGY

In this chapter, a novel real-time optimization-based EMS with a comprehensive structure of high-level and low-level controls for a hybrid power system. The proposed methodology is constructed based on an extremum seeking (ES) method, as the core idea, to achieve power distribution for the hybrid system powered by PEMFC, BAT, and SC. By using three components, a new equivalent SOC, which corresponds to equivalent energy storage devices ESDs, and a new adaptive co-state are introduced for ES-based EMS implementation. The ES approach is used to obtain the reference optimal power of the PEMFC. Comparative simulations are carried out between the proposed strategy with rule-based EMS, and fuzzy-based EMS in two case studies: with step-changing load and specific driving cycle load to verify the effectiveness and feasibility of the proposed methodology in stabilizing ESDs' SOC. Briefly, the simulations show good results of the ES-based method with fewer internal dynamics required compared to the other two and indicate the potential for expanding on other hybrid systems with multiple ESDs, respectively.

5.1 Introduction

From the EMS design point of view, the rule-based EMS (such as state machine, deterministic method, fuzzy-based EMS) is of real-time control strategy, but it cannot be generalized to any objective because the implementation of the rule-base EMS significantly depends on expert knowledge of designers, which cannot satisfy the optimal solution. Therefore, this type of EMS is considered as a baseline control strategy for comparison.

The global optimization approach can exhibit global optima; however, it belongs to the offline control strategy that remains a drawback of requiring a well-known or prior determined load profile; thus, restricting the real-time implementations. Moreover, some of the global optimization-based EMS, such as dynamic programming, genetic algorithm, and so forth, require a burden calculation because they demand a library of all driving cycles information, or some, like the ECMS and Pontragin minimum principle, need the parameters of the system dynamics and components to generate the objective function, which requires more effort in practical applications. Hence, they are mostly considered as a benchmark for comparisons.

On the contrary, the local optimization-based EMS, such as extremum-seeking, model predictive control, adaptive control, and so on, is not only suitable for real-time applications but also able to exhibit an optimal solution; however, it is easy to meet local optima. Among those, the model predictive control is a good choice for real-time EMS design due to its capability of predicting and solving optimization problems. Nevertheless, this method requires heavy computation [50]. The extremum seeking, on the contrary, offers a simpler calculation to seek out the maximum efficiency of the PEMFC. Despite the local optimization category, it is suitable for the EMS design because the PEMFC efficiency map uniquely exists one highest efficiency point; thus, the problem of local optima does not affect this situation [50, 54]. To this end, the state-of-the-art with merits and demerits for each control strategy is summarized in Table 5.1.

Table 5.1 Comparison of existing control strategies for the HPS.

	Rule-based EMS	**Optimization-based EMS**	
		Global	Local
Category	Online control strategy	Offline control strategy	Online control strategy
Merits	- Real-time applications	- Can achieve a globally optimal solution	- Real-time applications
Demerits	- Cannot exhibit an optimal solution	- Require information driving cycles and system dynamics → Burden calculation - Not real-time applications	- Get trapped in local optima

Compared to other optimal strategies, the ES, apart, functions as the model-free method where it also does not require internal parameters of energy storage devices. Only the current system state such as fuel cell power and its change rate and energy storage device SOC are required for the optimal reference PEMFC power. Furthermore, the PEMFC efficiency is also necessary for the optimal power calculation and this parameter can be online obtained. Regarding the equivalent model of the ESDs (BAT and/or SC), the SOCs can be calculated through instant power, initial SOC, maximum capacity, and rated voltage which are available in commercialized products. To this end, the ES can be constructed based on the system states and parameters that are available and/or can be instantly online obtained.

From the configuration point of view, besides, several studies just considered two devices for the hybrid power system, one primary source of the PEMFC and one supplementary source of either the battery or the SC. Some studies dealt with the PEMFC-BAT-SC hybridization; however, the dynamical behavior of the SC was ignored in the cost function and optimization problem.

Therefore, this work applies a new methodology to facilitate the ES-based control framework to deal with multiple supplements for power distribution by expressing an equivalent component. With a new penalty function, the PEMFC power can be more effectively regulated to operate in the high-efficiency region with smooth response whereas the SOCs of the BAT and SC are maintained to vary in the suitable intervals.

5.2 Proposed Extremum Seeking-Based Optimization

This section presents a comprehensive control scheme with high-level control for the EMS and low-level control for the DC/DC converter for PWM implementations. The high-level control aims to determine the appropriate power command for each source whereas the low-level control is to regulate the DC bus voltage and generate output power to meet the reference one obtained from the high-level control. The overall diagram of the proposed control strategy is presented in Figure 5.1.
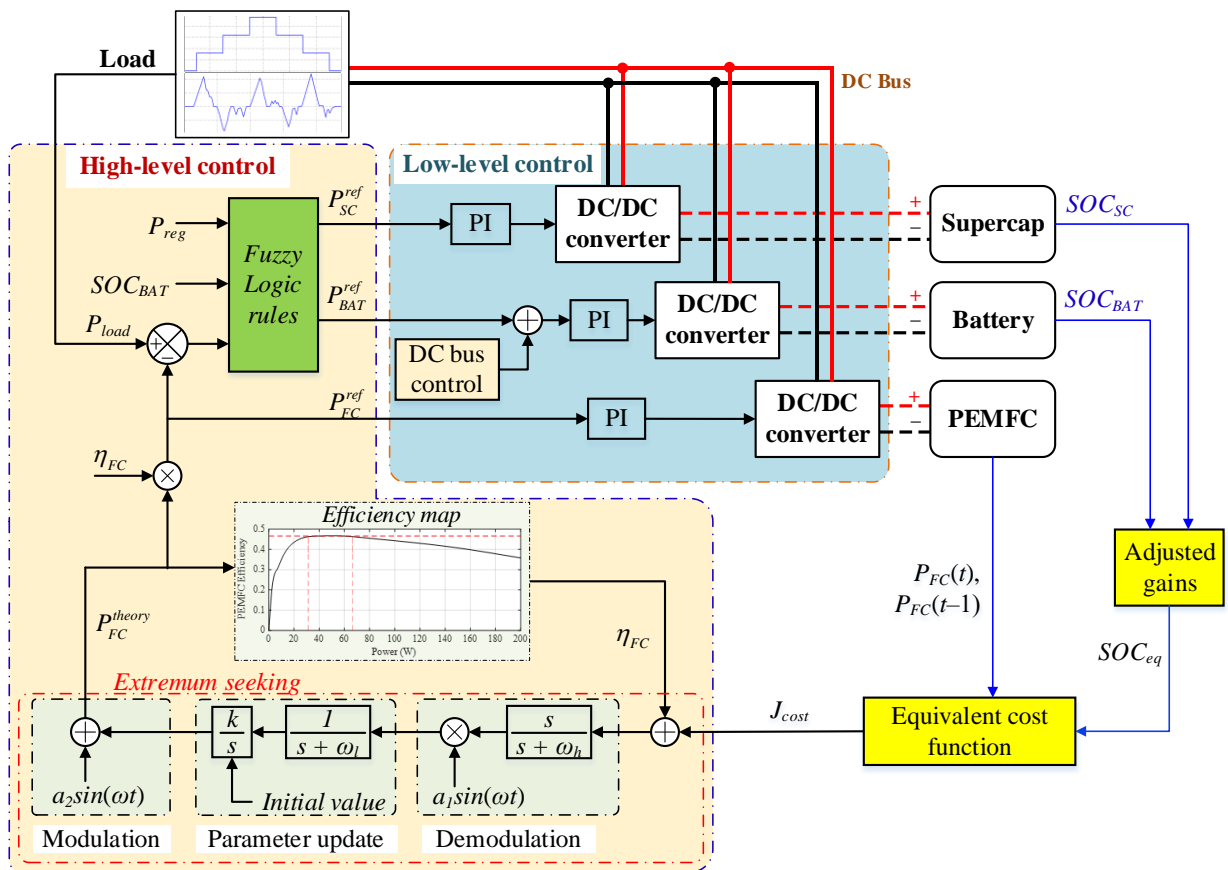
Figure 5.1 Multi-level control scheme of the proposed ES-based EMS.

5.3 High-Level Control

In this section, the proposed EMS based on the ES algorithm is dedicatedly explained for the power distribution of electrical sources.

5.3.1 PEMFC Reference Power

The goal of the ES optimization technique is to seek out the optimal power of the PEMFC, in which the system efficiency is maximized, whereas the SOCs of both BAT and SC are regulated within the suitable range to avoid over-charging or over-discharging. For this purpose, the SOC_{BAT} and SOC_{SC} are considered as constraints in the cost function, along with the PEMFC efficiency. However, the difficulty remaining is how to derive this objective function to effectively find out the extremum value and split the power for supplements when using more than two devices.

In order to solve this regard, an equivalent SOC, the so-called SOC_{eq}, is considered which reduces these auxiliaries to one equivalent device. Hereafter, the new hybridization of three sources is now equivalently converted to the former of two hybrid power sources. The proposed control scheme for the ES-based EMS is displayed in Fig. 5.1. As seen, the input of the ES is the penalty function attainted from the PEMFC efficiency and equivalent SOC. To appropriately obtain this parameter, an adaptive law was constructed which defines a suitable coefficient regarding the current SOCs of the BAT and SC.

The output of the ES is the optimal PEMFC reference power. The remained power load is then distributed to the BAT and SC through a fuzzy logic system. This process returns the BAT and SC reference power. Then, these references are used for the low-level control to execute PWM for DC/DC converters. The detailed control scheme with multi-level control of the proposed ES-based EMS is displayed in Figure 5.1, where P_{reg} is regenerative power in the case of braking, and P_{FC}^{theory} stands for optimal theoretical power obtained from the ES mechanism.

Based on the relationship between the input of PEMFC current, I_{FC}, or power P_{FC} in equivalence, and the output of PEMFC efficiency, η_{FC}, through the efficiency map, the ES mechanism will take care of the cost function J_{cost} obtained from the system output to adjust the control input P_{FC} such that this variable reaches to the optimum value P_{FC}^{theory}; thus, exhibiting the maximized steady-state output $\eta_{FC}^* = f\left(P_{FC}^{theory}\right)$. The core of this technique relies on the periodic perturbation sinusoidal signal added to the cost function with modulation, parameter update, and demodulation filter mechanisms to force the PEMFC current to move toward the optimal point where optimal efficiency η_{FC}^* is exhibited. The implementation for the ES is derived by the following equations:

$$\begin{cases} \dot{\phi}(t) = \left(\dot{\eta}_{FC}(t) + \dot{J}_{cost}(t) \right) F_h(s) \\ \dot{\xi}(t) = \phi(t) a_1 \sin(\omega t) F_l(s) \\ \dot{\hat{\theta}} = -k\xi(t) \\ I_{FC}^{theory} = a_2 \sin(\omega t) + \hat{\theta} \end{cases} \tag{5.1}$$

where $F_h(s) = \dfrac{s}{s+\omega_h}$ and $F_l(s) = \dfrac{1}{s+\omega_l}$ are the high-pass and low-pass filter functions, respectively; ω_h and ω_l stand for high- and low-pass filter cutoff frequencies, respectively; k is the learning rate, and two terms $a_1 \sin(\omega t)$ and $a_2 \sin(\omega t)$ are demodulation and modulation signals.

The cost function J_{cost} is expressed as

$$\begin{aligned} J_{cost} = &\left(-\alpha_{ES} \max\left(\frac{SOC_{eq}^{min} - SOC_{eq}}{SOC_{eq}^{min}}, 0, \frac{SOC_{eq} - SOC_{eq}^{max}}{SOC_{eq}^{max}} \right) \right)^2 \\ &- \beta_{ES} \left| P_{FC,t} - P_{FC,t-\Delta t} \right| - \gamma_{ES} \left| SOC_{eq}^{ini} - SOC_{eq} \right| \end{aligned} \tag{5.2}$$

where SOC_{eq} and SOC_{eq}^{ini} are instant equivalent SOC and initial equivalent SOC, respectively, determined as a new variable that represents the relationship between the SOC_{BAT} and SOC_{SC}; SOC_{eq}^{min} and SOC_{eq}^{max} are lower and upper bounds of the SOC_{eq}, respectively; α_{ES}, β_{ES}, and γ_{ES} are coefficients of the cost function; $P_{FC,t}$ and $P_{FC,t-\Delta t}$ denote current and one-step previous PEMFC power.

The equivalent SOC, SOC_{eq}, is expressed as

$$SOC_{eq} = rSOC_{BAT} + (1-r)SOC_{SC} \tag{5.3}$$

where $r \in (0,1)$ is an adaptive ratio determined based on the current SOCs of the BAT and SC.

In the simplest case, r can be defined as

$$r = \begin{cases} 1 & , if\ SOC_{BAT} > SOC_{SC} \\ \dfrac{SOC_{BAT}}{SOC_{SC}}, & \text{otherwise} \end{cases} \tag{5.4}$$

Thus, an initial equivalent SOC_{eq}^{ini} can be obtained based on the initial values of SOC_{BAT} and SOC_{SC}. Different from the original work [50] and [54], the cost function (5.2) is modified with two more terms $\beta_{ES} \left| P_{FC,t} - P_{FC,t-\Delta t} \right|$ and $\gamma_{ES} \left(SOC_{eq}^{ini} - SOC_{eq} \right)^2$ added where the first term is to regulate the change rate of the PEMFC power such that smooth power can be exhibited while the second term is to assure that at the end of the driving cycle, the final SOC_{eq} will be regulated to be as same as the initial one; thus, stabilizing the energy storage performance. This cost function is more generalized than existing ones as if setting $\beta_{ES} = 0$ and $\gamma_{ES} = 0$, then the cost function (5.2)

becomes the former. The stability of the ES approach can be referred to [49]. Then, the final step in this high-level control is defining individual reference power for each BAT and SC device.

5.3.2 Battery and Supercapacitor Reference Power

The aim is to diminish the remaining load power required from the auxiliary in the case of only considering the BAT and ignoring the SC in the objective function. In this step, the remaining load power and BAT SOC are assigned as two inputs and the output is the BAT reference power gain. Another fuzzy mechanism is employed for this purpose.

Instead of directly using the load remained as one input, the load ratio is considered. The reason for using this ratio is to make the remained load automatically scaled down to be constrained in a range of $[-1,1]$ regardless of its bounds changed due to using another size of PEMFC or a different size of hybrid power source. The calculation for this load factor is expressed by:

$$g_{r-load} = \begin{cases} -1 & , \text{if } \left|P_{load} - P_{FC}^{ref}\right| \geq \max\left(\left|P_{load}\right|\right) - P_{FC}^{ref} \\ \dfrac{P_{load} - P_{FC}^{ref}}{\max\left(\left|P_{load}\right|\right) - P_{FC}^{ref}} & ,\text{otherwise} \end{cases} \tag{4.5}$$

where $\max\left(\left|P_{load}\right|\right)$ is the maximum load that can be determined based on the load workability.

The SOC_{BAT} is required to vary in the range of [0.5, 0.9] where five membership functions (MFs) of very low (VL), low (L), medium (M), high (H), and very high (VH) are utilized to specify the SOC_B. The load factor is specified by five MFs of negative high (NH), negative medium (NM), zero (Z), positive medium (PM), and positive high (PH). For the output of the fuzzy operator, seven MFs are employed as negative big (NB), negative medium (NM), negative small (NS), zero (Z), positive small (PS), positive medium (PM), and positive big (PB). The MFs of the inputs and output are depicted in Figure 5.2 and the fuzzy rules table is described in Table 5.2.
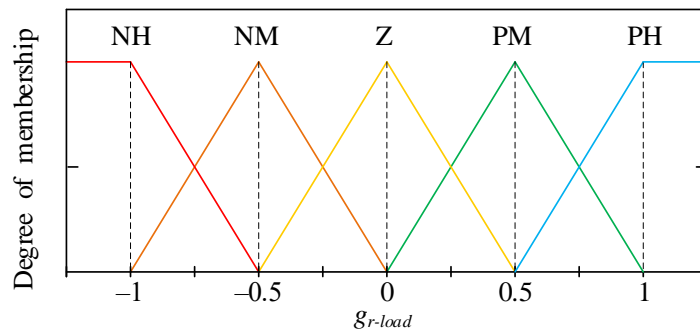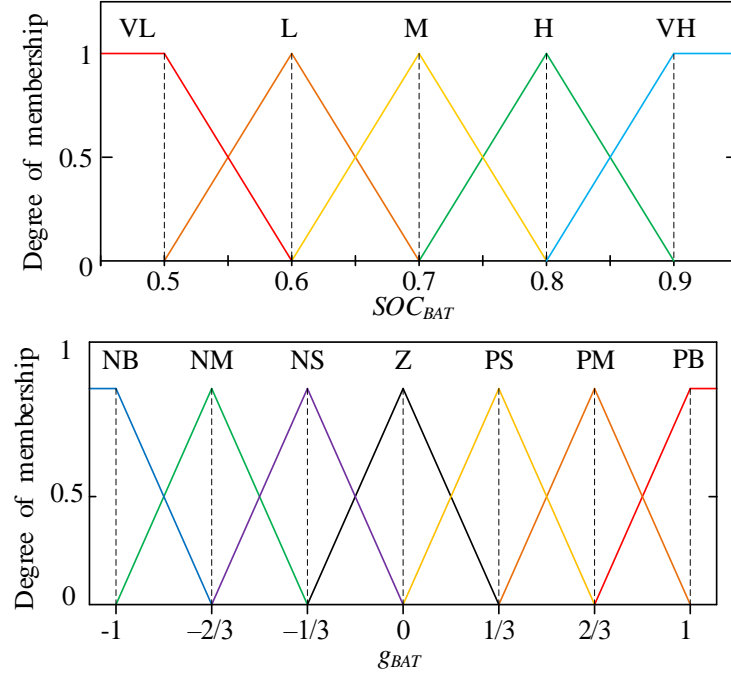
Figure 5.2 MFs of inputs and output of the fuzzy operator for the BAT and SC power split.

Table 5.2 Fuzzy rules for output battery power reference gain

g_{BAT}		$g_{r\text{-}load}$				
		NH	**NM**	**Z**	**PM**	**PH**
SOC_{BAT}	**VL**	NB	NB	NM	NS	Z
	L	NB	NM	NS	Z	PS
	M	NM	NS	Z	PS	PM
	H	NS	Z	PS	PM	PB
	VH	Z	PS	PM	PB	PB

From the output of the fuzzy rules, the reference power of the BAT is determined as

$$P_{BAT}^{ref} = g_{BAT}\left(P_{load} - P_{FC}^{ref}\right) \tag{5.6}$$

As a result, the SC will take care of the left load power and also absorb fluctuation induced by transient or peak load demand, i.e.

$$P_{SC}^{ref} = P_{load} - P_{FC}^{ref} - P_{BAT}^{ref} \tag{5.7}$$

5.4 Low-Level Control

Low-level control aims to generate the PWM signals for controlling DC/DC converters to satisfy the demand energy of power sources and compensate for DC bus fluctuation. This

compensation is executed by the modified power reference of the BAT, which is determined in high-level control. Then, proportional-integral (PI) controllers are employed to generate PWM signals for each respective power source. The architecture of the low-level control is presented in Figure 5.3.
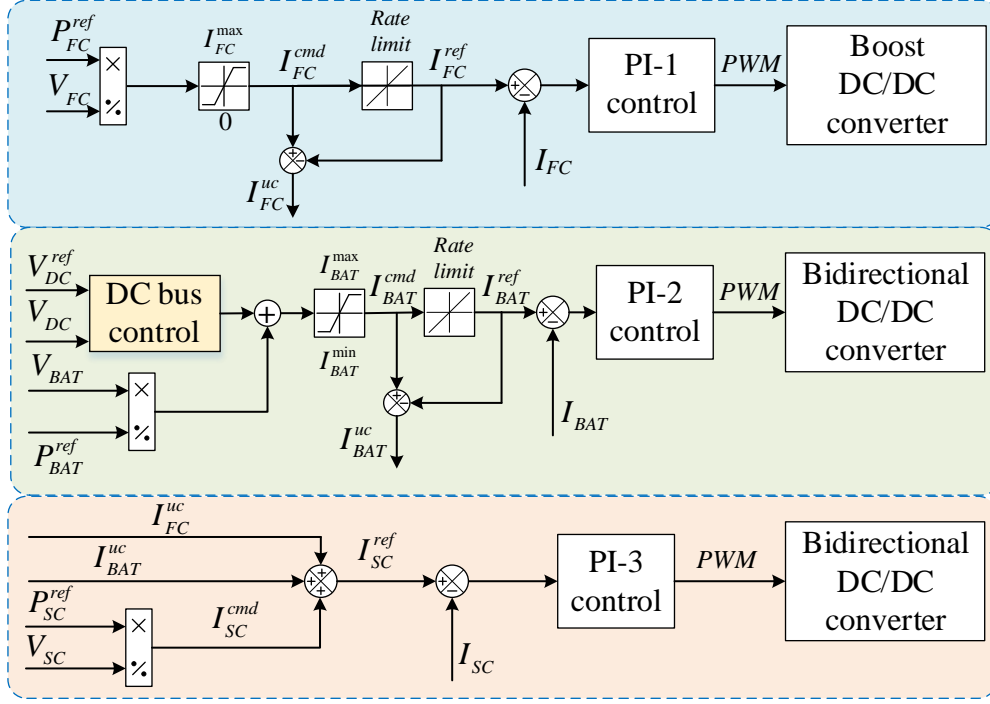
Figure 5.3 Structure of low-level control.

For the PEMFC, the reference current is computed as

$$I_{FC}^{ref} = f_{R1}\left(I_{FC}^{cmd}\right) \tag{5.8}$$

where I_{FC}^{ref} is the PEMFC reference current (A), $f_{R1}(.)$ is the function of the rate limiter for the PEMFC current, and I_{FC}^{cmd} is the command current of the PEMFC that is limited to maximum and minimum current values (A).

The uncompensated PEMFC current by using the rate limiter is given as follows:

$$\boldsymbol{I}_{FC}^{uc} = \boldsymbol{I}_{FC}^{ref} - \boldsymbol{I}_{FC}^{cmd} \tag{5.9}$$

where I_{FC}^{uc} is the uncompensated PEMFC current (A).

For the BAT, the reference and uncompensated currents can be defined as follows:

$$I_{BAT}^{ref} = f_{R2}\left(I_{BAT}^{cmd}\right) \tag{5.10}$$

$$\boldsymbol{I}_{BAT}^{uc} = \boldsymbol{I}_{BAT}^{ref} - \boldsymbol{I}_{BAT}^{cmd} \tag{5.11}$$

where I_{BAT}^{ref} is the BAT reference current (A), $f_{R2}(.)$ is the function of the rate limiter for the BAT current, I_{BAT}^{cmd} is the command current of the BAT that is limited to maximum and minimum current values (A), and I_{BAT}^{uc} is the uncompensated BAT current (A).

It is noteworthy that due to using the new command variable, the SC duties are to not only suppress the peak phenomenon but also release power to satisfy the power requirement. Thus, the SC, with its high power density and fast dynamics response, is employed to accommodate the uncompensated currents due to the slow dynamics of the PEMFC and BAT. The reference SC current is given by

$$I_{SC}^{ref} = I_{FC}^{uc} + I_{BAT}^{uc} + I_{SC}^{cmd} \tag{5.12}$$

where I_{SC}^{ref} is the SC reference current (A) and I_{SC}^{cmd} is the SC command current (A).

5.5 Simulation Results

In this section, a comparative simulation between the proposed optimization-based strategy and previous methods is conducted to access and analyze the effectiveness of EMS strategies for the HPS under different operating conditions. In this chapter, the proposed strategy is developed to solve several optimal requirements for HPS consisting of improving the PEMFC stack efficiency, reducing hydrogen consumption, increasing load power adaptation, and minimizing ripples of the DC bus. In detail, the proposed extremum seeking-based optimization EMS (proposed ES-EMS) is implemented and compared with the two other strategies: DFD-EMS (chapter 3), and fuzzy-EMS (chapter 4), in which a continuous black line representing the reference power of the load, a dashed-dot blue line indicating the power of the DFD-EMS, a dashed-dot green line showing the load power adaptation of the fuzzy-EMS, and a dashed-dot red line displaying the load power adaptation of the proposed extremum seeking-based optimization EMS (proposed ES-EMS). To comprehensively investigate EMS approaches with various operating situations, two load profiles as in Fig. 2.8 are considered with several load levels such as acceleration, deceleration, and regeneration in practical working conditions. In addition, the modeling of the HPS has deployed in Matlab/Simulink 2021b environment with a sampling time for displaying simulation results at 0.05 ms. By reasonably selecting components, characteristics of energy sources, and parameters of the proposed EMS are listed in Tables 3.4 – 3.7.

5.5.1 Step-Changing Load

The system performance and effectiveness of three EMSs are described in Figures 5.4 – 5.9.
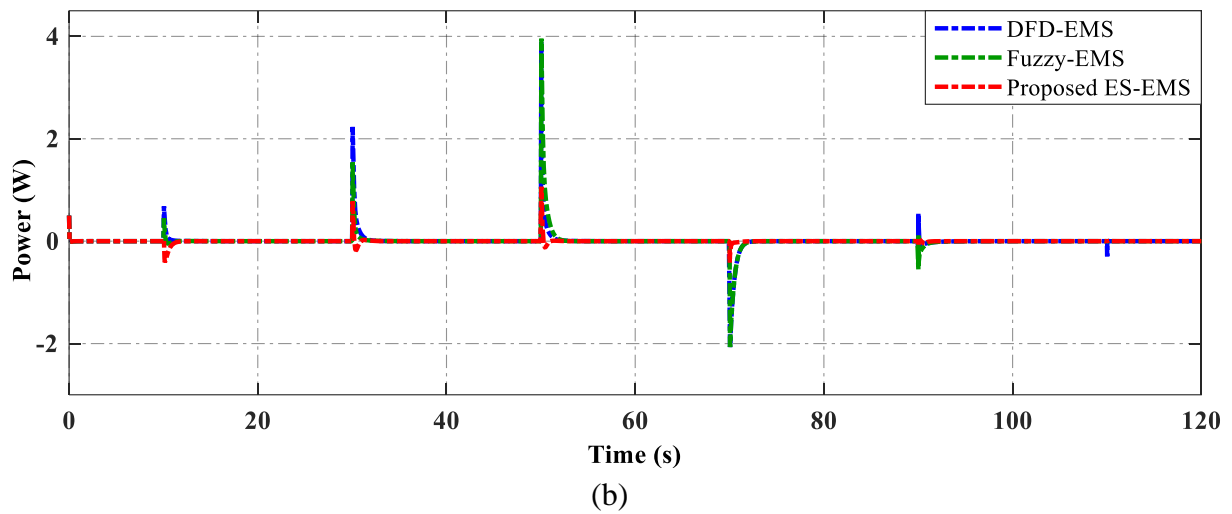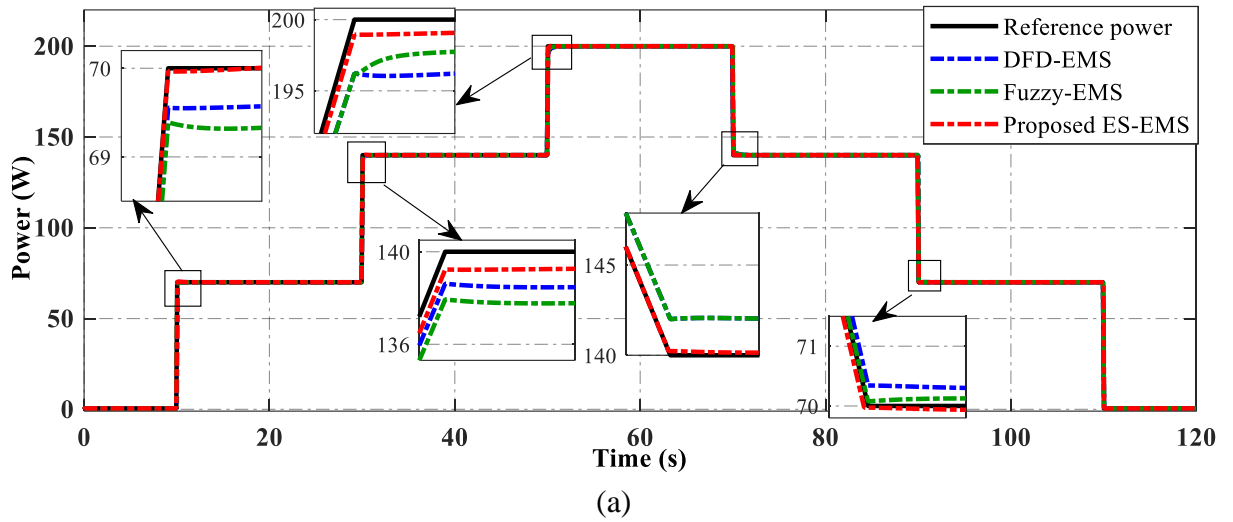
Figure 5.4 The comparison of load power adaptation based on three EMSs. (a) The load power adaptation. (b) The power tracking error.

Firstly, Figure 5.4 depicts the comparison of load power adaptation based on three EMSs. As shown in Figure 5.4 (a), it can be seen that three strategies can achieve a good performance of power adaptation to the load power demand. When the load power is abruptly changed at the time of the 10th, 30th, 50th, 70th, 90th, and 110th, these strategies can guarantee the fast transient state of the load power. However, there are some differences in the power tracking error of these EMSs as presented in Figure 5.4 (b). The proposed ES-EMS gets the optimum distributed accuracy with the error in the range of $(-0.5 \rightarrow 1)$ W, while the DFD-EMS and fuzzy-EMS have an inadequate power approximated $(-2 \rightarrow 4)$ W. The obtained results show that the proposed strategy has the best power adaptation with the smallest power fluctuations.
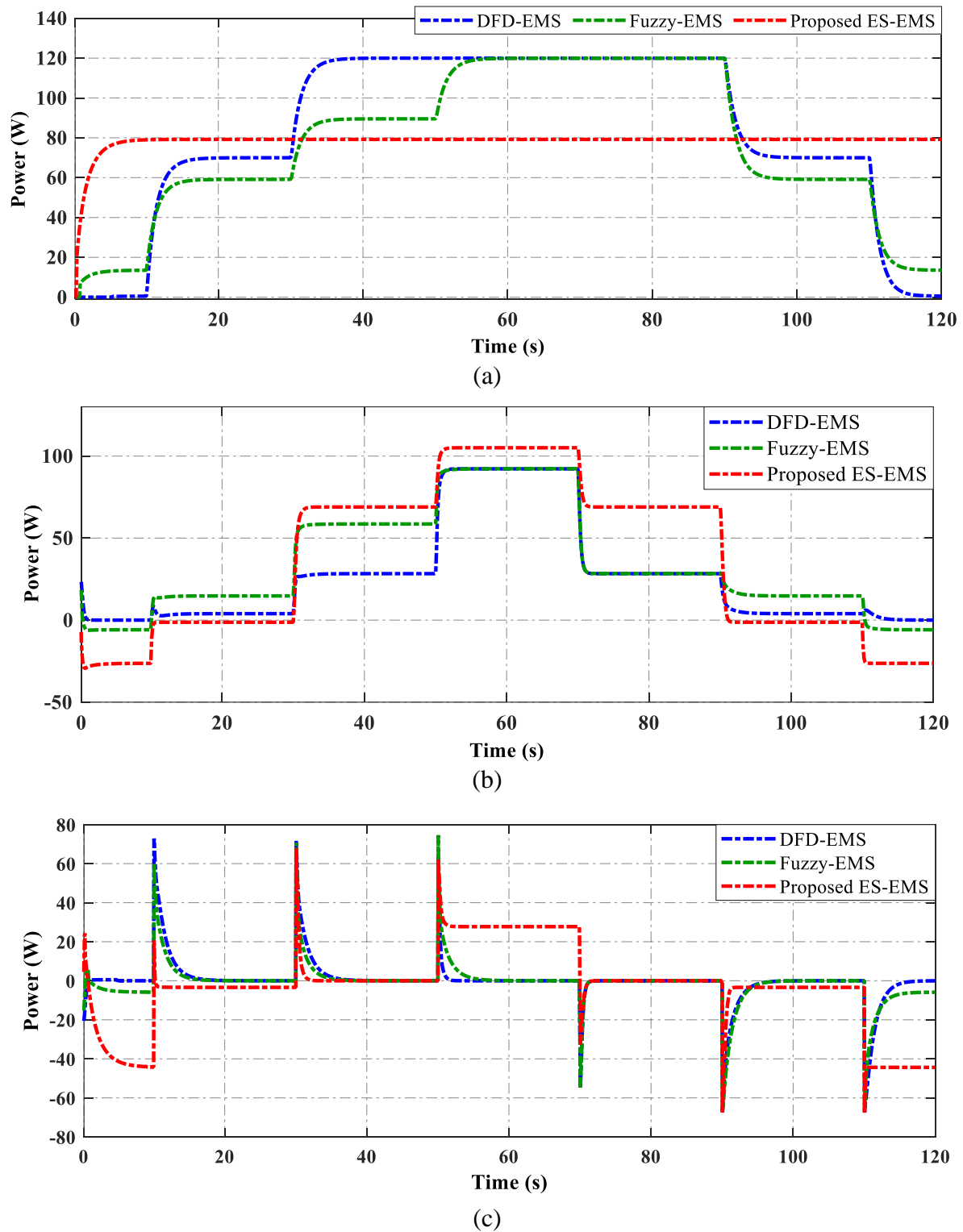
Figure 5.5 The power distribution of energy sources. (a) PEMFC. (b) BAT. (c) SC.

Next, the power distributions of the PEMFC, BAT, and SC in the hybrid system are shown in Figure 5.5. For the proposed strategy, the PEMFC supplies optimal power that corresponds optimal working point of the PEMFC stack as shown in Figure 5.5 (a). Then, the constraints of the cost function will regulate the power distribution of BAT and SC, which can guarantee not only the load power demand but also the fuel cell efficiency.
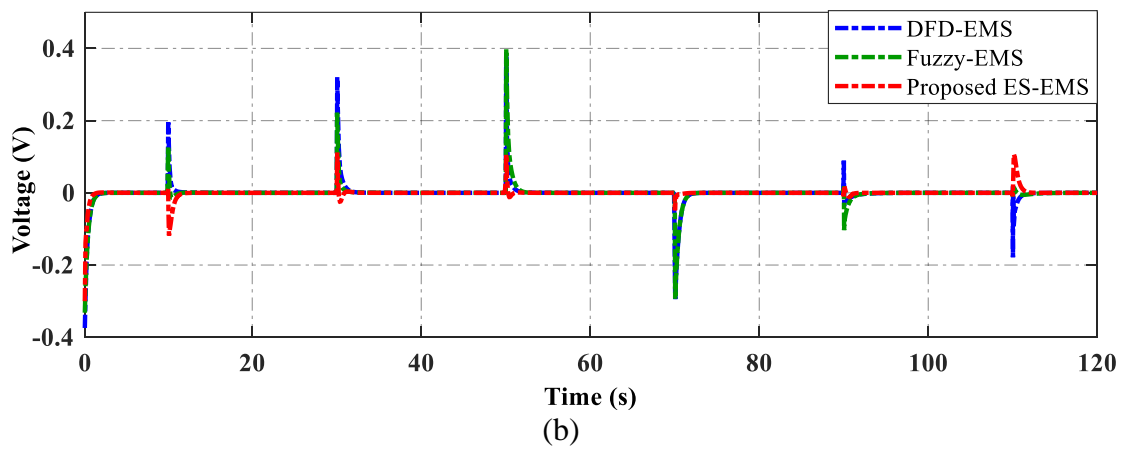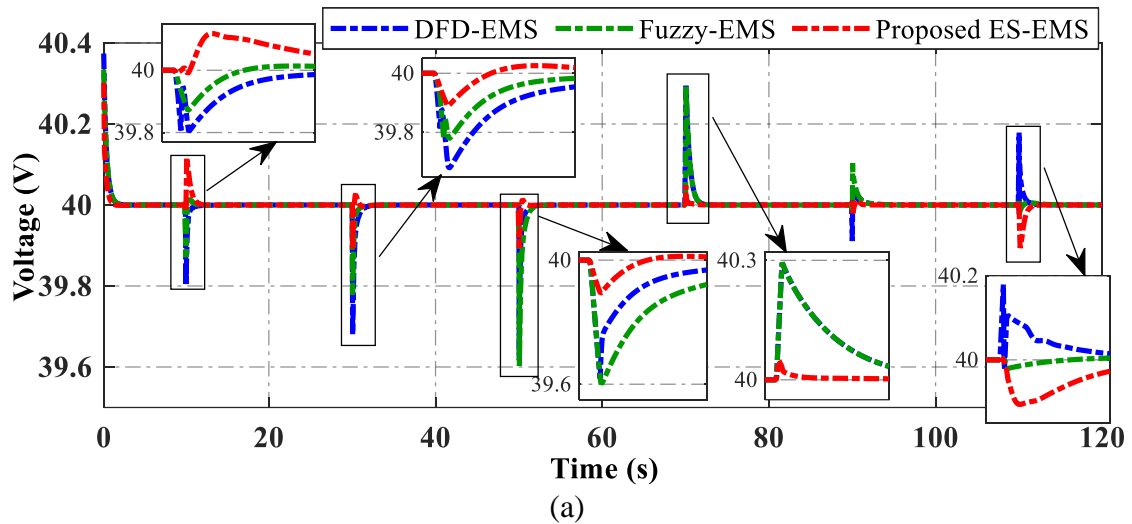
Figure 5.6 The DC bus voltage regulation. (a) Voltage tracking. (b) Tracking error.

The comparison of DC bus voltage regulation under different working load conditions is shown in Figure 5.6. It can be seen that the DC bus voltage is steadily maintained at around 40 V with a very small fluctuation, despite the abrupt change of the load, as displayed in Figures 5.6 (a) and (b). In particular, the proposed strategy has the peak voltage of the DC bus in the range of (39.9 → 40.1) V, which is the best voltage ripple approximated by 0.5 %. Meanwhile, the DC bus voltages fluctuate of two other strategies in the range of (39.6 → 40.3) V with about 1.75 % voltage ripple.
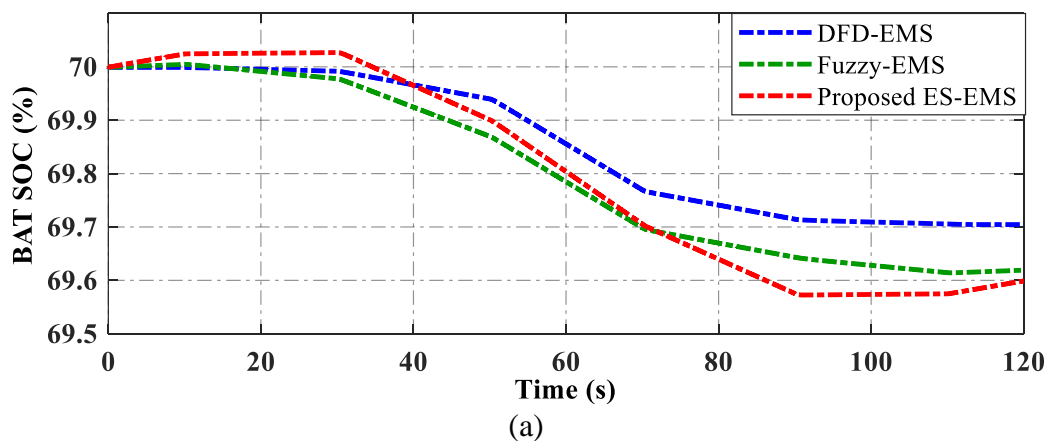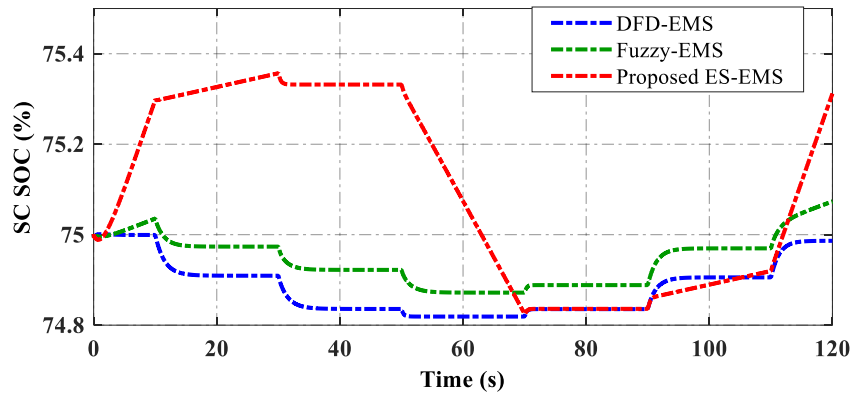
(b)

Figure 5.7 The SOC status. (a) BAT SOC. (b) SC SOC.

The SOC levels of both BAT and SC are performed in Figure 5.7, which describes the charged and discharged status. As shown in Figure 5.7 (a), the proposed approach could maintain the fluctuation of BAT SOC level in the range of (69.55 → 70.5) % with the charging and discharging mechanism clearly. The DFD-EMS and fuzzy-EMS show a decreased trend of the SOC BAT and keep the SOC range within (69.6 → 70) %. For the SC, the proposed EMS shows a higher SOC variation that corresponds to the charge and discharge status with the range of (74.85 → 73.5) %. Meanwhile, the DFD-EMS and fuzzy-EMS have a SOC varying range within (74.81 → 75) %.
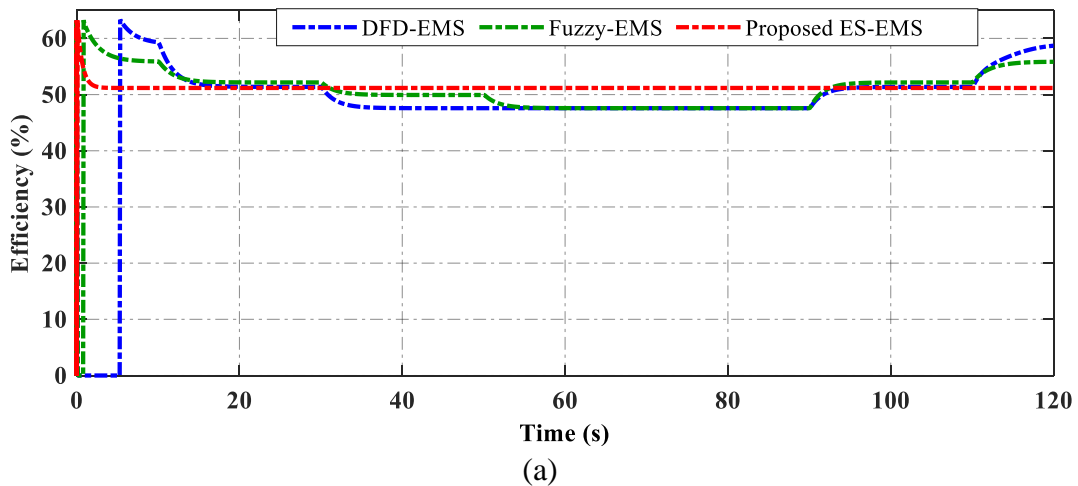
(a)
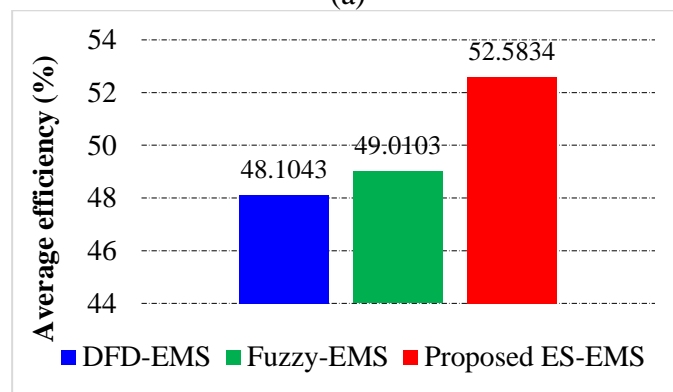
(b)

Figure 5.8 The PEMFC stack efficiency. (a) Efficiency status. (b) Average efficiency.

The PEMFC stack efficiency is investigated to evaluate the effectiveness of three EMSs as depicted in Figure 5.8. The efficiency status corresponding to PEMFC power change is depicted in Figure 5.8 (a). In addition, the average efficiency of the PEMFC stack is presented in Figure 5.8 (b). It can be seen that the average PEMFC stack efficiency can increase by 3.5731 % by using the proposed ES-EMS and reaches 52.5834 %, while the efficiency of fuzzy-EMS is 49.0103 %. Meanwhile, the average efficiency of the DFD-EMS has the lowest efficiency of 48.1043 (%).

(a)

(b)
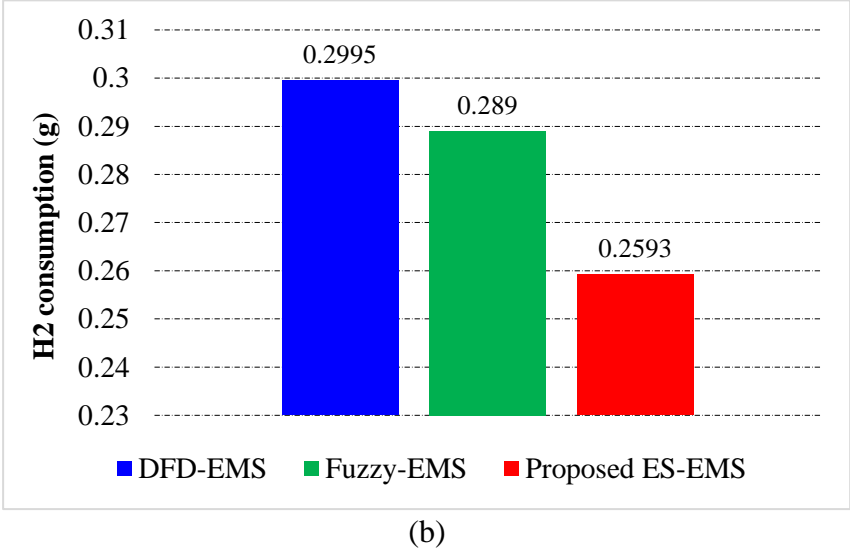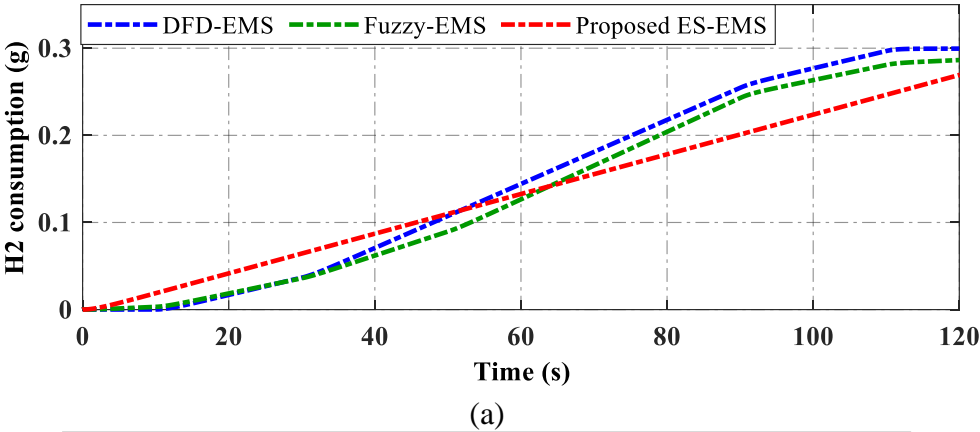
Figure 5.9 The comparison of fuel consumption. (a) H2 consumption status. (b) Total H2 consumption.

Finally, Figure 5.9 describes the hydrogen consumption of three EMSs. As a result, the total hydrogen consumption of the proposed ES-EMS is less than the fuzzy-EMS and the DFD-EMS. In detail, the DFD-EMS and the fuzzy-EMS have a hydrogen fuel consumption of 0.2995 (g) and 0.2890 (g) in comparable operating conditions, respectively. In contrast, in the case of the proposed approach, hydrogen consumption is 0.2593 (g) which reduces 0.0402 (g) (13.42 %) and 0.0297 (g) (10.28 %) in comparison to the DFD-EMS and fuzzy-EMS, respectively. This result demonstrates

that the proposed optimal strategy can save the fuel economy with hydrogen consuming less than compared to other ways.

5.5.2 Specific Driving Cycle Load

Here in this simulation, examined specific driving cycle along with the workability of load satisfaction under three strategies is shown in Figure 5.10. The behaviors of electrical devices, the DC bus voltage regulation, and the SOC status of BAT and SC are described in Figures 5.11, 5.12, and 5.13, respectively. Then, the PEMFC stack efficiency and hydrogen fuel consumption are depicted in Figure 5.14 and Figure 5.15, respectively. Generally, the use of the battery could help maintain the DC bus voltage to meet the desired one at 40 V.
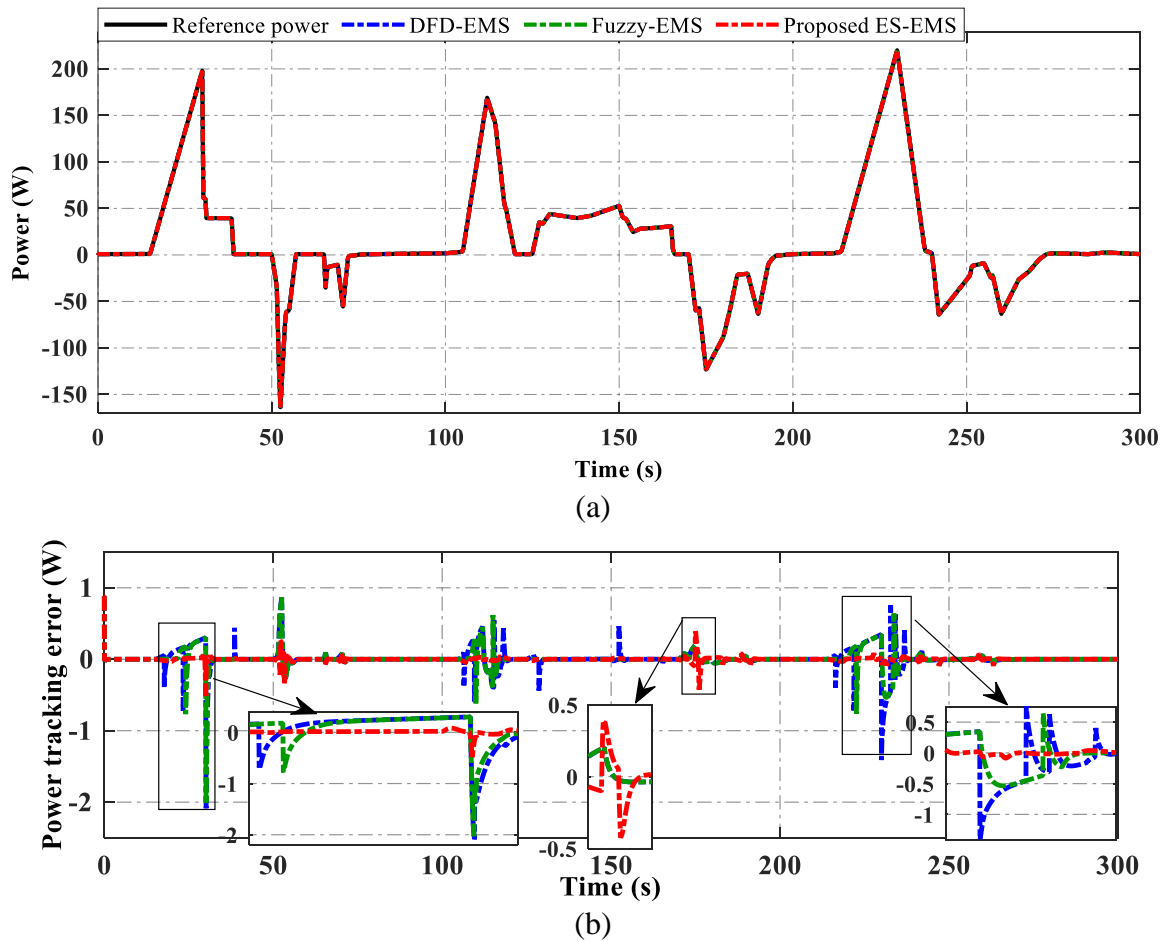
Figure 5.10 Load satisfaction under three strategies. (a) Load tracking performance. (b) Tracking error performance.

Firstly, the load power adaptation of three EMSs is presented in Figure 5.10. In general, all three algorithms could satisfy the load requirement as shown in Figure 5.10 (a). In Figure 5.10 (b), the tracking error performance of three strategies is described detail. It can be seen that the proposed strategy achieves the least power tracking error in the range of (−0.5 → 0.5) W. Meanwhile, the

DFD-EMS and the fuzzy-EMS take an insufficient power in the range of $(-2 \rightarrow 0.8)$ W, respectively. This result proves that the proposed strategy can improve the accuracy of load power adaptation under different operating conditions.
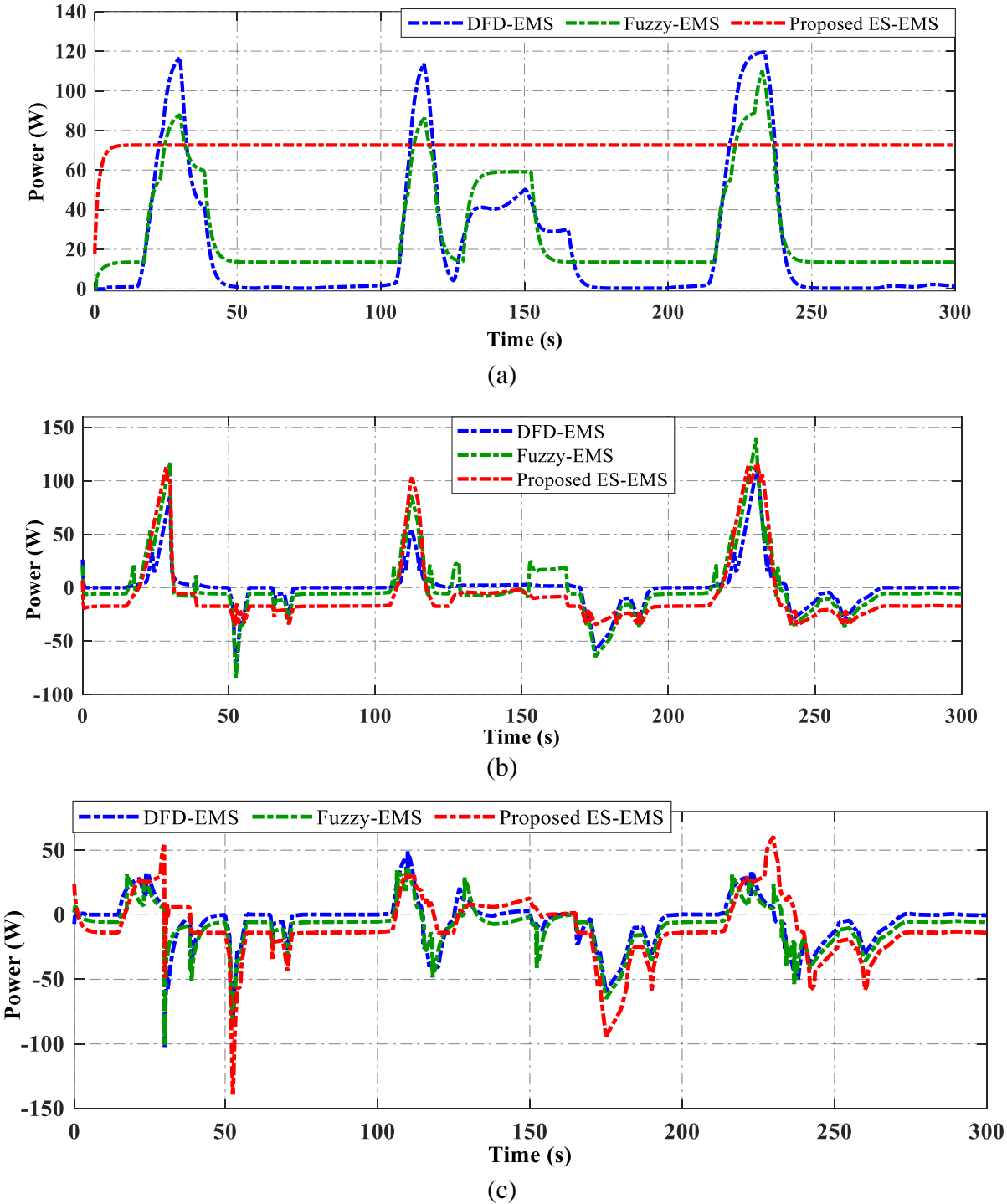
Figure 5.11 The power distribution of energy sources. (a) PEMFC. (b) BAT. (c) SC.

The power distributions of the PEMFC, BAT, and SC in the hybrid system are shown in Figure 5.11. For the PEMFC, the proposed strategy generates the optimal power distribution at the high-efficiency region as the efficiency map in Figure 2.4. This optimal PEMFC power can ensure a stable

adaptation for load power demand, which can improve the fuel economy and durability of the PEMFC system. The power capability of the BAT and SC under three EMSs are depicted in Figures 5.11 (b) and (c). It can be seen that the distribution of BAT and SC is employed to supplement the slow power response of the PEMFC as well as guarantee a smooth power response to charge the redundant power from the DC bus to the BAT and charge the redundant power in the regenerative mode.
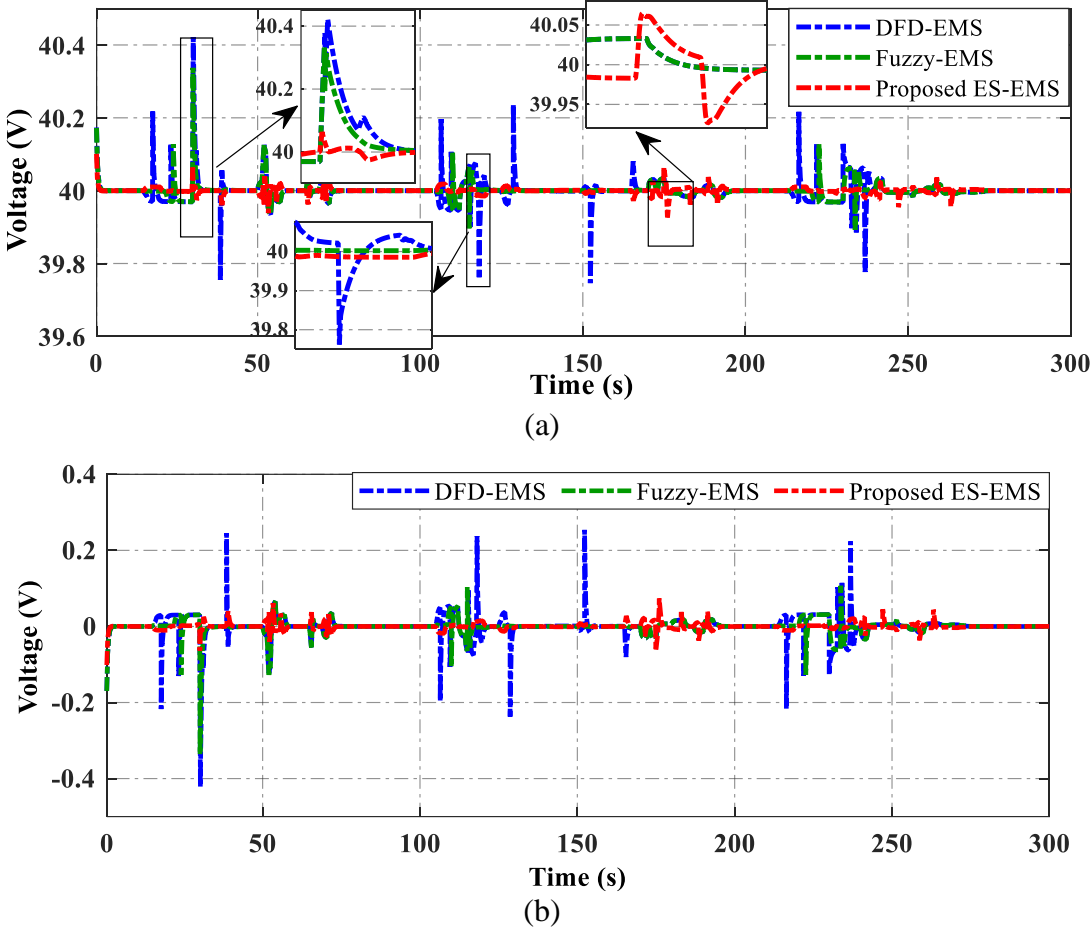
Figure 5.12 The DC bus voltage regulation. (a) Voltage tracking. (b) Tracking error.

Figure 5.12 shows the DC bus voltage regulation of three EMSs. Three strategies can maintain the DC bus voltage steadily at around 40 V. In detail, the proposed ES-EMS maintains the DC bus peak voltage in the range of $(39.9 \rightarrow 40.1)$ V with the tracking error of 0.2 V, approximated by a 0.5 % voltage ripple. Meanwhile, the fuzzy-EMS and DFD-EMS have a tracking error of 0.45 V and 0.7 V, which takes the voltage ripple of 1.13% and 1.68 %, respectively.
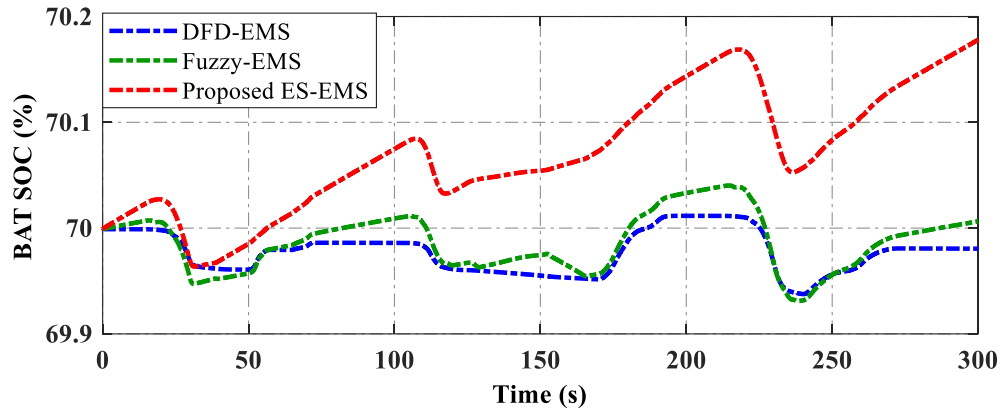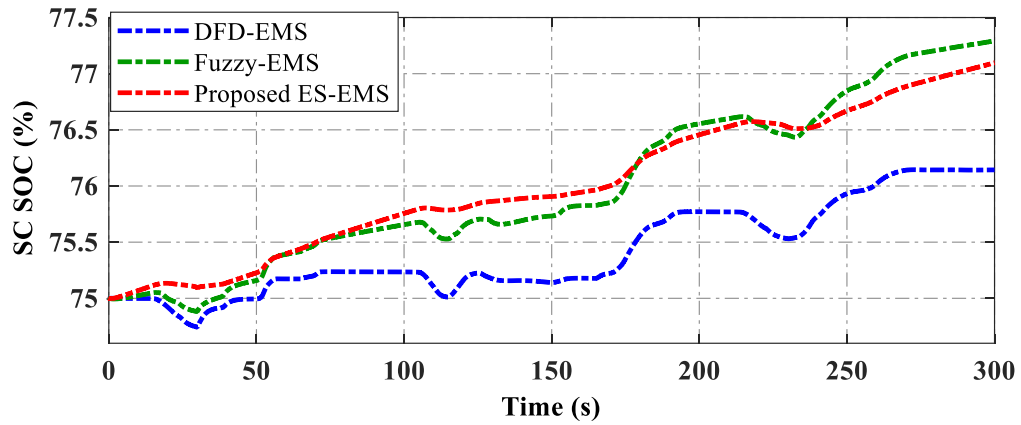
Figure 5.13 The SOC status. (a) BAT SOC. (b) SC SOC.

The SOC levels of both BAT and SC are depicted in Figure 5.13. In detail, the BAT SOC of the two strategies can maintain the low fluctuated range of (69.9 → 70.05) %, while the proposed ES-EMS varies in the range of (69.97 → 70.18) % as shown in Figure 5.13 (a). For the SC, the SOC level of the proposed strategy increase in the range of (75 → 77.1) %, while the DFD-EMS and fuzzy-EMS vary between (74.9 → 76.1) % and (74.9 → 77.3) %, respectively.
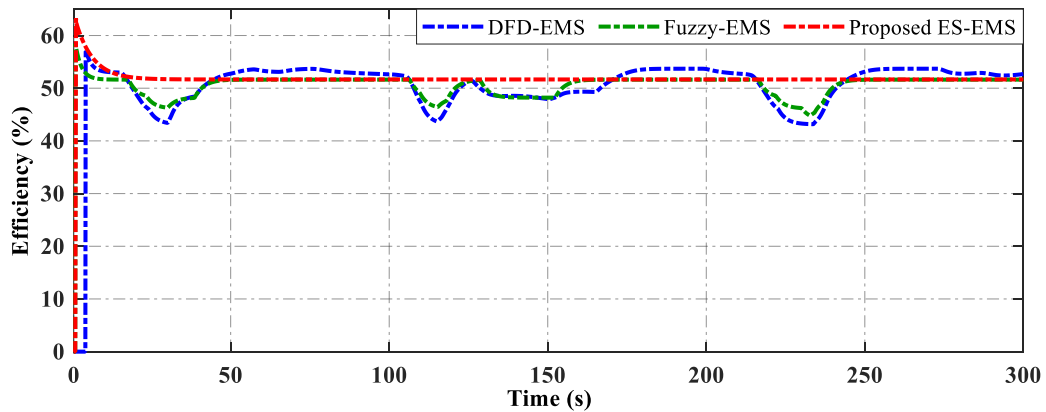
(a)
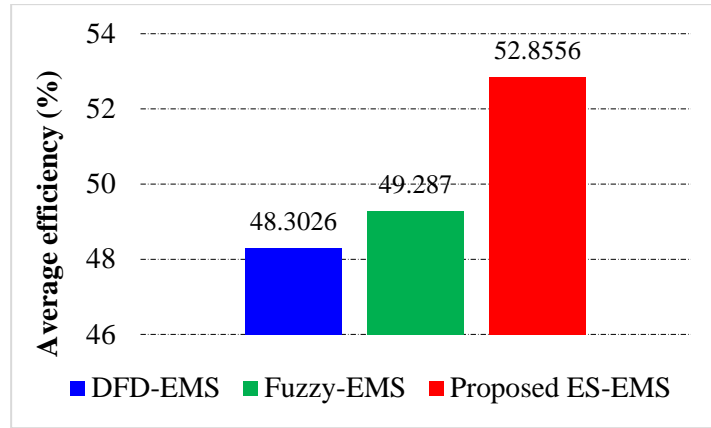
(b)

Figure 5.14 The comparison of PEMFC stack efficiency of PEMFC stack. (a) Efficiency status. (b) Average stack efficiency.

The PEMFC stack efficiency of three EMSs is evaluated as presented in Figure 5.14. From the above figure, the average PEMFC stack efficiency of the proposed strategy achieves 52.8556 % which increases by 3.5686 % in comparison to the efficiency of fuzzy-EMS with 49.287 %. Meanwhile, the average efficiency of the DFD-EMS has the lowest efficiency of 48.3026 (%).
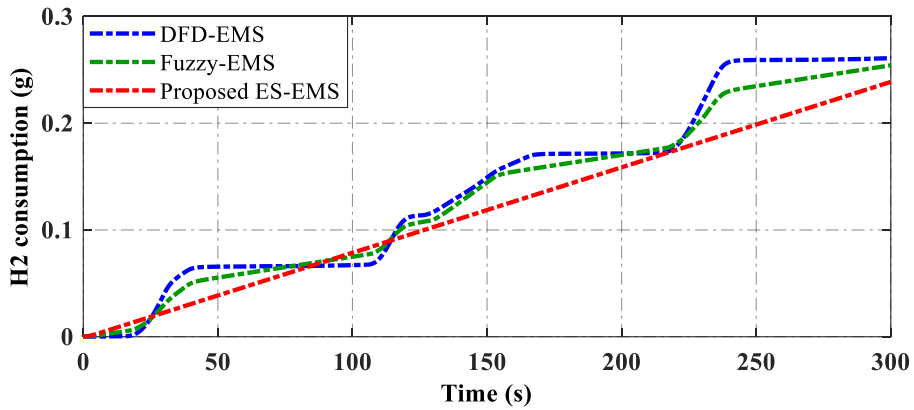
(a)
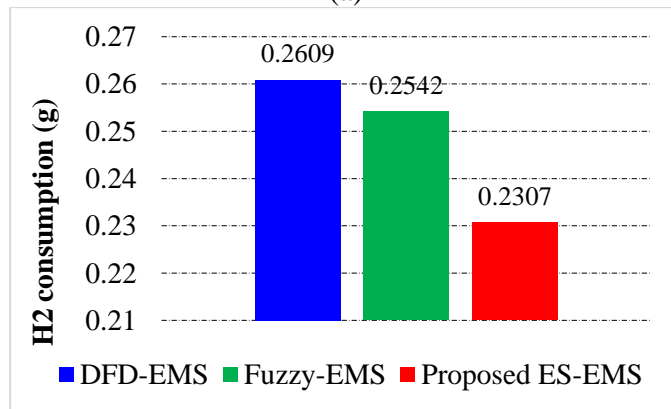
(b)

Figure 5.15 The comparison of hydrogen consumption. (a) H2 consumption status. (b) Total H2 consumption.

The hydrogen consumption of three EMSs is described in Figure 5.15. In detail, the proposed ES-EMS has the least total hydrogen consumption. In detail, the DFD-EMS and the fuzzy-EMS have a hydrogen fuel consumption of 0.2609 (g) and 0.2542 (g) in comparable operating conditions, respectively. In contrast, in the case of the proposed approach, hydrogen consumption is 0.2307 (g) which reduces 0.0302 (g) (11.58 %) and 0.0235 (g) (9.24 %) in comparison to the DFD-EMS and fuzzy-EMS, respectively. This result demonstrates that the proposed optimal strategy can save the fuel economy with hydrogen consuming less than compared to other ways.

5.6 Conclusion

This chapter presents the optimization EMS based on the ES algorithm with comprehensive multi-level control HPS to not only minimize fuel consumption but also maintain the system qualification. The proposed methodology is constructed based on the framework of ES for three power sources. To make this setup implementable, equivalent SOC, regarding the auxiliary SOCs, with adaptive co-state are introduced, to reduce the number of ESDs. Besides, the penalty cost function is developed with the PEMFC change rate added for the ES progress to determine the PEMFC optimal power. As for the remained power for the ESDs, other FLRs are employed to split suitable power for each source. From the reference obtained power in high-level control, the corresponding reference currents are calculated and thus assigned as input in the low-level control. At this level, actual command currents are used as the input signals for the PI controllers to generate a PWM signal that regulates the switching action in the DC/DC converters such that the output power matched the reference ones. The comparative simulations are conducted between the proposed ES-EMS, fuzzy-EMS, and DFD-EMS under two case studies: step-changing load and specific driving cycle. The obtained results show that the proposed strategy achieves effectiveness and feasibility in ensuring the DC bus stability with 0.5 % voltage ripple, increasing the PEMFC stack efficiency by 3.5731 % and 3.5686 % for the step-changing load and specific driving cycle, respectively. In addition, the hydrogen consumption reduces by 0.0297 (g) (10.28 %) and 0.0235 (g) (9.24 %) for the step-changing load and specific driving cycle, respectively.

In conclusion, the proposed methodology can stabilize the ESDs' SOC while still satisfying load requirements. Besides, this method can be considered as a premise for expansion on any hybrid electric system with more than two power sources by using an equivalent variable to reduce the number of auxiliary ESDs. Future works may focus on employing this methodology of using equivalent system states to investigate system dynamics under other strategies such as model predictive control, forgetting factor, global optimization approaches, and expanding on new configurations with multi-PEMFCs and multi-ESDs.

Simulation and experimental results are summarized as follows:

		Step-changing load			Specific driving cycle		
		DFD-EMS	Fuzzy-EMS	Proposed	DFD-EMS	Fuzzy-EMS	Proposed
Power tracking error	*RMSE*	0.176	0.147	**0.04**	0.107	0.103	**0.029**
	Me	3.955	3.895	**1.062**	2.029	2.005	**0.88**
	SD	0.176	0.146	**0.039**	0.106	0.103	**0.03**
DCbus voltage ripple (%)		1.75	1.75	**0.5**	1.68	1.13	**0.5**
FC stack efficiency (%)		48.1043	49.0103	**52.5834**	48.3026	49.287	**52.8556**
H2 consumption (g)		0.2995	0.289	**0.2593**	0.2609	0.2542	**0.2307**

Chapter 6

CONCLUSIONS AND FUTURE WORKS

6.1 Conclusions

This dissertation presents a comprehensive energy control strategy for the hybrid power system powered by PEMFC, BAT, and SC to enhance the power distribution accuracy, regulate the DC bus voltage, and improve fuel cell stack efficiency as well as hydrogen consumption. First of all, the dissertation describes the overall configuration, the characteristics of the power sources, and the requirements for energy management design in the hybrid power source. Then, control schemes have been proposed to improve the system control performance. The reliability and effectiveness of the proposed strategies are validated by simulation and experimental employment. The summarized conclusions of this dissertation are listed in the following.

In chapter 2, the key characteristics of power sources and electric components are captured and modeled to develop a hybrid power system for the analysis and energy management algorithm design. Dynamic models of PEMFC, BAT, SC, DC/DC converter, and load profile models are described with detailed characteristic functions. Finally, several techniques and requirements of EMS are illustrated as the theoretical background for the following chapters.

In order to improve the system performance for the hybrid power source, a comprehensive energy management strategy with high- and low-level control is proposed in chapter 3. In the high-level control, a deterministic rule-based strategy combined with a frequency decoupling (FD) method is developed to ensure accurate power distribution under different working conditions. Then, the low-level control is designed to maintain the stability of DC bus voltage based on the analysis of the dynamics response of converters through the Bode diagram. Finally, the simulation and experiment on the real hybrid power system test bench are implemented to evaluate the effectiveness of the proposed strategy. The obtained simulation results with the step-changing load reveal that the proposed strategy achieves the DC bus voltage at 1.75% ripple, while the specific driving cycle has a DC bus voltage ripple of 1.68 %. For the experiment performance, the proposed strategy maintains the DC bus voltage ripple at 3.5 % in the case of a step-changing load.

To deal with model uncertainty and complex decisions when using the deterministic rule-based method, the FLRs and FD method are developed in the high-level control to determine the flexible power-sharing of power sources based on their dynamic response. In addition, this hierarchical approach considers DC bus voltage regulation to correctly distribute energy while also maintaining DC bus voltage stability. Simulation and experiment results are employed to evaluate

the effectiveness of the proposed strategy. The issues of achieving optimum fuel economy and enhancing PEMFC efficiency, however, were not thoroughly covered in this chapter and need to be further investigated.

In order to improve the PEMFC stack efficiency and hydrogen consumption, a comprehensive multi-level control is developed in chapter 5, in which the extremum-seeking-based optimization in high-level control not only minimizes fuel consumption but also maintains the system qualification. Then, equivalent SOC, regarding the auxiliary SOCs, with adaptive co-state are introduced, to reduce the number of ESDs. Besides, the penalty cost function is developed to determine the PEMFC optimal power and fuzzy rules are employed to split suitable power for ESDs from the remained power. At low-level control, actual command currents are used as the input signals for the PI controllers to generate a PWM signal that regulates the switching action in the DC/DC converters such that the output power matched the reference ones. The comparative simulations depict that the proposed strategy achieves effectiveness and feasibility in maintaining the DC bus stability with a ripple voltage of 0.5 % while increasing the PEMFC stack efficiency by 3.5731 % and 3.5686 %, and reducing the hydrogen consumption by 0.0297 (g) (10.28 %) and 0.0235 (g) (9.24 %) for the step-changing load and specific driving cycle, respectively. As a result, the proposed methodology can stabilize the ESDs' SOC while still satisfying load requirements, and expanding on any hybrid systems with more than two ESDs.

6.2 Future Works

Although control strategies have been proposed to address existing problems in this dissertation, some areas needed to be investigated further in the future, such as:

- The advanced configuration of DC-DC converters and controllers should be considered to reduce the voltage ripple of the DC bus, which can increase the system performance and quickly adapt to the high peak power.
- The balance-of-plant (BOP) control issues for the PEMFC system such as hydrogen/oxygen supply control, humidity/thermal control, and so forth, need to be developed to protect the stack operation and improve the system efficiency.
- Fuel cell degradation and battery degradation metrics should be considered when designing the EMS to prolong the PEMFC stack and the battery lifetime.
- Advanced control strategies continue to develop such as online optimization-based algorithms and learning-based strategies to enhance the system performance, increase the PEMFC stack efficiency, and reduce hydrogen consumption.

- Experimental implementations need to be conducted with more load profile models of the driving cycle to validate the effectiveness of the proposed strategy under multiple working modes such as accelerator, decelerator, and regenerative.

As a result, this dissertation can be served as a foundation for the future development of sophisticated EMSs for hybrid PEMFC applications.

Publications

A.   International Journal

1. **Hoai-An Trinh**, Duc Giap Nguyen, Van-Du Phan, Tan-Quoc Duong, Hoai-Vu-Anh Truong, Sung-Jin Choi, and Kyoung Kwan Ahn, "Robust adaptive control strategy for a bidirectional DC-DC converter based on extremum seeking and sliding mode control," *Sensors*, vol. 23, no. 1, p. 457, Jan. 2023. doi: 10.3390/s23010457. (SCIE)

2. **Hoai-An Trinh**, Hoai-Vu-Anh Truong, Minh Duc Pham, Tri Cuong Do, Hong-Hee Lee, and Kyoung Kwan Ahn, "Comprehensive Control Strategy and Verification for PEM Fuel Cell/Battery/Supercapacitor Hybrid Power Source," *International Journal of Precision Engineering and Manufacturing-Green Technology*, vol. 10, p. 421-436, Dec. 2022. doi: 10.1007/s40684-022-00498-w. (SCIE)

3. **Hoai-An Trinh**, Hoai-Vu-Anh Truong, Tri Cuong Do, Manh Hung Nguyen, Van-Du Phan, and Kyoung Kwan Ahn, "Optimization-based energy management strategies for Hybrid construction machinery: A review," *Energy Reports*, vol. 8, pp. 6035-6057, Nov. 2022. doi: 10.1016/j.egyr.2022.04.050. (SCIE)

4. **Hoai-An Trinh**, Van-Du Phan, Hoai-Vu-Anh Truong, and Kyoung Kwan Ahn, "Energy Management Strategy for PEM Fuel Cell Hybrid Power System Considering DC Bus Voltage Regulation," *Electronics,* vol. 11, no. 17, p. 2722, Aug. 2022, doi: 10.3390/electronics11172722. (SCIE)

5. **Hoai-An Trinh**, Hoai-Vu-Anh Truong, and Kyoung Kwan Ahn, "Development of Fuzzy-Adaptive Control Based Energy Management Strategy for PEM Fuel Cell Hybrid Tramway System," *Applied Sciences*, vol. 12, no. 8, p. 3880, Apr. 2022, doi: 10.3390/app12083880. (SCIE)

6. **Hoai-An Trinh**, Hoai-Vu-Anh Truong, and Kyoung Kwan Ahn, "Fault Estimation and Fault-Tolerant Control for the Pump-Controlled Electrohydraulic System," *Actuators,* vol. 9, no. 4, p. 132, Dec. 2020, doi: 10.3390/act9040132. (SCIE)

7. Tri Cuong Do, **Hoai-An Trinh**, and Kyoung Kwan Ahn, "Hierarchical Control Strategy with Battery Dynamic Consideration for a Dual Fuel Cell/Battery Tramway," Mathematics, vol. 11, no. 10, p. 2269, May. 2023, doi: 10.3390/math11102269. (SCIE)

8. Van Du Phan, **Hoai-An Trinh**, and Kyoung Kwan Ahn, "Finite-Time Command Filtered Control for Oxygen-Excess Ratio of Proton Exchange Membrane Fuel Cell Systems with Prescribed Performance," *Mathematics*, vol. 11, no. 4, p. 914, Feb. 2023, doi: 10.3390/math11040914. (SCIE)

9. Van Du Phan, **Hoai-An Trinh**, and Kyoung Kwan Ahn, "Design and evaluation of adaptive neural fuzzy-based pressure control for PEM fuel cell system," *Energy Reports*, vol.8, pp.12026-12037, Nov. 2022. doi: 10.1016/j.egyr.2022.09.036. (SCIE)

10. Hoai-Vu-Anh Truong, **Hoai-An Trinh**, and Kyoung Kwan Ahn, "Backstepping Sliding Mode-based Model-free Control of Electro-hydraulic Systems," *Journal of Drive and Control*, vol.19, no.1, pp. 51-61, Mar. 2022. doi: 10.7839/ksfc.2022.19.1.051. (KCI)

11. Hoai-Vu-Anh Truong, **Hoai-An Trinh**, and Kyoung Kwan Ahn, "A Robust Observer for Sensor Faults Estimation on n-DOF Manipulator in Constrained Framework Environment," *IEEE Access*, vol. 9, pp. 88439- 88451, Jun. 2021. doi: 10.1109/ACCESS.2021.3087505. (SCIE)

12. Hoai-Vu-Anh Truong, **Hoai-An Trinh**, and Kyoung Kwan Ahn, "Safety Operation of n-DOF Serial Hydraulic Manipulator in Constrained Motion with Consideration of Contact-Loss Fault," *Applied Sciences*, vol. 10, no. 22, p. 8107, Nov. 2020, doi: 10.3390/app10228107. (SCIE)

B. International Conference

1. **H. -A. Trinh**, H. -V. -A. Truong and K. -K. Ahn, "An improved Energy Management Strategy for Fuel Cell Hybrid Power System Based on Compensator Design of DC-DC Converters," *2022 25th International Conference on Mechatronics Technology (ICMT)*, Kaohsiung, Taiwan, 2022, pp. 1-6, doi: 10.1109/ICMT56556.2022.9997745.

2. **H. -A. Trinh**, H. -V. -A. Truong and K. -K. Ahn, "Fault-tolerant control for a pump-controlled electro-hydraulic system," *2022 13th Asian Control Conference (ASCC),* Jeju, Korea, Republic of, 2022, pp. 1167-1173, doi: 10.23919/ASCC56756.2022.9828270.

3. **H. -A. Trinh**, H. -V. -A. Truong and K. -K. Ahn, "Energy Management Strategy for Fuel Cell Hybrid Power System using Fuzzy Logic and Frequency Decoupling Methods," *2021 24th International Conference on Mechatronics Technology (ICMT)*, Singapore, 2021, pp. 1-6, doi: 10.1109/ICMT53429.2021.9687291. ***(Best paper award)***

4. H. -V. -A. Truong, **H. -A. Trinh**, and K. -K. Ahn, "Optimization-based Energy Management Strategy for Hybrid Electric Tramways," *2022 22nd International Conference on Control, Automation and Systems (ICCAS)*, Jeju, Korea, Republic of, 2022, pp. 574-579, doi: 10.23919/ICCAS55662.2022.10003964.

C. Domestic Conference

1. **H.-A. Trinh**, V. D. Phan, K. K. Sin and K. K. Ahn. "Optimized energy management based on equivalent consumption minimization strategy for a hybrid electric excavator". *2023 Spring Conference on Drive and Control*, 18-19 May, 2023.

2. V. D. Phan, **H.-A. Trinh**, and K. K. Ahn. "Parameter Identification of a Real Electro-hydraulic Servo System using the Least Mean Square Method". *2023 Spring Conference on Drive and Control*, 18-19 May, 2023.

3. **H.-A. Trinh**, K. K. Sin and K. K. Ahn. "Development of fuzzy-based energy management strategy for fuel cell hybrid excavator". *2022 Autumn Conference on Drive and Control*, Gunsan, Korea, Republic of, 2022, pp. 99-104.

Bibliography

[1]   Z. Li, A. Khajepour, and J. Song, "A comprehensive review of the key technologies for pure electric vehicles," *Energy,* vol. 182, pp. 824-839, 2019/09/01/ 2019.

[2]   H.-A. Trinh, H. V. A. Truong, T. C. Do, M. H. Nguyen, V. D. Phan, and K. K. Ahn, "Optimization-based energy management strategies for hybrid construction machinery: A review," *Energy Reports,* vol. 8, pp. 6035-6057, 2022/11/01/ 2022.

[3]   I. E. Agency, "CO2 Emissions in 2022," 2022.

[4]   IEA. (2018). *Renewable electricity generation by source, World 1990-2018.* Available: https://www.iea.org/data-and-statistics/

[5]   R. MacEwen, "The Hidden Problems Within the Electric Vehicle Battery Supply Chain," in *Ballard Power Systems Inc.* vol. 2021, ed, 2019.

[6]   Q. Li, W. Chen, Z. Liu, M. Li, and L. Ma, "Development of energy management system based on a power sharing strategy for a fuel cell-battery-supercapacitor hybrid tramway," *Journal of Power Sources,* vol. 279, pp. 267-280, 2015/04/01/ 2015.

[7]   T. C. Do *et al.*, "Energy Management Strategy of a PEM Fuel Cell Excavator with a Supercapacitor/Battery Hybrid Power Source," vol. 12, no. 22, p. 4362, 2019.

[8]   T. A. Fagundes, G. H. F. Fuzato, P. G. B. Ferreira, M. Biczkowski, and R. Q. Machado, "Fuzzy Controller for Energy Management and SoC Equalization in DC Microgrids Powered by Fuel Cell and Energy Storage Units," *IEEE Journal of Emerging and Selected Topics in Industrial Electronics,* vol. 3, no. 1, pp. 90-100, 2022.

[9]   C. R. d. Aguiar, G. H. F. Fuzato, R. Q. Machado, and J. M. Guerrero, "An Adaptive Power Sharing Control for Management of DC Microgrids Powered by Fuel Cell and Storage System," *IEEE Transactions on Industrial Electronics,* vol. 67, no. 5, pp. 3726-3735, 2020.

[10]   Y. Liu *et al.*, "A Novel Adaptive Model Predictive Control for Proton Exchange Membrane Fuel Cell in DC Microgrids," *IEEE Transactions on Smart Grid,* vol. 13, no. 3, pp. 1801-1812, 2022.

[11]   T. X. Dinh *et al.*, "Modeling and Energy Management Strategy in Energetic Macroscopic Representation for a Fuel Cell Hybrid Electric Vehicle," *Journal of Drive and Control,* vol. 16, no. 2, p. 11, 2019.

[12]   H. Li, A. Ravey, A. N'Diaye, and A. Djerdir, "A novel equivalent consumption minimization strategy for hybrid electric vehicle powered by fuel cell, battery and supercapacitor," *Journal of Power Sources,* vol. 395, pp. 262-270, 2018/08/15/ 2018.

[13]   Z. Fu, Z. Li, P. Si, and F. Tao, "A hierarchical energy management strategy for fuel cell/battery/supercapacitor hybrid electric vehicles," *International Journal of Hydrogen Energy,* vol. 44, no. 39, pp. 22146-22159, 2019/08/13/ 2019.

[14]   T. D. Dang *et al.*, "Design, Modeling and Analysis of a PEM Fuel Cell Excavator with Supercapacitor/Battery Hybrid Power Source," *Journal of Drive and Control,* vol. 16, no. 1, 2019.

[15]   T. Li, H. Liu, D. Zhao, and L. Wang, "Design and analysis of a fuel cell supercapacitor hybrid construction vehicle," *International Journal of Hydrogen Energy,* vol. 41, no. 28, pp. 12307-12319, 2016/07/27/ 2016.

[16]   F. Peng *et al.*, "Development of master-slave energy management strategy based on fuzzy logic hysteresis state machine and differential power processing compensation for a PEMFC-LIB-SC hybrid tramway," *Applied Energy,* vol. 206, pp. 346-363, 2017/11/15/ 2017.

[17]   F. Piraino and P. Fragiacomo, "A multi-method control strategy for numerically testing a fuel cell-battery-supercapacitor tramway," *Energy Conversion and Management,* vol. 225, 2020.

[18]   H.-A. Trinh, H.-V.-A. Truong, and K. K. Ahn, "Development of Fuzzy-Adaptive Control Based Energy Management Strategy for PEM Fuel Cell Hybrid Tramway System," *Applied Sciences,* vol. 12, no. 8, p. 3880, 2022.

[19]   Y. Wang, Z. Sun, and Z. Chen, "Development of energy management system based on a rule-based power distribution strategy for hybrid power sources," *Energy,* vol. 175, pp. 1055-1066, 2019.

[20]   H. Marzougui, M. Amari, A. Kadri, F. Bacha, and J. Ghouili, "Energy management of fuel cell/battery/ultracapacitor in electrical hybrid vehicle," *International Journal of Hydrogen Energy,* vol. 42, no. 13, pp. 8857-8869, 2017/03/30/ 2017.

[21]   Q. Xun, S. Lundberg, and Y. Liu, "Design and experimental verification of a fuel cell/supercapacitor passive configuration for a light vehicle," *Journal of Energy Storage,* vol. 33, p. 102110, 2021/01/01/ 2021.

[22]   Y. Wang, Z. Sun, and Z. Chen, "Energy management strategy for battery/supercapacitor/fuel cell hybrid source vehicles based on finite state machine," *Applied Energy,* vol. 254, p. 113707, 2019/11/15/ 2019.

[23]   K. Kaya and Y. Hames, "Two new control strategies: For hydrogen fuel saving and extend the life cycle in the hydrogen fuel cell vehicles," *International Journal of Hydrogen Energy,* vol. 44, no. 34, pp. 18967-18980, 2019/07/12/ 2019.

[24]   Q. Li, H. Yang, Y. Han, M. Li, and W. Chen, "A state machine strategy based on droop control for an energy management system of PEMFC-battery-supercapacitor hybrid tramway," *International Journal of Hydrogen Energy,* vol. 41, no. 36, pp. 16148-16159, 2016/09/28/ 2016.

[25]   Q. Li, T. Wang, C. Dai, W. Chen, and L. Ma, "Power Management Strategy Based on Adaptive Droop Control for a Fuel Cell-Battery-Supercapacitor Hybrid Tramway," *IEEE Transactions on Vehicular Technology,* vol. 67, no. 7, pp. 5658-5670, 2018.

[26]   K. Yedavalli, L. Guo, and D. S. Zinger, "Simple Control System for a Switcher Locomotive Hybrid Fuel Cell Power System," *IEEE Transactions on Industry Applications,* vol. 47, no. 6, pp. 2384-2390, 2011.

[27]   P. García, L. M. Fernández, J. P. Torreglosa, and F. Jurado, "Operation mode control of a hybrid power system based on fuel cell/battery/ultracapacitor for an electric tramway," *Computers & Electrical Engineering,* vol. 39, no. 7, pp. 1993-2004, 2013/10/01/ 2013.

[28]   P. Garcia, L. M. Fernandez, C. A. Garcia, and F. Jurado, "Energy Management System of Fuel-Cell-Battery Hybrid Tramway," *IEEE Transactions on Industrial Electronics,* vol. 57, no. 12, pp. 4013-4023, 2010.

[29]   F. Tao, L. Zhu, Z. Fu, P. Si, and L. Sun, "Frequency Decoupling-Based Energy Management Strategy for Fuel Cell/Battery/Ultracapacitor Hybrid Vehicle Using Fuzzy Control Method," *IEEE Access,* vol. 8, pp. 166491-166502, 2020.

[30]   J. Snoussi, S. B. Elghali, M. Benbouzid, and M. F. Mimouni, "Optimal Sizing of Energy Storage Systems Using Frequency-Separation-Based Energy Management for Fuel Cell Hybrid Electric Vehicles," *IEEE Transactions on Vehicular Technology,* vol. 67, no. 10, pp. 9337-9346, 2018.

[31]   J. Snoussi, S. Ben Elghali, M. Benbouzid, and M. F. Mimouni, "Auto-Adaptive Filtering-Based Energy Management Strategy for Fuel Cell Hybrid Electric Vehicles," vol. 11, no. 8, p. 2118, 2018.

[32]   Q. Li, W. Chen, Y. Li, S. Liu, and J. Huang, "Energy management strategy for fuel cell/battery/ultracapacitor hybrid vehicle based on fuzzy logic," *International Journal of Electrical Power & Energy Systems,* vol. 43, no. 1, pp. 514-525, 2012/12/01/ 2012.

[33]   K. Ameu, A. Hadjaissa, M. S. A. Cheikh, A. Cheknane, and N. Essounbouli, "Fuzzy energy management of hybrid renewable power system with the aim to extend component lifetime," *International Journal of Energy Research,* vol. 41, no. 13, pp. 1867-1879, 2017.

[34] S. Ahmadi, S. M. T. Bathaee, and A. H. Hosseinpour, "Improving fuel economy and performance of a fuel-cell hybrid electric vehicle (fuel-cell, battery, and ultra-capacitor) using optimized energy management strategy," *Energy Conversion and Management,* vol. 160, pp. 74-84, 2018/03/15/ 2018.

[35] P. Fragiacomo and F. Piraino, "Numerical modelling of a PEFC powertrain system controlled by a hybrid strategy for rail urban transport," *Journal of Energy Storage,* vol. 17, pp. 474-484, 2018/06/01/ 2018.

[36] K. Song *et al.*, "Multi-mode energy management strategy for fuel cell electric vehicles based on driving pattern identification using learning vector quantization neural network algorithm," *Journal of Power Sources,* vol. 389, pp. 230-239, 2018/06/15/ 2018.

[37] Z. Hu *et al.*, "Multi-objective energy management optimization and parameter sizing for proton exchange membrane hybrid fuel cell vehicles," *Energy Conversion and Management,* vol. 129, pp. 108-121, 2016/12/01/ 2016.

[38] T. Li, H. Liu, H. Wang, and Y. Yao, "Multiobjective Optimal Predictive Energy Management for Fuel Cell/Battery Hybrid Construction Vehicles," *IEEE Access,* vol. 8, pp. 25927-25937, 2020.

[39] H.-S. Yi, J.-B. Jeong, S.-W. Cha, and C.-H. Zheng, "Optimal component sizing of fuel cell-battery excavator based on workload," *International Journal of Precision Engineering and Manufacturing-Green Technology,* vol. 5, no. 1, pp. 103-110, 2018/01/01 2018.

[40] Y. Yan, Q. Li, W. Chen, B. Su, J. Liu, and L. Ma, "Optimal Energy Management and Control in Multimode Equivalent Energy Consumption of Fuel Cell/Supercapacitor of Hybrid Electric Tram," *IEEE Transactions on Industrial Electronics,* vol. 66, no. 8, pp. 6065-6076, 2019.

[41] Y. Yan, Q. Li, W. Huang, and W. Chen, "Operation Optimization and Control Method Based on Optimal Energy and Hydrogen Consumption for the Fuel Cell/Supercapacitor Hybrid Tram," *IEEE Transactions on Industrial Electronics,* vol. 68, no. 2, pp. 1342-1352, 2021.

[42] P. Jiang, R. Li, and H. Li, "Multi-objective algorithm for the design of prediction intervals for wind power forecasting model," *Applied Mathematical Modelling,* vol. 67, pp. 101-122, 2019/03/01/ 2019.

[43] X. Lü, "Energy Optimization of Logistics Transport Vehicle Driven by Fuel Cell Hybrid Power System," *Energy conversion and management,* p. 2019, 2019-07-29 2019.

[44] S. Cheng, G. Zhao, M. Gao, Y. Shi, M. Huang, and N. Yousefi, "Optimal hybrid energy system for locomotive utilizing improved Locust Swarm optimizer," *Energy,* vol. 218, p. 119492, 2021/03/01/ 2021.

[45] J. Xie, J. Ma, and K. Bai, "State-of-charge estimators considering temperature effect, hysteresis potential, and thermal evolution for LiFePO4 batteries," *International Journal of Energy Research,* vol. 42, p. 18, 2018.

[46] H.-S. Yi and S. Cha, "Optimal Energy Management of the Electric Excavator Using Super Capacitor," *International Journal of Precision Engineering and Manufacturing-Green Technology,* vol. 8, no. 1, pp. 151-164, 2021/01/01 2021.

[47] H. Li, A. Ravey, A. N'Diaye, and A. Djerdir, "Online adaptive equivalent consumption minimization strategy for fuel cell hybrid electric vehicle considering power sources degradation," *Energy Conversion and Management,* vol. 192, pp. 133-149, 2019/07/15/ 2019.

[48] W. Zhang, J. Li, L. Xu, and M. Ouyang, "Optimization for a fuel cell/battery/capacity tram with equivalent consumption minimization strategy," *Energy Conversion and Management,* vol. 134, pp. 59-69, 2017/02/15/ 2017.

[49] T. Wang, Q. Li, L. Yin, W. Chen, E. Breaz, and F. Gao, "Hierarchical Power Allocation Method Based on Online Extremum Seeking Algorithm for Dual-PEMFC/Battery Hybrid Locomotive," *IEEE Transactions on Vehicular Technology,* vol. 70, no. 6, pp. 5679-5692, 2021.

[50] D. Zhou, A. Ravey, A. Al-Durra, and F. Gao, "A comparative study of extremum seeking methods applied to online energy management strategy of fuel cell hybrid electric vehicles," *Energy Conversion and Management,* vol. 151, pp. 778-790, 2017/11/01/ 2017.

[51] P. Thounthong, S. Raël, and B. Davat, "Energy management of fuel cell/battery/supercapacitor hybrid power source for vehicle applications," *Journal of Power Sources,* vol. 193, no. 1, pp. 376-385, 2009/08/01/ 2009.

[52] M. S. N, O. Tremblay, and L. Dessaint, "A generic fuel cell model for the simulation of fuel cell vehicles," in *2009 IEEE Vehicle Power and Propulsion Conference*, 2009, pp. 1722-1729.

[53] S. N. Motapon, L. Dessaint, and K. Al-Haddad, "A Comparative Study of Energy Management Schemes for a Fuel-Cell Hybrid Emergency Power System of More-Electric Aircraft," *IEEE Transactions on Industrial Electronics,* vol. 61, no. 3, pp. 1320-1334, 2014.

[54] D. Zhou, A. Al-Durra, I. Matraji, A. Ravey, and F. Gao, "Online Energy Management Strategy of Fuel Cell Hybrid Electric Vehicles: A Fractional-Order Extremum Seeking Method," *IEEE Transactions on Industrial Electronics,* vol. 65, no. 8, pp. 6787-6799, 2018.

[55] O. Tremblay, L. Dessaint, and A. Dekkiche, "A Generic Battery Model for the Dynamic Simulation of Hybrid Electric Vehicles," in *2007 IEEE Vehicle Power and Propulsion Conference*, 2007, pp. 284-289.

[56] K. B. Oldham, "A Gouy–Chapman–Stern model of the double layer at a (metal)/(ionic liquid) interface," *Journal of Electroanalytical Chemistry,* vol. 613, no. 2, pp. 131-138, 2008/02/15/ 2008.

[57] N. Xu and J. Riley, "Nonlinear analysis of a classical system: The double-layer capacitor," *Electrochemistry Communications,* vol. 13, no. 10, pp. 1077-1081, 2011/10/01/ 2011.

[58] H.-A. Trinh, H. V. A. Truong, M. D. Pham, T. C. Do, H.-H. Lee, and K. K. Ahn, "Comprehensive Control Strategy and Verification for PEM Fuel Cell/Battery/Supercapacitor Hybrid Power Source," *International Journal of Precision Engineering and Manufacturing-Green Technology,* 2022/12/30 2022.

[59] H.-A. Trinh, V.-D. Phan, H.-V.-A. Truong, and K. K. Ahn, "Energy Management Strategy for PEM Fuel Cell Hybrid Power System Considering DC Bus Voltage Regulation," vol. 11, no. 17, p. 2722, 2022.

[60] H. V. A. Truong *et al.*, "Mapping Fuzzy Energy Management Strategy for PEM Fuel Cell–Battery–Supercapacitor Hybrid Excavator," vol. 13, no. 13, p. 3387, 2020.

[61] H. V. Dao *et al.*, "Optimization-Based Fuzzy Energy Management Strategy for PEM Fuel Cell/Battery/Supercapacitor Hybrid Construction Excavator," *International Journal of Precision Engineering and Manufacturing-Green Technology,* vol. 8, no. 4, pp. 1267-1285, 2021/07/01 2021.

[62] H. Marzougui, A. Kadri, J.-P. Martin, M. Amari, S. Pierfederici, and F. Bacha, "Implementation of energy management strategy of hybrid power source for electrical vehicle," *Energy Conversion and Management,* vol. 195, pp. 830-843, 2019/09/01/ 2019.

[63] Y. Han, Q. Li, T. Wang, W. Chen, and L. Ma, "Multisource Coordination Energy Management Strategy Based on SOC Consensus for a PEMFC–Battery–Supercapacitor Hybrid Tramway," *IEEE Transactions on Vehicular Technology,* vol. 67, no. 1, pp. 296-305, 2018.

[64] S. Somkun and V. Chunkag, "Fast DC bus voltage control of single-phase PWM rectifiers using a ripple voltage estimator," in *IECON 2016 - 42nd Annual Conference of the IEEE Industrial Electronics Society*, 2016, pp. 2289-2294.

[65] K. Sabanci and S. Balci, "Development of an expression for the output voltage ripple of the DC-DC boost converter circuits by using particle swarm optimization algorithm," *Measurement,* vol. 158, p. 107694, 2020/07/01/ 2020.

[66] S. K. Kollimalla, M. K. Mishra, A. Ukil, and H. B. Gooi, "DC Grid Voltage Regulation Using New HESS Control Strategy," *IEEE Transactions on Sustainable Energy,* vol. 8, no. 2, pp. 772-781, 2017.

[67] R. W. Erickson and D. Maksimović, *Fundamentals of Power Electronics*, Third Edition ed. Springer, 2020.

[68] X. Li, Y. Wang, D. Yang, and Z. Chen, "Adaptive energy management strategy for fuel cell/battery hybrid vehicles using Pontryagin's Minimal Principle," *Journal of Power Sources,* vol. 440, p. 10, 2019.

[69] M. Zandi, A. Payman, J. Martin, S. Pierfederici, B. Davat, and F. Meibody-Tabar, "Energy Management of a Fuel Cell/Supercapacitor/Battery Power Source for Electric Vehicular Applications," *IEEE Transactions on Vehicular Technology,* vol. 60, no. 2, pp. 433-443, 2011.

[70] H. Hemi, J. Ghouili, and A. Cheriti, "A real time fuzzy logic power management strategy for a fuel cell vehicle," *Energy Conversion and Management,* vol. 80, pp. 63-70, 2014/04/01/ 2014.

[71] A. Badji, D. O. Abdeslam, D. Chabane, and N. Benamrouche, "Real-time implementation of improved power frequency approach based energy management of fuel cell electric vehicle considering storage limitations," *Energy,* vol. 249, p. 123743, 2022/06/15/ 2022.

[72] H. A. Trinh, H. V. A. Truong, and K. K. Ahn, "Energy management strategy for fuel cell hybrid power system using fuzzy logic and frequency decoupling methods," in *2021 24th International Conference on Mechatronics Technology (ICMT)*, 2021, pp. 1-6.